



World Scientific News

An International Scientific Journal

WSN 138(1) (2019) 1-64

EISSN 2392-2192

A Study on the Effects of Inclined Magnetic Field, Flow Medium Porosity and Thermal Radiation on Free Convection of Casson Nanofluid over a Vertical Plate

M. G. Sobamowo^{1,*}, A. A. Yinusa¹ and O. D. Makinde²

¹Department of Mechanical Engineering, University of Lagos, Akoka, Lagos, Nigeria

²Faculty of Military Science, Stellenbosch University, Saldanha, South Africa

*E-mail address: mikegbeminiyi@gmail.com

ABSTRACT

In this paper, variational homotopy perturbation method with Padé approximant technique is applied to investigate the impacts of inclined magnetic field, flow medium porosity and thermal radiation on free convection flow and heat transfer of Casson nanofluids over a vertical plate. The accuracies of the developed analytical methods are verified by comparing the results of the analytical solutions with the results of past works as presented in literature. Thereafter, the analytical solutions are used to investigate the effects of thermal radiation; Prandtl number, nanoparticles volume-fraction, shape and type on the flow and heat transfer behaviour of various nanofluids over the flat plate. It is observed that both the velocity and temperature of the nanofluid as well viscous and thermal boundary layers increase with increase in the radiation parameter. The velocity and temperature of the nanofluid decreases and increases, respectively as the Prandtl number and volume-fraction of the nanoparticles in the basefluid increase. The maximum decrease in velocity and maximum increase in temperature are caused lamina shaped nanoparticle and followed by platelets, cylinder, bricks and sphere-shaped nanoparticles, respectively. It is hoped that the present study will enhance the understanding of free convection boundary-layer problems under the influence of thermal radiation as applied in various engineering processes.

Keywords: Inclined magnetic field, Flow medium porosity, Thermal radiation, Casson nanofluid, Free convection, Variational homotopy perturbation method

1. INTRODUCTION

The importance and the wide applications of free convection flow and heat transfer in extrusion, melt spinning, glass-fibre production processes, food processing, mechanical forming processes, etc. have in recent times aroused renewed research interests and explorations. In the study of free convection and heat transfer problems, the analysis of incompressible laminar flow of viscous fluid in a steady state, two-dimensional free convection boundary-layer has over the years been a common area of increasing research interests following experimental investigations of Schmidt and Beckmann [1] and the pioneering theoretical work of Ostrach et al. [2]. In their attempts to study the laminar free convection flow and heat transfer problem in 1953, Ostrach et al. [2] applied method of iterative integration to analyze free convection over a semi-infinite isothermal flat plate.

The author obtained the numerical solutions for a wide range of Prandtl numbers from 0.01 to 1000 and validated their numerical results using experimental data of Schmidt and Beckmann [1]. Five years later, Sparrow and Gregg [3] presented a further study on numerical solutions for laminar free convection from a vertical plate with uniform surface heat flux. Considering the fact that the major part of low Prandtl-number boundary layer of free convection is inviscid, Lefevre [4] examined the laminar free convection of an inviscid flow from a vertical plane surface. In a further work, Sparrow and Gregg [5] developed similar solutions for free convection from a non-isothermal vertical plate. Meanwhile, a study on fluid flow over a heated vertical plate at high Prandtl number was presented by Stewartson and Jones [6]. Due to the disadvantages in the numerical methods in the previous studies [2, 3], Kuiken [7] adopted method of matched asymptotic expansion and established asymptotic solutions for large Prandtl number free convection. In the subsequent year, the same author applied the singular perturbation method and analyzed free convection at low Prandtl numbers [8].

Also, in another work on the asymptotic analysis of the same problem, Eshghy [9] studied free-convection boundary layers at large Prandtl number while Roy [10] investigated free convection for uniform surface heat flux at high Prandtl number. With the development of asymptotic solution, a combined study of the effects of small and high Prandtl numbers on the viscous fluid flow over a flat vertical plate was submitted by Kuiken and Rotem [11]. In the succeeding year, Na and Habib [12] utilized parameter differentiation method to solve the free convection boundary layer problem. Few years later, Merkin [13] presented the similarity solutions for free convection on a vertical plate while Merkin and Pop [14] used finite difference method to develop numerical solutions for conjugate free convection problem of boundary-layer flow over a vertical plate. Also, Ali et al. [15] submitted a study on numerical investigation of free convective boundary layer in a viscous fluid.

The various analytical and numerical studies of the past works have shown that the boundary layer problems are very difficult to solve. This is because, besides having very thin regions where there is rapid change of the fluid properties, they are defined on unbounded domains. Although, approximate analytical methods are being used to solve boundary layer problems, they converge very slowly for some boundary layer problems, particularly those with very large parameters. The numerical methods used to the flow process also encounter problems in resolving the solution of the governing equations in the very thin regions and in cases where singularities or multiple solutions exist. Moreover, in numerical analysis, it is absolutely required that the stability and convergence analysis should be carried so as to avoid divergence or inappropriate results.

Such analysis in the mathematical methods increases the computation time and cost. Therefore, in the quest of presenting symbolic solutions to the flow and heat transfer problem using one of the recently developed semi-analytical methods, Motsa et al. [16] adopted homotopy analysis of free convection boundary layer flow with heat and mass transfer. In another work, the authors used spectral local linearization approach for solving the natural convection boundary layer flow [17]. Ghotbi et al. [18] investigated the use of homotopy analysis method to natural convection boundary layer flow. Although, the homotopy analysis method (HAM) is a reliable and efficient semi-analytical technique, it suffers from a number of limiting assumptions such as the requirements that the solution ought to conform to the so-called rule of solution expression and the rule of coefficient ergodicity. Also, the use of HAM in the analysis of linear and nonlinear equations requires the determination of auxiliary parameter which will increase the computational cost and time. Additionally, the lack of rigorous theories or proper guidance for choosing initial approximation, auxiliary linear operators, auxiliary functions, and auxiliary parameters limits the applications of HAM. Moreover, such method requires high skill in mathematical analysis and the solution comes with large number of terms. Additionally, various analyses of nonlinear models and fluid flow problems under the influences of some internal and external factors using different approximate analytical and numerical methods have been presented in literature [19-47].

However, the relative simplicity coupled with ease of applications of differential transformation method (DTM) has made the method to be more effective than most of the other approximate analytical methods. The method was introduced by Zhou [48] and it has fast gained ground as it appeared in many engineering and scientific research papers. This is because, with the applications of DTM, a closed form series solution or approximate solution can be provided for nonlinear integral and differential equations without linearization, restrictive assumptions, perturbation and discretization or round-off error. It reduces complexity of expansion of derivatives and the computational difficulties of the other traditional or recently developed methods.

Therefore, Yu and Chen [49] applied the differential transformation method to provide approximate analytical solutions to Blasius equation. Also, Kuo [50] adopted the same method to determine the velocity and temperature profiles of the Blasius equation of forced convection problem for fluid flow passing over a flat plate. An extended work on the applications of differential transformation method to free convection boundary-layer problem of two-dimensional steady and incompressible laminar flow passing over a vertical plate was presented by the same author [51]. However, in the later work, the nonlinear coupled boundary value governing equations of the flow and heat transfer processes are reduced to initial value equations by a group of transformations and the resulting coupled initial-value equations are solved by means of the differential transformation method.

The reduction or the transformation of the boundary value problems to the initial value problems was carried out due to the fact that the developed systems of nonlinear differential equations contain an unbounded domain of infinite boundary conditions. Moreover, in order to obtain the numerical solutions that are valid over the entire large domain of the problem, Ostrach et al. [2] estimated the values of $f''(0)$ and $\theta'(0)$ during the analysis of the developed systems of fully coupled nonlinear ordinary differential equations. Following the Ostrach et al's approach, most of the subsequent solutions provided in literature [3, 9, 10, 12, 14, 15, 50, and 51] were based on the estimated boundary conditions given by Ostrach et al [1]. Additionally, the limitations of power series solutions to small domain problems have been well established

in literature. However, in some recent studies, the use of power series methods coupled with Padé-approximant technique has shown to be very effective way of developing accurate analytical solutions to nonlinear problems of large or unbounded domain problems of infinite boundary conditions. The application of Padé-approximant technique with power series method increases the rate and radius of convergence of power series solution. Therefore, in a recent work, Rashidi et al. [52] applied differential transformation method coupled with Padé-approximant technique to develop a novel analytical solution for mixed convection about an inclined flat plate embedded in a porous medium.

Casson fluid is a non-Newtonian fluid that was first invented by Casson in 1959 [53]. It is a shear thinning liquid which is assumed to have an infinite viscosity at zero rate of shear, a yield stress below which no flow occurs, and a zero viscosity at an infinite rate of shear [54]. If yield stress is greater than the shear stress then it acts as a solid, whereas if yield stress lesser than the shear stress is applied then the fluid would start to move. The fluid is based on the structure of liquid phase and interactive behaviour of solid of a two-phase suspension. It is able to capture complex rheological properties of a fluid, unlike other simplified models like the power law [55] and second, third or fourth-grade models [56]. Some examples of Casson fluid are Jelly, honey, tomato sauce and concentrated fruit juices. Human blood is also treated as a Casson fluid in the presence of several substances such as fibrinogen, globulin in aqueous base plasma, protein, and human red blood cells. Concentrated fluids like sauces, honey, juices, blood, and printing inks can be well described using this model. It has various applications in fibrinogen, cancer homeo-therapy, protein and red blood cells form a chain type structure. Due to these applications many researchers are concentrating characteristics of Casson fluid. Application of Casson fluid for flow between two rotating cylinders is performed in [57]. The effect of magnetohydrodynamic (MHD) Casson fluid flow in a lateral direction past linear stretching sheet was explained by Nadeem et al. [58].

The role of thermal radiation is a major important in some industrial applications such as glass production and furnace design, and also in space technology applications, such as comical flight aerodynamics rocket, space vehicles, propulsion systems, plasma physics and space craft re-entry aerodynamics which operates at high temperatures, in the flow structure of atomic plants, combustion processes, internal combustion engines, ship compressors and solar radiations.

The effect of thermal radiation on magnetohydrodynamics flow was examined Raptis et al. [59] while Seddeek [60] investigated the impacts of thermal radiation and variable viscosity on magnetohydrodynamics in free convection flow over a semi-infinite flat plate. In another study, Mehmood et al. [61] analyzed unsteady stretched flow of Maxwell fluid in presence of nonlinear thermal radiation and convective condition while Hayat et al. [62] addressed the effects of nonlinear thermal radiation and magnetohydrodynamics on viscoelastic nanofluid flow. Effects of nonlinear thermal radiation on stagnation point flow Farooq et al. [63]. Also, Shehzad et al. [64] presented a study on MHD three-dimensional flow of Jeffrey nanofluid with internal heat generation and thermal radiation. Further studies on the effects of transverse magnetic field, chemical reaction, heat generation, radiation on the free convection flow of viscous and nanofluid over stretching surfaces have been carried out in literature [65-107].

The previous studies on fluid flow over stretching plate focus on the analysis of Newtonian and non-Newtonian fluids under the influences of thermal radiation, internal heat generation and magnetic field. To the best of the author's knowledge, a study on the simultaneous effects of inclined magnetic field, flow medium porosity and thermal radiation on

free convection flow and heat transfer of Casson nanofluids over a vertical plate has not been presented in literature. Moreover, different analytical, approximate analytical, semi-numerical and numerical methods have been used to analyze different flow problems. However, the relatively new approximate analytical method called variational homotopy perturbation method which is a modified variation iteration method has shown to have improved accuracy, very rapid rate of convergence and wide range of applications.

The method combines the variational iteration technique and the homotopy perturbation method. It provides solutions to problems in a rapid convergent series which may lead the solution in a closed form. It is very reliable and highly efficient. It solves nonlinear problems without using the so-called Adomian's polynomials. The VHPM is applied without any discretization, restrictive assumption, or transformation and is free from round-off errors. Unlike the method of separation of variables that require initial and boundary conditions, the VHPM provides an analytical solution by using the initial conditions only. The boundary conditions can be used only to justify the obtained result. The method is considered as an important and significant refinement of the previously developed techniques and can be viewed as an alternative to the recently developed methods such as Adomian's decomposition, variational iterations and homotopy perturbation methods [108-111]. Therefore, in the present study, variational homotopy perturbation method coupled with Padé-approximant technique is applied to investigate the simultaneous effects of inclined magnetic field, flow medium porosity, thermal radiation and nanoparticles on free convective flow of Casson nanofluid past a vertical plate. Also, the influences of low and high Prandtl numbers on the free convection boundary-layer flow and heat transfer of nanofluids are examined and discussed.

2. PROBLEM FORMULATION AND MATHEMATICAL ANALYSIS

Consider a laminar free-convection flow of an incompressible Casson nanofluid over a vertical plate parallel to the direction of the generating body force as shown in Fig. 1. The plate is embedded in a porous medium, and subjected to an inclined magnetic field and thermal radiation. Using the rheological equation for an isotropic and incompressible Casson fluid, reported by Casson [65], is

$$\tau = \tau_0 + \mu \dot{\gamma} \tag{1}$$

or

$$\begin{aligned} \tau &= \left\{ 2 \left(\mu_B + \frac{p_y}{\sqrt{2\pi}} \right) e_{ij}, \pi > \pi_c \right\} \\ &= \left\{ 2 \left(\mu_B + \frac{p_y}{\sqrt{2\pi_c}} \right) e_{ij}, \pi_c < \pi \right\} \end{aligned} \tag{2}$$

where τ is the shear stress, τ_0 is the Casson yield stress, μ is the dynamic viscosity, $\dot{\gamma}$ is the shear rate, $\pi = e_{ij}e_{ij}$ and e_{ij} is the $(i,j)th$ component of the deformation rate, π is the product of

the component of deformation rate with itself, π_c is a critical value of this product based on the non-Newtonian model, μ_B the is plastic dynamic viscosity of the non-Newtonian fluid and p_y is the yield stress of the fluid. The velocity as well as the temperature is functions of y, t only.

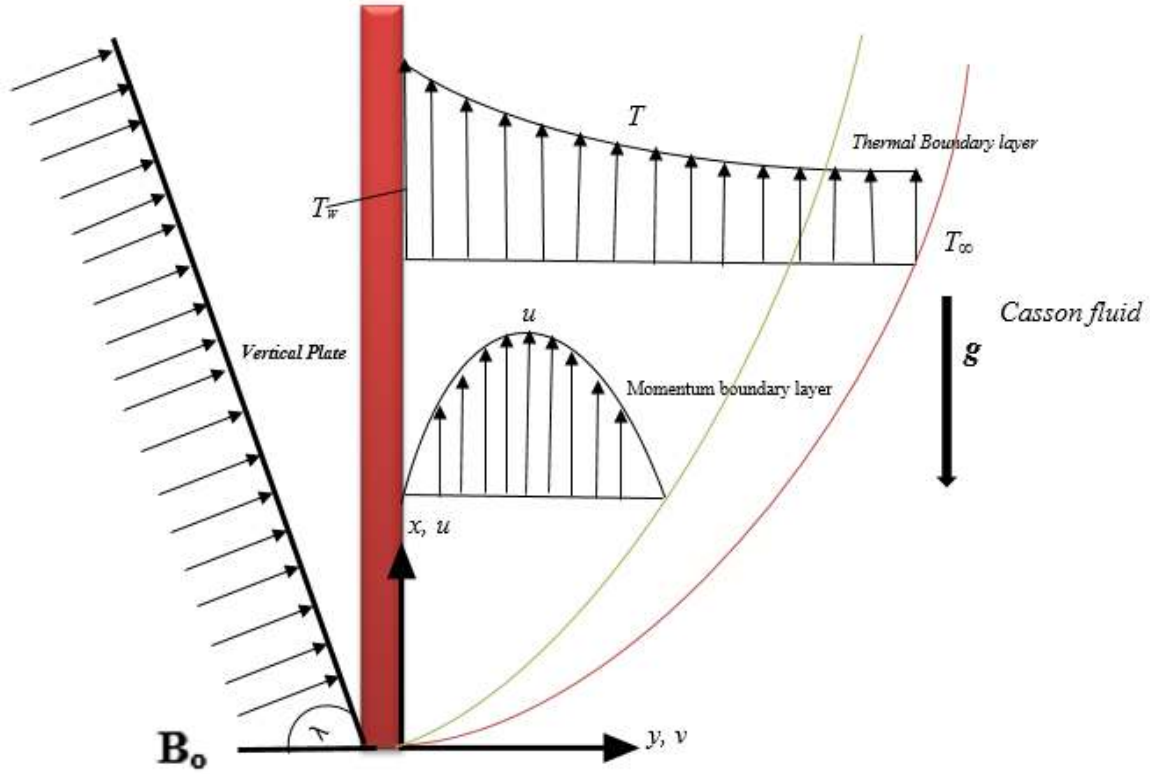


Fig. 1. Velocity and temperature profiles in free convection flow over a vertical plate under the influence of inclined magnetic field

Assuming that the flow in the laminar boundary layer is two-dimensional and steady, the heat transfer from the plate to the fluid is proportional to the local surface temperature T , using the Boussinesq approximation along with the assumption that the pressure is uniform across the boundary layer, the equations for continuity and motion are given as

$$\frac{\partial u}{\partial x} + \frac{\partial v}{\partial y} = 0 \tag{3}$$

$$\rho_{nf} \left(u \frac{\partial u}{\partial x} + v \frac{\partial u}{\partial y} \right) = \left(1 + \frac{1}{\gamma} \right) \mu_{nf} \frac{\partial^2 u}{\partial y^2} + g(\rho\beta)_{nf} (T - T_{\infty}) - \sigma B_0^2 u (\sin^2 \lambda) - \frac{\mu u}{K} \tag{4}$$

$$(\rho c_p)_{nf} \left(u \frac{\partial T}{\partial x} + v \frac{\partial T}{\partial y} \right) = k_{nf} \frac{\partial^2 T}{\partial y^2} - \frac{\partial q_r}{\partial y} \tag{5}$$

Assuming no slip conditions, the appropriate boundary conditions are given as

$$u = 0, \quad v = 0, \quad T = T_s \quad \text{at} \quad y = 0 \tag{6a}$$

$$u = 0, \quad T = T_w, \quad \text{at} \quad y \rightarrow \infty \tag{6b}$$

where the various physical and thermal properties in the Eq. (3-5) are given as

$$\rho_{nf} = \rho_f(1 - \phi) + \rho_s\phi \tag{7a}$$

$$(\rho c_p)_{nf} = (\rho c_p)_f(1 - \phi) + (\rho c_p)_s\phi \tag{7b}$$

$$(\rho\beta)_{nf} = (\rho\beta)_f(1 - \phi) + (\rho\beta)_s\phi \tag{7c}$$

$$\mu_{nf} = \frac{\mu_f}{(1 - \phi)^{2.5}} \tag{7d}$$

$$\sigma_{nf} = \sigma_f \left[1 + \frac{3 \left\{ \frac{\sigma_s}{\sigma_f} - 1 \right\} \phi}{\left\{ \frac{\sigma_s}{\sigma_f} + 2 \right\} \phi - \left\{ \frac{\sigma_s}{\sigma_f} - 1 \right\} \phi} \right], \tag{8}$$

$$k_{nf} = k_f \left[\frac{k_s + (m - 1)k_f - (m - 1)\phi(k_f - k_s)}{k_s + (m - 1)k_f + \phi(k_f - k_s)} \right] \tag{9}$$

$$\frac{\partial q_r}{\partial y} = -\frac{4\sigma}{3K} \frac{\partial T^4}{\partial y} \cong -\frac{16\sigma T_s^3}{3K} \frac{\partial^2 T}{\partial y^2} \quad (\text{using Rosseland's approximation}) \tag{10}$$

where m in the above Hamilton Crosser's model in Eq. (8) is the shape factor which numerical values for different shapes are given in Table 1.

It should be noted that the shape factor, $m = \frac{3}{\lambda}$, where λ is the sphericity (the ratio of the surface area of the sphere and the surface area of the real particles with equal volumes). For sphericity of sphere, platelet, cylinder, laminar and brick are 1.000, 0.526, 0.625, 0.185 and 0.811 respectively. The Hamilton Crosser's model becomes a Maxwell-Garnett's model, when the shape factor of the nanoparticle, $m=3$.

Table 1. The values of different shapes of nanoparticles [66, 67]

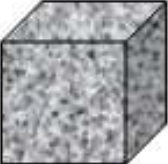
S/N	Name	Shape	Shape factor (m)	Sphericity (ψ)
1	Sphere		3.0	1.000
2	Platelet		5.7	0.526
3	Cylinder		4.8	0.625
4	Lamina		16.2	0.185
5	Brick		3.7	0.811

Table 2. Physical and thermal properties of the base fluid [66-71]

Base fluid	ρ (kg/m ³)	c_p (J/kgK)	k (W/mK)
Pure water	997.1	4179	0.613
Ethylene Glycol	1115	2430	0.253
Engine oil	884	1910	0.144
Kerosene	783	2010	0.145

Table 3. Physical and thermal properties of nanoparticles [66-71]

Nanoparticles	ρ (kg/m ³)	c_p (J/kgK)	k (W/mK)
Copper (Cu)	8933	385	401
Aluminum oxide (Al ₂ O ₃)	3970	765	40
SWCNTs	2600	42.5	6600
Silver (Ag)	10500	235.0	429
Titanium dioxide (TiO ₂)	4250	686.2	8.9538
Copper (II) Oxide (CuO)	783	540	18

Table 2 and 3 present the physical and thermal properties of the base fluid and the nanoparticles, respectively. SWCNTs mean single-walled carbon nanotubes.

Going back to Eq. (3), (4) and (5) and if one introduces a stream function, $\psi(x, y)$ such that

$$u = \frac{\partial \psi}{\partial y}, \quad v = -\frac{\partial \psi}{\partial x}, \tag{11}$$

and use the following similarity and dimensionless variables

$$\eta = \left[\frac{\rho_f^2 (g\beta_f (T_w - T_\infty) x_0^3)}{\mu_f^2 x} \right]^{\frac{1}{4}} \frac{y}{(x - x_0)}, \quad \psi = \left[\frac{\rho_f^2 (g\beta_f (T_w - T_\infty)) x_0^3}{\mu_f^2} \right]^{\frac{1}{4}} f(\eta), \tag{12}$$

$$T = T + (T_1 - T)_0 \left(\frac{x_0}{x_0 - x} \right)^3 \theta(\eta), \quad Pr = \frac{\mu_f c_p}{k_f}, \quad R = \frac{4\sigma T_\infty^3}{3kK}$$

one arrives at fully coupled third and second orders ordinary differential equations

$$\left(1 + \frac{1}{\gamma} \right) f''' - (1 - \phi)^{2.5} \left\{ \left[(1 - \phi) + \phi \left(\frac{\rho_s}{\rho_f} \right) \right] (f')^2 + \left[(1 - \phi) + \phi \left[(\rho\beta)_s / (\rho\beta)_f \right] \right] \theta \right\} - Ha (\sin^2 \lambda) f' - \frac{1}{Da} f' = 0 \tag{13}$$

$$\left(1 + \frac{4}{3}R\right)\theta'' - 3 \left[\frac{1}{(1-\phi) + \phi \left[\frac{(\rho C_p)_s}{(\rho C_p)_f} \right]} \right] \left[\frac{k_s + (m-1)k_f - (m-1)\phi(k_f - k_s)}{k_s + (m-1)k_f + \phi(k_f - k_s)} \right] Prf \theta' = 0 \tag{14}$$

and the boundary conditions as

$$f = 0, \quad f' = 0, \quad \theta = 1, \quad \text{when } \eta = 0 \tag{15}$$

$$f' = 0, \quad \theta = 0, \quad \text{when } \eta = \infty$$

It should be noted that for a viscous fluid which does not have nanoparticles with negligible radiation and magnetic field, embedded in a non-porous medium, the nanoparticle volume fraction is zero i.e. $\phi = 0, Ha = R = 0, Da \rightarrow \infty$ and $\beta \rightarrow \infty$ then one recovers the earlier models [2-15] from Eq. (13) and (14) which are

$$f''' - (f')^2 + \theta = 0 \tag{16}$$

$$\theta'' - 3Prf\theta' = 0 \tag{17}$$

and the boundary conditions remain the same as in Eq. (15)

3. METHOD OF SOLUTION: VARIATIONAL HOMOTOPY PERTURBATION METHOD

As the name implies, variational homotopy perturbation method is based on variational iteration and homotopy perturbation methods. In the algorithm of the variational homotopy perturbation method, the correct functional is developed and the Lagrange multipliers are calculated optimally via variational theory [108-111]. Finally, the homotopy perturbation is implemented on the correct functional and the comparison of like powers of given solutions of various orders are made. The developed algorithm takes full advantage of variational iteration the homotopy perturbation methods. Therefore, in order to illustrate the basic concept of the hybrid technique, we first consider the two methods that make up the hybrid method.

3. 1. Variational iteration method

In finding direct and practical solutions to the problem, variational iteration method is applied to the simultaneous nonlinear equations. As pointed previously, the variational iteration method is an approximate analytical method for solving differential equations [112-117].

The basic definitions of the method are as follows.

The differential equation to be solved can be written in the form

$$Lu + Nu = g(x) \tag{18}$$

where L is a linear operator, N is a nonlinear operator and $g(x)$ is an inhomogeneous term in the differential equation.

Following VIM procedure, we have a correction functional as

$$u_{n+1}(x) = u_n(x) + \int_0^x \lambda(\xi) \{Lu_n(\xi) + N\tilde{u}_n(\xi)\} d\xi \tag{19}$$

λ is a general Lagrange multiplier, the subscript n is the n th approximation and \tilde{u}_n is a restricted variation $\delta\tilde{u}_n$

3. 2. Homotopy perturbation method

The comparative advantages and the provision of acceptable analytical results with convenient convergence and stability coupled with total analytic procedures of homotopy perturbation method [118-125] compel us to consider the method for solving the system of nonlinear differential equations in Eqs. (14) and (15) with the the boundary conditions in Eq. (16).

3. 2. 1. The basic idea of homotopy perturbation method

In order to establish the basic idea behind homotopy perturbation method, consider a system of nonlinear differential equations given as

$$A(U) - f(r) = 0, \quad r \in \Omega, \tag{20}$$

with the boundary conditions

$$B\left(u, \frac{\partial u}{\partial \eta}\right) = 0, \quad r \in \Gamma, \tag{21}$$

where A is a general differential operator, B is a boundary operator, $f(r)$ a known analytical function and Γ is the boundary of the domain Ω

The operator A can be divided into two parts, which are L and N , where L is a linear operator, N is a non-linear operator. Eq. (20) can be therefore rewritten as follows

$$L(u) + N(u) - f(r) = 0. \tag{22}$$

By the homotopy technique, a homotopy $U(r, p): \Omega \times [0, 1] \rightarrow R$ can be constructed, which satisfies

$$H(U, p) = (1-p)[L(U) - L(U_o)] + p[A(U) - f(r)] = 0, \quad p \in [0, 1], \tag{23}$$

or

$$H(U, p) = L(U) - L(U_o) + pL(U_o) + p[N(U) - f(r)] = 0. \tag{24}$$

In the above Eqs. (23) and (24), $p \in [0,1]$ is an embedding parameter, u_o is an initial approximation of equation of Eq. (20), which satisfies the boundary conditions.

Also, from Eqs. (23) and Eq. (24), we will have

$$H(U,0) = L(U) - L(U_o) = 0, \tag{25}$$

or

$$H(U,0) = A(U) - f(r) = 0. \tag{26}$$

The changing process of p from zero to unity is just that of $U(r,p)$ from $u_o(r)$ to $u(r)$. This is referred to homotopy in topology. Using the embedding parameter p as a small parameter, the solution of Eqs. (23) and Eq. (24) can be assumed to be written as a power series in p as given in Eq. (27)

$$U = U_o + pU_1 + p^2U_2 + \dots \tag{27}$$

It should be pointed out that of all the values of p between 0 and 1, $p=1$ produces the best result. Therefore, setting $p = 1$, results in the approximation solution of Eq. (19)

$$u = \lim_{p \rightarrow 1} U = U_o + U_1 + U_2 + \dots \tag{28}$$

The basic idea expressed above is a combination of homotopy and perturbation method. Hence, the method is called homotopy perturbation method (HPM), which has eliminated the limitations of the traditional perturbation methods. On the other hand, this technique can have full advantages of the traditional perturbation techniques. The series Eq. (28) is convergent for most cases.

4. APPLICATION OF THE VARIATIONAL HOMOTOPY PERTURBATION METHOD TO THE PRESENT PROBLEM

The variational homotopy perturbation method is a combination of variational iteration technique and the homotopy perturbation method. In order to convey its basic ideas, we consider the following general differential equation

$$Lu + Nu = g(x) \tag{29}$$

where L is a linear operator, N is a nonlinear operator and $g(x)$ is an inhomogeneous term in the differential equation.

Following VIM procedure, we have a correction functional as

$$u_{n+1}(x) = u_n(x) + \int_0^x \lambda(\xi) \{Lu_n(\xi) + Ni \dots \dots \dots \} d\xi \tag{30}$$

As pointed in the previous section, λ is a general Lagrange multiplier, the subscript n is the n th approximation and \tilde{r} is a restricted variation $\delta \tilde{r}$, Now, we apply the homotopy perturbation method

$$\sum_{n=0}^{\infty} p^{(n)} u_n(x) = u_0(x) + p \int_0^x \lambda(\xi) \left\{ \sum_{n=0}^{\infty} p^{(n)} Lu_n(\xi) + \sum_{n=0}^{\infty} p^{(n)} N\tilde{r} \dots \right\} - \int_0^x \lambda(\xi) g(\xi) d\xi \quad (31)$$

The above procedure gives the variational homotopy perturbation method which is formulated by variational iteration technique and the homotopy perturbation method. A comparison of like powers of p gives the solutions of various orders.

Now, consider Eqs. (13) and (14), the correction functional is given by

$$f_{n+1}(\eta) = f_n(\eta) + \int_0^\eta \lambda(\xi) \left\{ \left(1 + \frac{1}{\gamma} \right) \frac{d^3 f_n}{d\xi^3} - (1-\phi)^{2.5} \left[\begin{aligned} & \left[(1-\phi) + \phi \left(\frac{\rho_s}{\rho_f} \right) \right] \left(\frac{df_n}{d\xi} \right)^2 \\ & - \left[(1-\phi) + \phi \left[(\rho\beta)_s / (\rho\beta)_f \right] \right] \theta_n(\xi) \end{aligned} \right] \right. \\ \left. - Ha(\sin^2 \lambda) \frac{df_n}{d\xi} - \frac{1}{Da} \frac{df_n}{d\xi} \right\} d\xi, \quad (32)$$

$$\theta_{n+1}(\eta) = \theta_n(\eta) + \int_0^\eta \lambda(\xi) \left\{ \left(1 + \frac{4}{3} R \right) \frac{d^2 \theta_n}{d\xi^2} - 3 \left[\frac{1}{\left[(1-\phi) + \phi \left[(\rho C_p)_s / (\rho C_p)_f \right] \right]} \times \left[\frac{k_s + (m-1)k_f - (m-1)\phi(k_f - k_s)}{k_s + (m-1)k_f + \phi(k_f - k_s)} \right] \right] \right. \\ \left. Pr f_n \left(\frac{d\theta_n}{d\xi} \right) \right\} d\xi \quad (33)$$

Making the correction functional stationary, the Lagrange multipliers for Eqs. (32) and (33) can easily be identified

$$\lambda_1(\xi) = -\frac{1}{2}(\xi - \eta)^2, \quad \lambda_2(\xi) = (\xi - \eta). \quad (34)$$

Consequently,

$$f_{n+1}(\eta) = f_n(\eta) - \frac{1}{2} \int_0^\eta (\xi - \eta)^2 \left(\left(1 + \frac{1}{\gamma} \right) \frac{d^3 f_n}{d\xi^3} - (1 - \phi)^{2.5} \left\{ \begin{aligned} & \left[(1 - \phi) + \phi \left(\frac{\rho_s}{\rho_f} \right) \right] \left(\frac{df_n}{d\xi} \right)^2 \\ & - \left[(1 - \phi) + \phi \left[(\rho\beta)_s / (\rho\beta)_f \right] \right] \theta_n(\xi) \end{aligned} \right\} \right. \\ \left. - Ha(\sin^2 \lambda) \frac{df_n}{d\xi} - \frac{1}{Da} \frac{df_n}{d\xi} \right) d\xi \tag{35}$$

$$\theta_{n+1}(\eta) = \theta_n(\eta) + \int_0^\eta (\xi - \eta) \left\{ \left(1 + \frac{4}{3} R \right) \frac{d^2 \theta_n}{d\xi^2} - 3 \left[\frac{1}{\left[(1 - \phi) + \phi \left[(\rho C_p)_s / (\rho C_p)_f \right] \right]} \right] \right. \\ \left. \times \left[\frac{k_s + (m - 1)k_f - (m - 1)\phi(k_f - k_s)}{k_s + (m - 1)k_f + \phi(k_f - k_s)} \right] \right. \left. Pr f_n \left(\frac{d\theta_n}{d\xi} \right) \right\} d\xi \tag{36}$$

Now, applying the He polynomial-variational iteration method, we have

$$\sum_{n=0}^{\infty} p^{(n)} f_n(\eta) = f_0(\eta) - \frac{1}{2} p \int_0^\eta (\xi - \eta)^2 \left(\left(1 + \frac{1}{\gamma} \right) \sum_{n=0}^{\infty} p^{(n)} \frac{d^3 f_n}{d\xi^3} - (1 - \phi)^{2.5} \left\{ \begin{aligned} & \left[(1 - \phi) + \phi \left(\frac{\rho_s}{\rho_f} \right) \right] \sum_{n=0}^{\infty} p^{(n)} \left(\frac{df_n}{d\xi} \right)^2 \\ & - \left[(1 - \phi) + \phi \left[(\rho\beta)_s / (\rho\beta)_f \right] \right] \sum_{n=0}^{\infty} p^{(n)} \theta_n(\xi) \end{aligned} \right\} \right. \\ \left. - Ha(\sin^2 \lambda) \sum_{n=0}^{\infty} p^{(n)} \frac{df_n}{d\xi} - \frac{1}{Da} \sum_{n=0}^{\infty} p^{(n)} \frac{df_n}{d\xi} \right) d\xi \tag{37}$$

$$\sum_{n=0}^{\infty} p^{(n)} \theta_n(\eta) = \theta_0(\eta) + p \int_0^\eta (\xi - \eta) \left\{ \left(1 + \frac{4}{3} R \right) \sum_{n=0}^{\infty} p^{(n)} \frac{d^2 \theta_n}{d\xi^2} - 3 \left[\frac{1}{\left[(1 - \phi) + \phi \left[(\rho C_p)_s / (\rho C_p)_f \right] \right]} \right] \right. \\ \left. \times \left[\frac{k_s + (m - 1)k_f - (m - 1)\phi(k_f - k_s)}{k_s + (m - 1)k_f + \phi(k_f - k_s)} \right] \right. \left. Pr \sum_{n=0}^{\infty} p^{(n)} f_n \left(\frac{d\theta_n}{d\xi} \right) \right\} d\xi \tag{38}$$

After expansion of the above equations, we have

$$f_0 + pf_1 + p^2 f_2 + p^3 f_3 + \dots = f_0(\eta) - \frac{1}{2} p \int_0^\eta (\xi - \eta)^2 \left\{ \begin{aligned} & \left(\left(1 + \frac{1}{\gamma} \right) \left(\frac{d^3 f_0}{d\xi^3} + p \frac{d^3 f_1}{d\xi^3} + p^2 \frac{d^3 f_2}{d\xi^3} + p^3 \frac{d^3 f_3}{d\xi^3} + \dots \right) \right. \\ & - (1 - \phi)^{2.5} \left\{ \begin{aligned} & \left[(1 - \phi) + \phi \left(\frac{\rho_s}{\rho_f} \right) \right] \left(\frac{df_0}{d\xi} + p \frac{df_1}{d\xi} + p^2 \frac{df_2}{d\xi} + p^3 \frac{df_3}{d\xi} + \dots \right)^2 \\ & - \left[(1 - \phi) + \phi \left[(\rho\beta)_s / (\rho\beta)_f \right] \right] (\theta_0 + p\theta_1 + p^2\theta_2 + p^3\theta_3 + \dots) \end{aligned} \right\} \\ & - \left(Ha(\sin^2 \lambda) + \frac{1}{Da} \right) \left(\frac{df_0}{d\xi} + p \frac{df_1}{d\xi} + p^2 \frac{df_2}{d\xi} + p^3 \frac{df_3}{d\xi} + \dots \right) \end{aligned} \right\} d\xi \end{aligned} \tag{39}$$

$$\theta_0 + p\theta_1 + p^2\theta_2 + p^3\theta_3 + \dots = \theta_0(\eta) + p \int_0^\eta (\xi - \eta) \left\{ -3 \left[\begin{aligned} & \left(1 + \frac{4}{3} R \right) \left(\frac{d^2 \theta_0}{d\xi^2} + p \frac{d^2 \theta_1}{d\xi^2} + p^2 \frac{d^2 \theta_2}{d\xi^2} + p^3 \frac{d^2 \theta_3}{d\xi^2} + \dots \right) \right. \\ & \left. \left[\frac{1}{\left[(1 - \phi) + \phi \left[(\rho C_p)_s / (\rho C_p)_f \right] \right]} \right] Pr \right. \\ & \left. \times \left[\frac{k_s + (m - 1)k_f - (m - 1)\phi(k_f - k_s)}{k_s + (m - 1)k_f + \phi(k_f - k_s)} \right] \right. \\ & \left. \times \left[(f_0 + pf_1 + p^2 f_2 + p^3 f_3 + \dots) \left(\frac{d\theta_0}{d\xi} + p \frac{d\theta_1}{d\xi} + p^2 \frac{d\theta_2}{d\xi} + p^3 \frac{d\theta_3}{d\xi} + \dots \right) \right] \right] \end{aligned} \right\} d\xi \end{aligned} \tag{40}$$

Comparing the coefficient of like powers of p , we obtain

$$p^0 : f_0(\eta) = \left(\frac{\alpha_1}{2} \right) \eta^2,$$

$$p^1 : f_1(\eta) = - \left(\frac{1}{6} \right) \left[(1 - \phi) + \phi \left[(\rho\beta)_s / (\rho\beta)_f \right] \right] \eta^3 + \left(\frac{1}{24} \right) \left\{ \begin{aligned} & \left(Ha(\sin^2 \lambda) + \frac{1}{Da} \right) \alpha_1 \\ & - \left[(1 - \phi) + \phi \left[(\rho\beta)_s / (\rho\beta)_f \right] \right] \alpha_2 \end{aligned} \right\} \eta^4 \\ + \left(\frac{\alpha_1^2}{60} \right) (1 - \phi)^{2.5} \left[(1 - \phi) + \phi \left(\frac{\rho_s}{\rho_f} \right) \right] \eta^5,$$

$$p^2 : f_2(\eta) = \frac{1}{2} \left\{ \begin{aligned} & \left[\frac{1}{3} \left[\frac{1}{2} \left(1 + \frac{1}{\gamma} \right) - 1 \right] \left[(1-\phi) + \phi \left[(\rho\beta)_s / (\rho\beta)_f \right] \right] \eta^3 \right. \\ & - \frac{1}{3} \left\{ \left\{ \left(Ha(\sin^2 \lambda) + \frac{1}{Da} \right) \alpha_1 - \left[(1-\phi) + \phi \left[(\rho\beta)_s / (\rho\beta)_f \right] \right] \alpha_2 \right\} \right. \\ & \left. \left. + \frac{1}{4} \left[(1-\phi) + \phi \left[(\rho\beta)_s / (\rho\beta)_f \right] \right] \alpha_2 - \frac{1}{8} \left(Ha(\sin^2 \lambda) + \frac{1}{Da} \right) \alpha_1 \right\} \right\} \eta^4 \\ & - \frac{1}{30} \left\{ \left\{ \left(1 + \frac{1}{\gamma} \right) \left(\frac{\alpha_1^2}{30} \right) (1-\phi)^{2.5} \left[(1-\phi) + \phi \left(\frac{\rho_s}{\rho_f} \right) \right] \right\} - \alpha_1^2 (1-\phi)^{2.5} \left[(1-\phi) + \phi \left(\frac{\rho_s}{\rho_f} \right) \right] \right\} \eta^5 \\ & \left. + \frac{1}{6} \left(Ha(\sin^2 \lambda) + \frac{1}{Da} \right) \left[(1-\phi) + \phi \left[(\rho\beta)_s / (\rho\beta)_f \right] \right] \right\} \\ & \left. \left(\frac{1}{180} (1-\phi)^{2.5} \left[(1-\phi) + \phi \left(\frac{\rho_s}{\rho_f} \right) \right] \left[(1-\phi) + \phi \left[(\rho\beta)_s / (\rho\beta)_f \right] \right] \alpha_1 \right. \right. \\ & \left. \left. + \frac{1}{1440} \left(Ha(\sin^2 \lambda) + \frac{1}{Da} \right) \left\{ \left(Ha(\sin^2 \lambda) + \frac{1}{Da} \right) \alpha_1 - \left[(1-\phi) + \phi \left[(\rho\beta)_s / (\rho\beta)_f \right] \right] \alpha_2 \right\} \right. \right. \\ & \left. \left. + \frac{5\alpha_1 \alpha_2}{24} \left[(1-\phi) + \phi \left[(\rho\beta)_s / (\rho\beta)_f \right] \right] \left[\frac{1}{\left[(1-\phi) + \phi \left[(\rho C_p)_s / (\rho C_p)_f \right] \right]} \right. \right. \right. \\ & \left. \left. \left. \times \frac{k_s + (m-1)k_f - (m-1)\phi(k_f - k_s)}{k_s + (m-1)k_f + \phi(k_f - k_s)} \right] \right] \right\} Pr \eta^6 \\ & - \frac{\alpha_1 \alpha_2}{10} \left[(1-\phi) + \phi \left[(\rho\beta)_s / (\rho\beta)_f \right] \right] \left[\frac{1}{\left[(1-\phi) + \phi \left[(\rho C_p)_s / (\rho C_p)_f \right] \right]} \right. \\ & \left. \left. \times \frac{k_s + (m-1)k_f - (m-1)\phi(k_f - k_s)}{k_s + (m-1)k_f + \phi(k_f - k_s)} \right] \right] Pr \right\} \\ & \left. \left(\frac{2\alpha_1}{105} (1-\phi)^{2.5} \left[(1-\phi) + \phi \left(\frac{\rho_s}{\rho_f} \right) \right] \left\{ \left(Ha(\sin^2 \lambda) + \frac{1}{Da} \right) \alpha_1 - \left[(1-\phi) + \phi \left[(\rho\beta)_s / (\rho\beta)_f \right] \right] \alpha_2 \right\} \right. \right. \\ & \left. \left. + \frac{2}{105} \left(\frac{\alpha_1^2}{60} \right) (1-\phi)^{2.5} \left[(1-\phi) + \phi \left(\frac{\rho_s}{\rho_f} \right) \right] \left(Ha(\sin^2 \lambda) + \frac{1}{Da} \right) \right. \right. \\ & \left. \left. + \frac{3\alpha_1 \alpha_2}{35} \left[(1-\phi) + \phi \left[(\rho\beta)_s / (\rho\beta)_f \right] \right] \left[(1-\phi) + \phi \left[(\rho\beta)_s / (\rho\beta)_f \right] \right] \left[\frac{1}{\left[(1-\phi) + \phi \left[(\rho C_p)_s / (\rho C_p)_f \right] \right]} \right. \right. \right. \\ & \left. \left. \left. \times \frac{k_s + (m-1)k_f - (m-1)\phi(k_f - k_s)}{k_s + (m-1)k_f + \phi(k_f - k_s)} \right] \right] \right] Pr \right\} \eta^7 \\ & \left. + \left(\frac{\alpha_1^3}{4800} (1-\phi)^{2.5} \left[(1-\phi) + \phi \left(\frac{\rho_s}{\rho_f} \right) \right] \right) \eta^8, \right\} \end{aligned} \right.$$

In the same manner, the expressions for $f_3(\eta)$, $f_4(\eta)$, $f_5(\eta)$... were found which are too large expressions to be included in this paper.

Similarly,

$$p^0 : \theta_0(\eta) = 1 + \alpha_2 \eta,$$

$$\begin{aligned}
 p^1 : \theta_1(\eta) &= Pr \left[\frac{1}{\left[(1-\phi) + \phi \left[\frac{(\rho C_p)_s}{(\rho C_p)_f} \right] \right]} \right] \left[\left(\frac{\alpha_1 \alpha_2}{2} \right) \eta^3 + \left(\frac{\alpha_1 \alpha_2}{4} \right) \eta^4 \right], \\
 p^2 : \theta_2(\eta) &= \left(1 + \frac{4}{3} R \right) Pr \left[\frac{1}{\left[(1-\phi) + \phi \left[\frac{(\rho C_p)_s}{(\rho C_p)_f} \right] \right]} \right] \left[\frac{1}{3} \left(\frac{\alpha_1 \alpha_2}{2} \right) \eta^3 - \left(\frac{\alpha_1 \alpha_2}{4} \right) \eta^4 \right] \\
 &\quad - \left(\frac{\alpha_1 \alpha_2}{120} \right) \left[(1-\phi) + \phi \left[\frac{(\rho \beta)_s}{(\rho \beta)_f} \right] \right]^2 \eta^5 \\
 &\quad + \left(\frac{\alpha_2}{720} \left[(1-\phi) + \phi \left[\frac{(\rho \beta)_s}{(\rho \beta)_f} \right] \right] \left[\left(Ha (\sin^2 \lambda) + \frac{1}{Da} \right) \alpha_1 - \left[(1-\phi) + \phi \left[\frac{(\rho \beta)_s}{(\rho \beta)_f} \right] \right] \alpha_2 \right] \right) \\
 &\quad + \left(\frac{\alpha_1}{20} \left[(1-\phi) + \phi \left[\frac{(\rho \beta)_s}{(\rho \beta)_f} \right] \right] \left[\frac{1}{\left[(1-\phi) + \phi \left[\frac{(\rho C_p)_s}{(\rho C_p)_f} \right] \right]} \right] \left[\frac{k_s + (m-1)k_f - (m-1)\phi(k_f - k_s)}{k_s + (m-1)k_f + \phi(k_f - k_s)} \right] \left(\frac{\alpha_1 \alpha_2}{2} \right) Pr \right) \eta^6 \\
 &\quad + \left(\frac{\alpha_1}{210} \left[(1-\phi) + \phi \left[\frac{(\rho \beta)_s}{(\rho \beta)_f} \right] \right] \left[\frac{1}{\left[(1-\phi) + \phi \left[\frac{(\rho C_p)_s}{(\rho C_p)_f} \right] \right]} \right] \left[\frac{k_s + (m-1)k_f - (m-1)\phi(k_f - k_s)}{k_s + (m-1)k_f + \phi(k_f - k_s)} \right] \left(\frac{\alpha_1 \alpha_2}{4} \right) Pr \right) \eta^7, \\
 &\quad + \left(\frac{\alpha_2}{42} \left[(1-\phi) + \phi \left[\frac{(\rho \beta)_s}{(\rho \beta)_f} \right] \right] \left[\frac{\alpha_1^2}{60} \right] (1-\phi)^{2.5} \left[(1-\phi) + \phi \left(\frac{\rho_s}{\rho_f} \right) \right] \right)
 \end{aligned}$$

Also, the expressions for $\theta_3(\eta)$, $\theta_4(\eta)$, $\theta_5(\eta)$... were found which are too large expressions to be included in this paper.

From the definition, the solution could be written as

$$f(\eta) = f_0(\eta) + f_1(\eta) + f_2(\eta) + \dots,$$

$$\theta(\eta) = \theta_0(\eta) + \theta_1(\eta) + \theta_2(\eta) + \dots,$$

Therefore, the series solutions are given by

$$\begin{aligned}
 f(\eta) = & \left(\frac{\alpha_1}{2}\right)\eta^2 - \left(\frac{1}{6}\right)\left[(1-\phi) + \phi\left[\frac{(\rho\beta)_s}{(\rho\beta)_f}\right]\right]\eta^3 + \left(\frac{1}{24}\right)\left\{\left[\left(Ha(\sin^2\lambda) + \frac{1}{Da}\right)\alpha_1\right. \right. \\
 & \left. \left. - \left[(1-\phi) + \phi\left[\frac{(\rho\beta)_s}{(\rho\beta)_f}\right]\right]\alpha_2\right]\right\}\eta^4 + \left(\frac{\alpha_1^2}{60}\right)(1-\phi)^{2.5}\left[(1-\phi) + \phi\left(\frac{\rho_s}{\rho_f}\right)\right]\eta^5 \\
 & \left. + \left\{\frac{1}{3}\left[\frac{1}{2}\left(1 + \frac{1}{\gamma}\right) - 1\right]\left[(1-\phi) + \phi\left[\frac{(\rho\beta)_s}{(\rho\beta)_f}\right]\right]\eta^3 \right. \right. \\
 & \left. - \frac{1}{3}\left\{\left[\left(Ha(\sin^2\lambda) + \frac{1}{Da}\right)\alpha_1 - \left[(1-\phi) + \phi\left[\frac{(\rho\beta)_s}{(\rho\beta)_f}\right]\right]\alpha_2\right]\right\} \right. \\
 & \left. + \frac{1}{4}\left[(1-\phi) + \phi\left[\frac{(\rho\beta)_s}{(\rho\beta)_f}\right]\right]\alpha_2 - \frac{1}{8}\left(Ha(\sin^2\lambda) + \frac{1}{Da}\right)\alpha_1\right\}\eta^4 \right. \\
 & \left. - \frac{1}{30}\left\{\left[\left(1 + \frac{1}{\gamma}\right)\left(\frac{\alpha_1^2}{30}\right)(1-\phi)^{2.5}\left[(1-\phi) + \phi\left(\frac{\rho_s}{\rho_f}\right)\right]\right] - \alpha_1^2(1-\phi)^{2.5}\left[(1-\phi) + \phi\left(\frac{\rho_s}{\rho_f}\right)\right]\right\} \right. \\
 & \left. + \frac{1}{6}\left(Ha(\sin^2\lambda) + \frac{1}{Da}\right)\left[(1-\phi) + \phi\left[\frac{(\rho\beta)_s}{(\rho\beta)_f}\right]\right]\right\}\eta^5 \\
 & \left. + \left\{\frac{1}{180}(1-\phi)^{2.5}\left[(1-\phi) + \phi\left(\frac{\rho_s}{\rho_f}\right)\right]\left[(1-\phi) + \phi\left[\frac{(\rho\beta)_s}{(\rho\beta)_f}\right]\right]\alpha_1 \right. \right. \\
 & \left. + \frac{1}{1440}\left(Ha(\sin^2\lambda) + \frac{1}{Da}\right)\left\{\left[Ha(\sin^2\lambda) + \frac{1}{Da}\right]\alpha_1 - \left[(1-\phi) + \phi\left[\frac{(\rho\beta)_s}{(\rho\beta)_f}\right]\right]\alpha_2\right\} \right. \\
 & \left. + \frac{5\alpha_1\alpha_2}{24}\left[(1-\phi) + \phi\left[\frac{(\rho\beta)_s}{(\rho\beta)_f}\right]\right]\left[\frac{1}{\left[(1-\phi) + \phi\left[\frac{(\rho C_p)_s}{(\rho C_p)_f}\right]\right]}\right] \right. \\
 & \left. \times \left[\frac{k_s + (m-1)k_f - (m-1)\phi(k_f - k_s)}{k_s + (m-1)k_f + \phi(k_f - k_s)}\right]\right\}Pr\eta^6 \\
 & \left. - \frac{\alpha_1\alpha_2}{10}\left[(1-\phi) + \phi\left[\frac{(\rho\beta)_s}{(\rho\beta)_f}\right]\right]\left[\frac{1}{\left[(1-\phi) + \phi\left[\frac{(\rho C_p)_s}{(\rho C_p)_f}\right]\right]}\right] \right. \\
 & \left. \times \left[\frac{k_s + (m-1)k_f - (m-1)\phi(k_f - k_s)}{k_s + (m-1)k_f + \phi(k_f - k_s)}\right]\right\}Pr\eta^6 \\
 & \left. + \left\{\frac{2\alpha_1}{105}(1-\phi)^{2.5}\left[(1-\phi) + \phi\left(\frac{\rho_s}{\rho_f}\right)\right]\left\{\left[Ha(\sin^2\lambda) + \frac{1}{Da}\right]\alpha_1 - \left[(1-\phi) + \phi\left[\frac{(\rho\beta)_s}{(\rho\beta)_f}\right]\right]\alpha_2\right\} \right. \right. \\
 & \left. + \frac{2}{105}\left(\frac{\alpha_1^2}{60}\right)(1-\phi)^{2.5}\left[(1-\phi) + \phi\left(\frac{\rho_s}{\rho_f}\right)\right]\left(Ha(\sin^2\lambda) + \frac{1}{Da}\right) \right. \\
 & \left. + \frac{3\alpha_1\alpha_2}{35}\left[(1-\phi) + \phi\left[\frac{(\rho\beta)_s}{(\rho\beta)_f}\right]\right]\left[(1-\phi) + \phi\left[\frac{(\rho\beta)_s}{(\rho\beta)_f}\right]\right]\left[\frac{1}{\left[(1-\phi) + \phi\left[\frac{(\rho C_p)_s}{(\rho C_p)_f}\right]\right]}\right] \right. \\
 & \left. \times \left[\frac{k_s + (m-1)k_f - (m-1)\phi(k_f - k_s)}{k_s + (m-1)k_f + \phi(k_f - k_s)}\right]\right\}Pr\eta^7 \\
 & \left. + \left(\frac{\alpha_1^3}{4800}\right)(1-\phi)^{2.5}\left[(1-\phi) + \phi\left(\frac{\rho_s}{\rho_f}\right)\right]\eta^8, \right. \\
 & \left. \right\}
 \end{aligned}$$

(41)

$$\begin{aligned}
 \theta(\eta) = & 1 + \alpha_2 \eta + Pr \left[\frac{1}{\left[\frac{(1-\phi) + \phi \left[\frac{(\rho C_p)_s}{(\rho C_p)_f} \right]}{k_s + (m-1)k_f - (m-1)\phi(k_f - k_s)} \right]} \right] \left[\left(\frac{\alpha_1 \alpha_2}{2} \right) \eta^3 + \left(\frac{\alpha_1 \alpha_2}{4} \right) \eta^4 \right] \\
 & + \left(1 + \frac{4}{3} R \right) Pr \left[\frac{1}{\left[\frac{(1-\phi) + \phi \left[\frac{(\rho C_p)_s}{(\rho C_p)_f} \right]}{k_s + (m-1)k_f - (m-1)\phi(k_f - k_s)} \right]} \right] \left[\frac{1}{3} \left(\frac{\alpha_1 \alpha_2}{2} \right) \eta^3 - \left(\frac{\alpha_1 \alpha_2}{4} \right) \eta^4 \right] \\
 & - \left(\frac{\alpha_1 \alpha_2}{120} \right) \left[(1-\phi) + \phi \left[\frac{(\rho \beta)_s}{(\rho \beta)_f} \right] \right]^2 \eta^5 \\
 & + \left(\frac{\alpha_2}{720} \left[(1-\phi) + \phi \left[\frac{(\rho \beta)_s}{(\rho \beta)_f} \right] \right] \left[\left(Ha(\sin^2 \lambda) + \frac{1}{Da} \right) \alpha_1 - \left[(1-\phi) + \phi \left[\frac{(\rho \beta)_s}{(\rho \beta)_f} \right] \right] \alpha_2 \right] \right. \\
 & \left. + \frac{\alpha_1}{20} \left[(1-\phi) + \phi \left[\frac{(\rho \beta)_s}{(\rho \beta)_f} \right] \right] \left[\frac{1}{\left[\frac{(1-\phi) + \phi \left[\frac{(\rho C_p)_s}{(\rho C_p)_f} \right]}{k_s + (m-1)k_f - (m-1)\phi(k_f - k_s)} \right]} \right] \left(\frac{\alpha_1 \alpha_2}{2} \right) Pr \right] \eta^6 \\
 & + \left(\frac{\alpha_1}{210} \left[(1-\phi) + \phi \left[\frac{(\rho \beta)_s}{(\rho \beta)_f} \right] \right] \left[\frac{1}{\left[\frac{(1-\phi) + \phi \left[\frac{(\rho C_p)_s}{(\rho C_p)_f} \right]}{k_s + (m-1)k_f - (m-1)\phi(k_f - k_s)} \right]} \right] \left(\frac{\alpha_1 \alpha_2}{4} \right) Pr \right. \\
 & \left. + \frac{\alpha_2}{42} \left[(1-\phi) + \phi \left[\frac{(\rho \beta)_s}{(\rho \beta)_f} \right] \right] \left(\frac{\alpha_1^2}{60} \right) (1-\phi)^{2.5} \left[(1-\phi) + \phi \left(\frac{\rho_s}{\rho_f} \right) \right] \right) \eta^7,
 \end{aligned}
 \tag{42}$$

While for viscous fluid where the volume fraction of the nanoparticle, thermal radiation and magnetic parameters are set to zero i.e. $\phi=R=Ha=0$ and $Da \rightarrow \infty$ and $\gamma \rightarrow \infty$.

$$p^0 : f_0(\eta) = \left(\frac{\alpha_1}{2} \right) \eta^2,$$

$$p^1 : f_1(\eta) = -\left(\frac{1}{6} \right) \eta^3 - \left(\frac{\alpha_2}{24} \right) \eta^4 + \left(\frac{\alpha_1^2}{60} \right) \eta^5,$$

$$p^2 : f_2(\eta) = -\left(\frac{\alpha_1 Pr}{240} + \frac{\alpha_1}{120} \right) \eta^6 + \left(\frac{\alpha_1 \alpha_2}{630} + \frac{\alpha_1 \alpha_2 Pr}{120} \right) \eta^7 + \left(\frac{\alpha_1^3}{2016} \right) \eta^8,$$

$$p^3 : f_2(\eta) = \left(\frac{\alpha_1 \alpha_2}{630} + \frac{\alpha_1 \alpha_2 Pr}{120} + \frac{\sigma}{1680} + \frac{1}{840} \right) \eta^7 + \left(\frac{\alpha_1^3}{2016} + \frac{\alpha_2 Pr}{3360} + \frac{\alpha_2}{2016} \right) \eta^8$$

$$+ \left(-\frac{\alpha_1^2 Pr^2}{10080} + \frac{\alpha_1^2 Pr}{8640} + \frac{\alpha_2^2 Pr}{130240} - \frac{11\alpha_1^2}{30240} + \frac{\alpha_2^2}{18144} \right) \eta^9 + \left(-\frac{\alpha_1^2 \alpha_2}{14400} - \frac{\alpha_1^2 \alpha_2 Pr}{604800} - \frac{\alpha_1^2 Pr^2 \alpha_2}{40320} \right) \eta^{10},$$

and

$$p^0 : \theta_0(\eta) = 1 + \alpha_2 \eta,$$

$$p^1 : \theta_1(\eta) = \left(\frac{\alpha_1 \alpha_2 Pr}{2} \right) \eta^3 + \left(\frac{\alpha_1 \alpha_2 Pr}{4} \right) \eta^4,$$

$$p^2 : \theta_2(\eta) = -\left(\frac{\alpha_1 \alpha_2}{10} \right) \eta^5 + \left(\frac{\alpha_1^2 Pr^2}{20} + \frac{\alpha_1^2 Pr}{120} - \frac{\alpha_2^2 Pr}{60} \right) \eta^6 + \left(\frac{\alpha_1^2 \alpha_2 Pr}{168} + \frac{\alpha_1^2 \alpha_2 Pr}{56} \right) \eta^7,$$

$$p^3 : \theta_3(\eta) = \left(-\frac{\alpha_1 Pr}{280} + \frac{\alpha_1 Pr^2}{35} \right) \eta^7 + \left(-\frac{11\alpha_1 \alpha_2 Pr}{3360} + \frac{41\alpha_1 \alpha_2 Pr^2}{2240} \right) \eta^8$$

$$+ \left(\frac{\alpha_1^2 \alpha_2^2 Pr^2}{360} + \frac{\alpha_1^2 Pr}{6048} + \frac{\alpha_1^3 Pr^3}{480} - \frac{\alpha_1 \alpha_2^2 Pr}{2160} \right) \eta^9$$

$$+ \left(\frac{\alpha_1^3 \alpha_2^3 Pr}{7560} + \frac{\alpha_1^2 \alpha_2 Pr^2}{1120} + \frac{\alpha_2 \alpha_1^3 Pr^3}{1680} \right) \eta^{10},$$

So, for the case when $\phi = R = Ha = 0$ and $Da \rightarrow \infty$ and $\gamma \rightarrow \infty$, the series solution is given by

$$f(\eta) = \left(\frac{\alpha_1}{2} \right) \eta^2 - \left(\frac{1}{6} \right) \eta^3 + \left(\frac{\alpha_2}{24} \right) \eta^4 + \left(\frac{\alpha_1^2}{60} \right) \eta^5 - \left(\frac{\alpha_1 Pr}{240} + \frac{\alpha_1}{120} \right) \eta^6 + \left(\frac{\alpha_1 \alpha_2}{630} + \frac{\alpha_1 \alpha_2 Pr}{120} + \frac{\sigma}{1680} + \frac{1}{840} \right) \eta^7$$

$$+ \left(\frac{\alpha_1^3}{2016} + \frac{\alpha_2 Pr}{3360} + \frac{\alpha_2}{2016} \right) \eta^8 + \left(-\frac{\alpha_1^2 Pr^2}{10080} + \frac{\alpha_1^2 Pr}{8640} + \frac{\alpha_2^2 Pr}{130240} - \frac{11\alpha_1^2}{30240} + \frac{\alpha_2^2}{18144} \right) \eta^9 + \quad (43)$$

$$\left(-\frac{\alpha_1^2 \alpha_2}{14400} - \frac{\alpha_1^2 \alpha_2 Pr}{604800} - \frac{\alpha_1^2 Pr^2 \alpha_2}{40320} \right) \eta^{10} + \dots$$

$$\theta(\eta) = 1 + \alpha_2 \eta^2 + \left(\frac{\alpha_1 \alpha_2 Pr}{2} \right) \eta^3 + \left(\frac{\alpha_1 \alpha_2 Pr}{4} \right) \eta^4 - \left(\frac{\alpha_1 \alpha_2}{10} \right) \eta^5 + \left(\frac{\alpha_1^2 Pr^2}{20} + \frac{\alpha_1^2 Pr}{120} - \frac{\alpha_2^2 Pr}{60} \right) \eta^6$$

$$+ \left(\frac{\alpha_1^2 \alpha_2 Pr}{168} + \frac{\alpha_1^2 Pr^2 \alpha_2}{56} - \frac{\alpha_1 Pr}{280} + \frac{\alpha_1 Pr^2}{35} \right) \eta^7 + \left(-\frac{11\alpha_1 \alpha_2 Pr}{3360} + \frac{41\alpha_1 \alpha_2 Pr^2}{2240} \right) \eta^8 + \quad (44)$$

$$\left(\frac{\alpha_1^2 \alpha_2^2 Pr^2}{360} + \frac{\alpha_1^2 Pr}{6048} + \frac{\alpha_1^3 Pr^3}{480} - \frac{\alpha_1 \alpha_2^2 Pr}{2160} \right) \eta^9 + \left(\frac{\alpha_1^3 \alpha_2^3 Pr}{7560} + \frac{\alpha_1^2 \alpha_2 Pr^2}{1120} + \frac{\alpha_2 \alpha_1^3 Pr^3}{1680} \right) \eta^{10} + \dots$$

5. THE BASIC CONCEPT AND THE PROCEDURE OF PADÉ APPROXIMANT

The limitation of power series methods to a small domain have been overcome by after-treatment techniques. These techniques increase the radius of convergence and also, accelerate the rate of convergence of a given series. Among the so-called after treatment techniques, Padé approximant technique has been widely applied in developing accurate analytical solutions to nonlinear problems of large or unbounded domain problems of infinite boundary conditions [73]. The Padé-approximant technique manipulates a polynomial approximation into a rational function of polynomials. Such a manipulation gives more information about the mathematical behaviour of the solution. The basic procedures are as follows.

Suppose that a function $f(\eta)$ is represented by a power series.

$$f(\eta) = \sum_{i=0}^{\infty} c_i \eta^i \tag{45}$$

This expression is the fundamental point of any analysis using Padé approximant. The notation $c_i, i = 0, 1, 2, \dots$ is reserved for the given set of coefficient and $f(\eta)$ is the associated function. $[L/M]$ Padé approximant is a rational function defined as

$$f(\eta) = \frac{\sum_{i=0}^L a_i \eta^i}{\sum_{i=0}^M b_i \eta^i} = \frac{a_0 + a_1 \eta + a_2 \eta^2 + \dots + a_L \eta^L}{b_0 + b_1 \eta + b_2 \eta^2 + \dots + b_M \eta^M} \tag{46}$$

which has a Maclaurin expansion, agrees with Eq. (45) as far as possible. It is noticed that in Eq. (46), there are $L+1$ numerator and $M+1$ denominator coefficients. So, there are $L+1$ independent number of numerator coefficients, making $L+M+1$ unknown coefficients in all. This number suggest that normally (L/M) out of fit the power series Eq. (45) through the orders $1, \eta, \eta^2, \dots, \eta^{L+M}$

In the notation of formal power series

$$\sum_{i=0}^{\infty} c_i \eta^i = \frac{a_0 + a_1 \eta + a_2 \eta^2 + \dots + a_L \eta^L}{b_0 + b_1 \eta + b_2 \eta^2 + \dots + b_M \eta^M} + O(\eta^{L+M+1}) \tag{47}$$

which gives

$$(b_0 + b_1 \eta + b_2 \eta^2 + \dots + b_M \eta^M)(c_0 + c_1 \eta + c_2 \eta^2 + \dots) = a_0 + a_1 \eta + a_2 \eta^2 + \dots + a_L \eta^L + O(\eta^{L+M+1}) \tag{48}$$

Expanding the LHS and equating the coefficients of $\eta^{L+1}, \eta^{L+2}, \dots, \eta^{L+M}$ we get

$$b_M c_{L-M+1} + b_{M-1} c_{L-M+2} + b_{M-2} c_{L-M+3} + \dots + b_2 c_{L-1} + b_1 c_L + b_0 c_{L+1} = 0$$

$$b_M c_{L-M+2} + b_{M-1} c_{L-M+3} + b_{M-2} c_{L-M+4} + \dots + b_2 c_L + b_1 c_{L+1} + b_0 c_{L+2} = 0$$

$$b_M c_{L-M+3} + b_{M-1} c_{L-M+4} + b_{M-2} c_{L-M+5} + \dots + b_2 c_{L+1} + b_1 c_{L+2} + b_0 c_{L+3} = 0$$

.....

$$b_M c_L + b_{M-1} c_{L+1} + b_{M-2} c_{L+2} + \dots + b_2 c_{L+M-2} + b_1 c_{L+M-1} + b_0 c_{L+M} = 0 \tag{49}$$

If $i < 0, c_i = 0$ for consistency. Since $b_0 = 1$, Eqn. (49) becomes a set of M linear equations for M unknown denominator coefficients

$$\begin{pmatrix} c_{L-M+1} & c_{L-M+2} & c_{L-M+3} & \dots & - \\ c_{L-M+2} & c_{L-M+3} & c_{L-M+4} & \dots & - \\ c_{L-M+3} & c_{L-M+4} & c_{L-M+4} & \dots & - \\ \vdots & \vdots & \vdots & \vdots & \vdots \\ c_L & c_{L+1} & c_{L+2} & \dots & - \dots 1 \end{pmatrix} \begin{pmatrix} b_M \\ b_{M-1} \\ b_{M-2} \\ \vdots \\ b_1 \end{pmatrix} = - \begin{pmatrix} c_{L+1} \\ c_{L+2} \\ c_{L+3} \\ \vdots \\ c_{L+M} \end{pmatrix} \tag{50}$$

From the above Eq. (50), b_i may be found. The numerator coefficient $a_0, a_1, a_2, \dots, a_L$ follow immediately from Eq. (51) by equating the coefficient of $1, \eta, \eta^2, \dots, \eta^{L+M}$ such that

$$\begin{aligned} a_0 &= c_0 \\ a_1 &= c_1 + b_1 c_0 \\ a_2 &= c_2 + b_1 c_1 + b_2 c_0 \\ a_3 &= c_3 + b_1 c_2 + b_2 c_1 + b_3 c_0 \\ a_4 &= c_4 + b_1 c_3 + b_2 c_2 + b_3 c_1 + b_4 c_0 \\ a_5 &= c_5 + b_1 c_4 + b_2 c_3 + b_3 c_2 + b_4 c_1 + b_5 c_0 \\ a_6 &= c_6 + b_1 c_5 + b_2 c_4 + b_3 c_3 + b_4 c_2 + b_5 c_1 + b_6 c_0 \\ &\vdots \\ a_L &= c_L + \sum_{i=1}^{\min[L/M]} b_i c_{L-i} \end{aligned} \tag{51}$$

The Eq. (51) and Eq. (52) normally determine the Pade numerator and denominator and are called Padé equations. The $[L/M]$ Pade approximant is constructed which agrees with the

equation in the power series through the order η^{L+M} . To obtain a diagonal Padé approximant of order [L/M], the symbolic calculus software Maple is used.

It should be noted as mentioned previously that Δ and Ω in the solutions are unknown constants. In order to compute their values for extended large domains solutions, the power series as presented in Eqs. (41) and (41) are converted to rational functions using [10/10] Pade approximation through the software Maple and then, the infinite boundary conditions i.e. $\eta \rightarrow \infty, f' = 0, \theta = 0$ are applied. The resulting simultaneous equations are solved to obtain the values of Δ and Ω for the respective values of the physical and thermal properties of the nanofluids under considerations.

6. FLOW AND HEAT TRANSFER PARAMETERS

In addition to the determination of the velocity and temperature distributions, it is often desirable to compute other physically important quantities (such as shear stress, drag, heat transfer rate and heat transfer coefficient) associated with the free convection flow and heat transfer problem. Consequently, two parameters, a flow parameter and a heat transfer parameter, are computed.

6. 1. Fluid flow parameter

Skin friction coefficient

$$c_f = \frac{\tau_w}{\rho_{nf} u^2} = \frac{\mu_{nf} \left. \frac{\partial u}{\partial y} \right|_{y=0}}{\rho_{nf} u^2} = \frac{\mu_{nf} \left(\frac{\partial u}{\partial \eta} \cdot \frac{\partial \eta}{\partial y} \right) \Big|_{y=0}}{\rho_{nf} u^2} \tag{52}$$

After the dimensionless exercise,

$$c_f (Re_x)^{1/2} = \frac{f''(0)}{(1-\phi)^{2.5}}$$

$$c_f (Re_x)^{1/2} \frac{\tau_w}{(4Gr_x^3)^{1/4} (\nu\mu)} = f''(0) \frac{f''(0)}{(1-\phi)^{2.5}}$$

6. 2. Heat transfer parameter

Heat transfer coefficient

$$h_x = -\frac{k_{nf}}{T_w - T_\infty} \left(\frac{\partial T}{\partial y} \right)_{y=0} = -k_{nf} \theta'(0) \frac{1}{x} \left(\frac{1}{4} Gr_x \right)^{1/4} \tag{53}$$

The local Nusselt number is

$$Nu_x = \frac{h_x x}{k_{nf}} = - \left(\frac{x}{T_w - T_\infty} \right) \left(\frac{\partial T}{\partial y} \right)_{y=0} = -\theta'(0) \left(\frac{1}{4} Gr_x \right)^{1/4} \tag{54}$$

$$Nu_x = - \frac{\theta'(0)}{\sqrt{2}} Gr_x^{1/4} = f((Pr) Gr_x^{1/4})$$

where $\phi(Pr) = -\frac{\theta'(0)}{\sqrt{2}}$ is a function of Prandtl number. The dependence of ϕ on the Prandtl number is evidenced by Eq. (54). It could also be shown that

$$\frac{Nu_x}{(Re_x)^{1/2}} = - \frac{k_{nf}}{k_f} \theta'(0) = - \left[\frac{k_s + (m-1)k_f - (m-1)\phi(k_f - k_s)}{k_s + (m-1)k_f + \phi(k_f - k_s)} \right] \theta'(0) \tag{55}$$

where Re_x and Gr_x are the local Reynold and Grashof numbers defined as:

$$Re_x = \frac{ux}{\nu_{nf}} \quad \text{and} \quad Gr_x = \frac{g\beta(T_w - T_\infty)x^3}{\nu^3}$$

7. RESULTS AND DISCUSSION

Table 4-6 presents the values of the unknown parameters $\alpha_1 = f''(0)$ and $\alpha_2 = \theta'(0)$ for different values of the models controlling parameters. Using the converged values of the unknown parameters, the solutions of DTM with [10/10] Padé approximation is presented in this section.

Table 4. Numerical values for $\alpha_1 = f''(0)$ at $\phi=0, Ha=R=0, Da \rightarrow \infty$ and $\gamma \rightarrow \infty$

<i>Pr</i>	[4,4]	[5,5]	[6,6]	α_1
0.001	1.1155529418	1.1272760416	1.1252849854	1.1231381347
0.01	1.0631737963	1.0741895683	1.0638385351	1.0633808585
0.1	0.9128082210	0.9238226280	0.9242158493	0.9240830397
1	0.6941230861	0.6929598014	0.6932195158	0.6932116298
10	0.4511240728	0.4502429544	0.4476712316	0.4471165250
100	0.2679197151	0.2681474363	0.2641295627	0.2645235434
1000	0.2204061432	0.1524783266	0.1500456755	0.1512901971
10000	0.0858587180	0.0858519249	0.0844775473	0.0855408524

Table 5. Numerical values for $\alpha_2 = \theta'(0)$ at $\phi=0, Ha=R=0, Da \rightarrow \infty$ and $\gamma \rightarrow \infty$

Pr	[4,4]	[5,5]	[6,6]	α_2
0.001	-0.0371141028	-0.0415417739	-0.0436188230	-0.0468074648
0.01	-0.1274922800	-0.1221616907	-0.1351353865	-0.1357607439
0.1	-0.3621215470	-0.3505589981	-0.3499273453	-0.3500596733
1	-0.7694165843	-0.7695971295	-0.7698955992	-0.7698611967
10	-1.5028543431	-1.5007437650	-1.4985484075	-1.4970992078
100	-2.7627624234	-2.7637067330	-2.7445541894	-2.7468855016
1000	-5.7787858408	-4.9468469883	-4.9104728566	-4.9349476252
10000	-8.8057265644	-8.8032691004	-8.7384279086	-8.8044492660

Table 6. Converged numerical values for $\alpha_1 = f''(0)$ and $\alpha_2 = \theta'(0)$ at $\phi = 0, Ha = R = 0, Da \rightarrow \infty$ and $\gamma \rightarrow \infty$

Pr	$\alpha_1 = f''(0)$	$\alpha_2 = \theta'(0)$
0.001	1.1231381347	-0.0468074648
0.01	1.0633808585	-0.1357607439
0.1	0.9240830397	-0.3500596733
1	0.6932116298	-0.7698611967
10	0.4471165250	-1.4970992078
100	0.2645235434	-2.7468855016
1000	0.1512901971	-4.9349476252
10000	0.0855408524	-8.8044492660

Table 7. Comparison of results for Comparison of results of $f''(\eta)$ and $\theta'(\eta)$ at different Prandtl numbers.

Pr	Kuo [51]		Na and Hibb [12]		Present study	
	$f''(0)$	$\theta'(0)$	$f''(0)$	$\theta'(0)$	$f''(0)$	$\theta'(0)$
0.72	0.6760	-0.5046	0.6760	-0.5046	0.6760	-0.5046
0.60	0.6947	-0.4721	0.6946	-0.4725	0.6947	-0.4721
0.50	0.7132	-0.4411	0.7131	-0.4420	0.7132	-0.4411

0.40	0.7356	-0.4053	0.7354	-0.4066	0.7356	-0.4053
0.30	0.7636	-0.3623	0.7633	-0.3641	0.7636	-0.3623
0.20	0.8015	-0.3078	0.8009	-0.3101	0.8015	-0.3078
0.10	0.8600	-0.2298	0.8590	-0.2326	0.8600	-0.2298
0.06	0.8974	-0.1834	0.8961	-0.1864	0.8974	-0.1834
0.04	0.9233	-0.1526	0.9221	-0.1556	0.9233	-0.1526
0.01	0.9845	-0.0832	0.9887	-0.0817	0.9885	-0.0832
1.00	0.6421	-0.5671	0.6421	-0.5671	0.6421	-0.5671
1.10	0.6323	-0.5862	0.6323	-0.5860	0.6323	-0.5862
1.20	0.6233	-0.6040	0.6234	-0.6036	0.6233	-0.6040
1.30	0.6151	-0.6208	0.6152	-0.6202	0.6151	-0.6208
1.40	0.6075	-0.6365	0.6076	-0.6358	0.6075	-0.6365
1.50	0.6005	-0.6515	0.6006	-0.6506	0.6005	-0.6515
1.60	0.5939	-0.6656	0.5940	-0.6646	0.5939	-0.6656
1.70	0.5877	-0.6792	0.5879	-0.6780	0.5877	-0.6792
1.80	0.5819	-0.6921	0.5821	-0.6908	0.5819	-0.6921
1.90	0.5764	-0.7045	0.5767	-0.7031	0.5764	-0.7045
2.00	0.5712	-0.7164	0.5715	-0.7149	0.5712	-0.7164
2.00	0.5712	-0.7164	0.5713	-0.7165	0.5712	-0.7164
3.00	0.5308	-0.8154	0.5312	-0.8145	0.5308	-0.8154
4.00	0.5029	-0.8914	0.5036	-0.8898	0.5029	-0.8914
5.00	0.4817	-0.9539	0.4827	-0.9517	0.4817	-0.9539
6.00	0.4648	-1.0073	0.4660	-1.0047	0.4648	-1.0073
7.00	0.4507	-1.0542	0.4522	-1.0512	0.4507	-1.0542
8.00	0.4387	-1.0961	0.4405	-1.0930	0.4387	-1.0961
9.00	0.4283	-1.1342	0.4304	-1.1309	0.4283	-1.1342
10.00	0.4191	-1.1692	0.4215	-1.1658	0.4191	-1.1692

Table 8. Comparison of results for Comparison of results of $f''(\eta)$ at different Prandtl number.

Pr	$f''(0)$		
	Kuiken [73]	Mosta [17]	Present study
0.001	1.12313813	1.12313813	1.12313813
0.01	1.06338086	1.06338086	1.06338086
0.1	0.92408304	0.92408304	0.92408304
1	0.69321163	0.69321163	0.69321163
10	0.44711652	0.44711652	0.44711652
100	0.26452354	0.26452354	0.26452354
1000	0.15129020	0.15129020	0.15129020
10000	0.08554085	0.08554085	0.08554085

Table 9. Comparison of results for Comparison of results of $f''(\eta)$ at different Prandtl number.

Pr	$-\theta'(0)$			
	Kuiken [73]	Mosta et al. [17]	Mosta et al. [17]	Present study
0.001	0.04680746	0.04680746	0.04680746	0.04680746
0.01	0.13576074	0.13576074	0.13576074	0.13576074
0.1	0.35005967	0.35005967	0.35005967	0.35005967
1	0.76986120	0.76986120	0.76986119	0.76986120
10	1.49709921	1.49709921	1.49709921	1.49709921
100	2.74688550	2.74688550	2.74688549	2.74688550
1000	4.93494763	4.93494763	4.93494756	4.93494763
10000	8.80444927	8.80444927	8.80444960	8.80444960

Tables 7-9 present various comparisons of results of the present study and the past works for viscous fluid i.e. when the volume fraction of the nanoparticle, thermal radiation and magnetic parameters are set to zero i.e. $\phi = R = Ha = 0$ and $Da \rightarrow \infty$ and $\gamma \rightarrow \infty$. It could be seen from the Tables that there are excellent agreements between the past results and the present study. Moreover, the Tables present the effects of Prandtl number on the flow and heat transfer processes.

Although, the nonlinear partial differential equations in Mosta et al. [17] are the same in all aspects to the present problems under investigation, there are slight differences between the transformed nonlinear ordinary differential equations in Mosta et al. [17] of Eq. (7) and developed Eq. (16) and (17) to this present study (where the volume-fraction of the nanoparticle, radiation and Casson parameters are set to zero) due to the differences in the adopted similarity variables. It is shown that using the VHPM-Padé approximant as applied in this work to the transformed nonlinear ordinary differential equations in Mosta et al. [17], excellent agreements are recorded between the results of the present study and that of Mosta et al. [17] and Kuiken [73] as shown in Tables 8 and 9.

The variations of nanoparticle volume fraction with dynamic viscosity and thermal conductivity ratios of Copper (II) Oxide-water nanofluid are shown in Fig 2 and 3, respectively. Also, Fig. 3 show the effects of nanoparticle shape on thermal conductivity ratio. It is depicted in the figure that the thermal conductivity of nanofluid varies linearly and increases with increase in nanoparticle volume fraction.

It is also observed that the suspensions of particles with high shape factor or low sphericity have higher thermal conductivity ratio of the nanofluid. With spherical shape nanoparticle have the lowest thermal conductivity ratio and lamina shape nanoparticle have the highest thermal conductivity ratio.

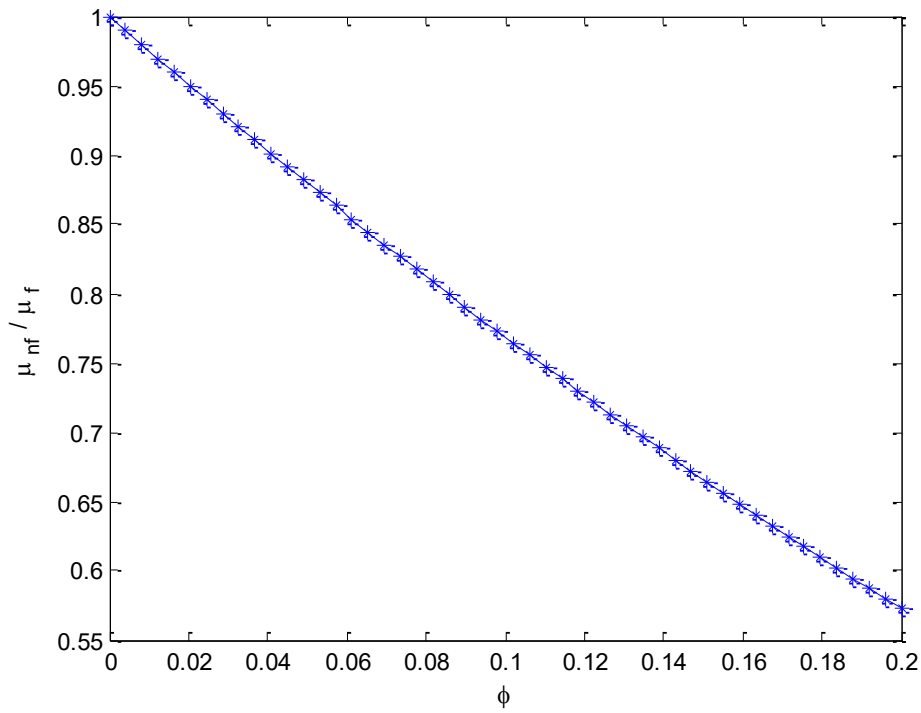


Fig. 2. Variation of nanofluid dynamic viscosity ratio with nanoparticle volume fraction

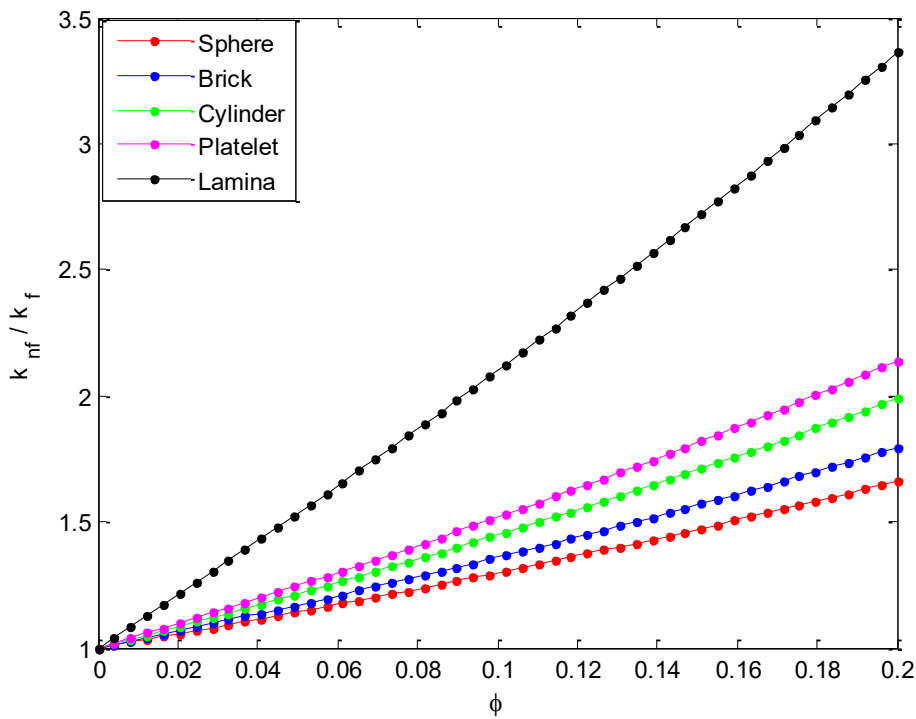


Fig. 3. Effects of nanoparticle shape on thermal conductivity ratio of nanofluid

The effects of the flow and heat transfer controlling parameters on the velocity and temperature distributions are shown in Figs. 4–17 for different shapes, type and volume-fraction of nanoparticles at Prandtl number of 0.01-1000.

7. 1. Effect of magnetic field inclination on the Casson nanofluid velocity and temperature distributions

Effect of inclination angle of the magnetic field on velocity profiles is shown in Fig. 4. It is evident that increasing in inclination angle of the magnetic field causes the decrease of fluid flow velocity. Also, it is established that the momentum boundary layer is thickened for the increasing values of the inclination angle of the magnetic field. As it is seen from Fig. 4, the magnetic field effect is minimum when the angle of inclination of the magnetic field, $\lambda = 0$ and it is maximum when $\lambda = \pi/2$. Going back to Eq. (2), it could be seen that the angle of inclination, λ appears in the magnetic field term (as $\sin \lambda$) of the momentum equation. Therefore, the flow velocity of the fluid attains minimum value when the plate inclination, $\lambda = 0$ and the fluid velocity reaches maximum value when the plate inclination, $\lambda = \pi/2$. Rising the inclined angle strengthens the applied magnetic field, this leads to increase the drag or Lorentz force. We conclude that decrease in inclination angle of the magnetic field, reduces the magnetic field effect. And when $\lambda = \pi/2$, the inclined magnetic field acts like transverse magnetic field. It is observed that decrease in inclination angle shows slight increase in temperature profiles.

Therefore, it could be extended that increasing magnetic field inclination parameter tends to decrease the fluid velocity and increase fluid temperature within the boundary layer, consequently, the skin friction factor in terms of shear stress and heat transfer rate in terms of Nusselt number are decreased.

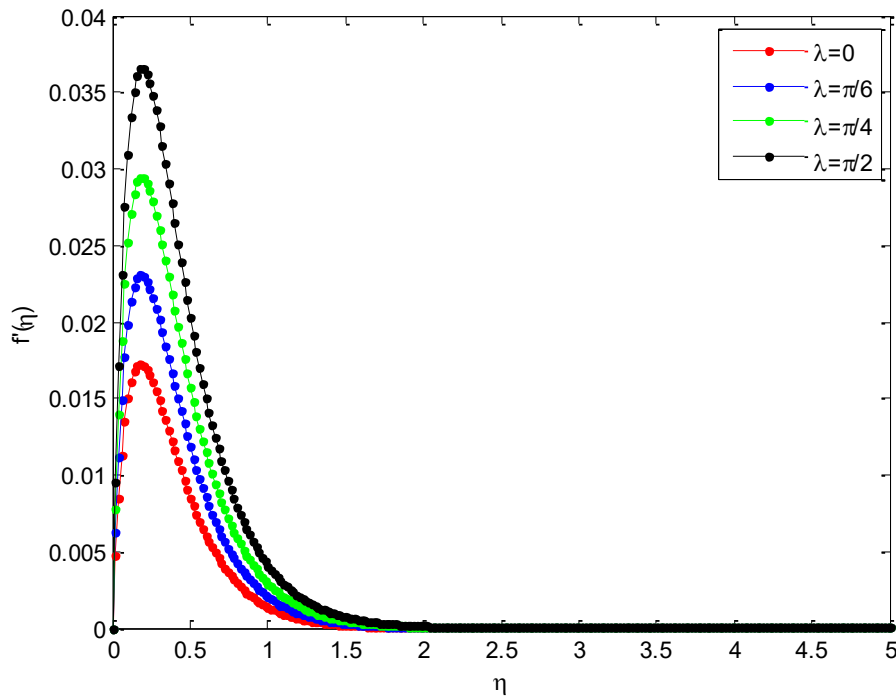


Fig. 4a. Effects of inclination angle on the velocity profile

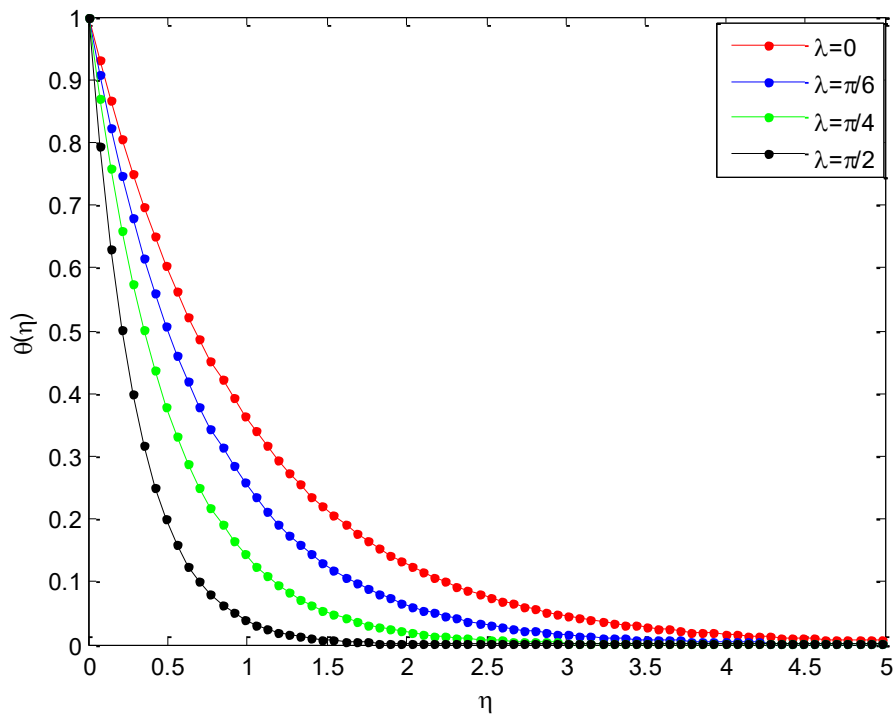


Fig. 4b. Effects of inclination angle on temperature profile

7. 2. Effect of magnetic field on Casson nanofluid velocity and temperature distributions

The influence of magnetic parameter on the flow velocity and the temperature of the fluid are shown in Figures 5a and 5b, respectively. It is inferred from the figures that the velocity of the fluid and the temperature gradient of the flow decrease as the magnetic field increases. As magnetic parameter increases, the velocity distribution decreases due to the Lorentz force as a result of the presence of magnetic field which slows fluid motion at boundary layer on the plates. Also, it is established that the momentum boundary layer is thickened for the increasing values of the magnetic term. Increasing magnetic field parameter tends to decrease the fluid velocity and increase fluid temperature within the boundary layer, consequently, the skin friction factor in terms of shear stress and heat transfer rate in terms of Nusselt number are decreased. The skin friction and heat transfer factor are reduced with increasing of magnetic field parameter. The physics behind it's that the applied magnetic force works against the fluid flow and also reduces the temperature difference between the plate and ambient fluid. It is clear that the temperature profiles increase with the increasing values of magnetic field parameter. This is because, interaction of magnetic field with flowing fluid particles produces heat in the fluid region and creates a hot fluid layer within the boundary layer. It should be noted that the velocity profiles increase with decrease of magnetic field M , at lower values of the magnetic field parameter, velocity profiles attain its maximum values near the plate. And at higher values of the magnetic field parameter, velocity decreases rapidly to the minimum values. This is due to the fact that the application of magnetic field to an electrically conducting fluid gives rise to a resistive force called Lorentz force which retards the flow of fluid.

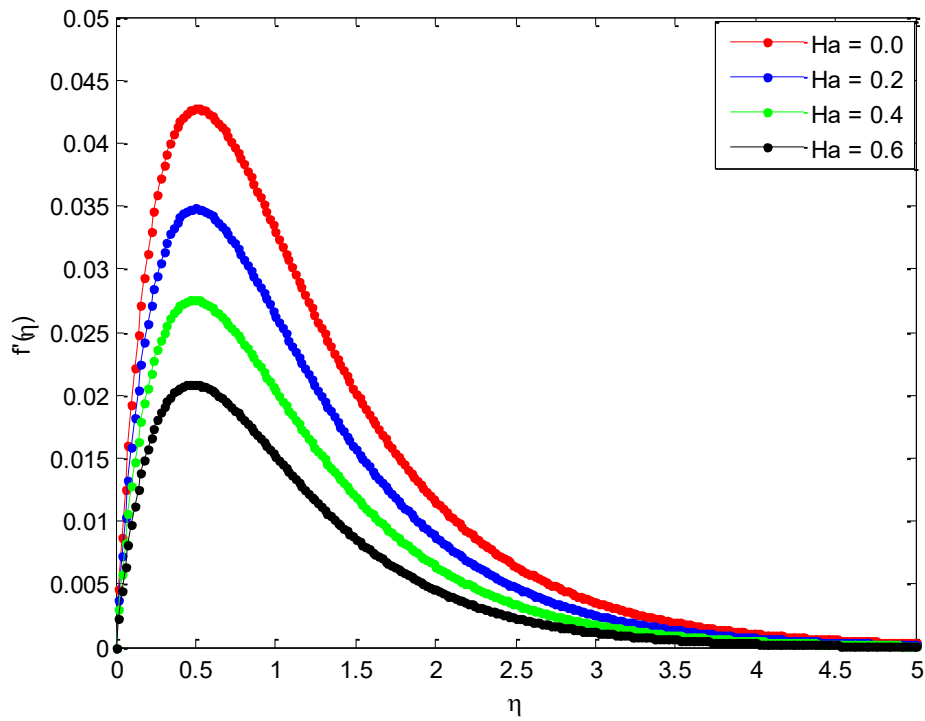


Fig. 5a. Effects of magnetic field on the velocity profile

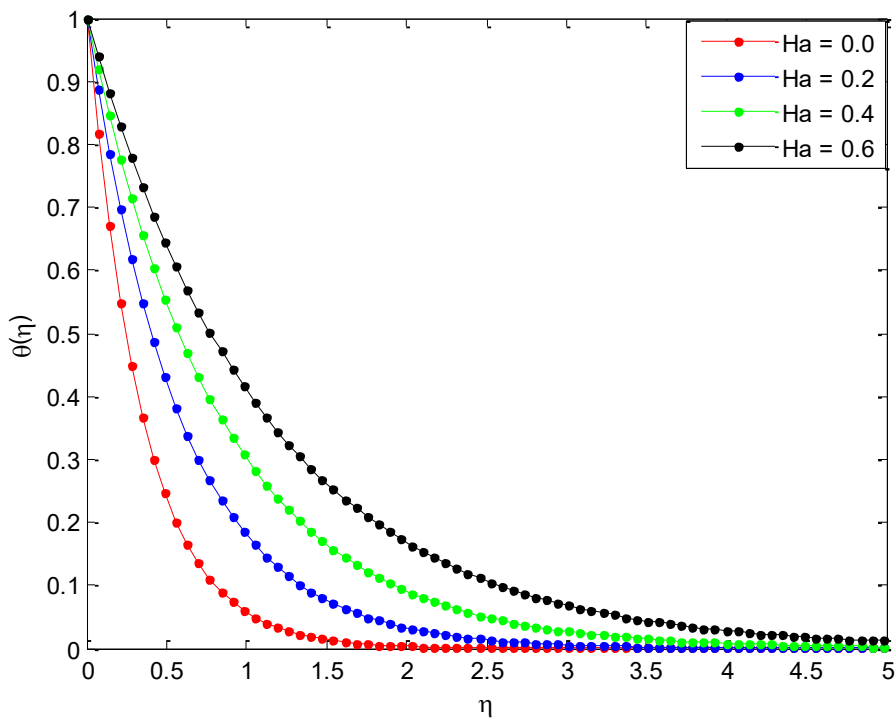


Fig. 5b. Effects of magnetic field on temperature profile

7. 3. Effect of flow medium porosity on Casson nanofluid velocity and temperature distributions

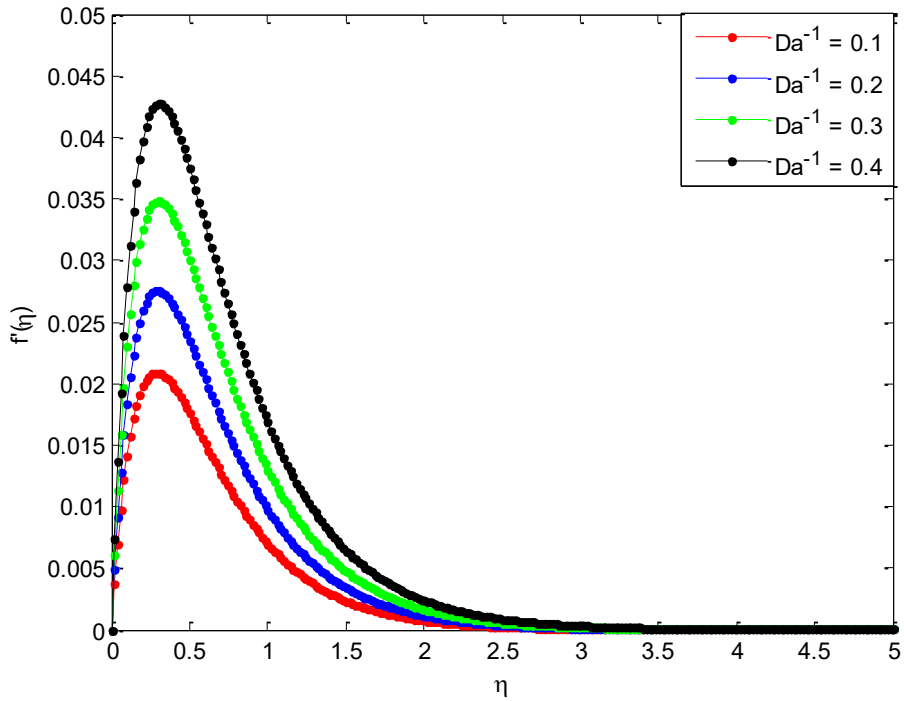


Fig. 6a. Effects of flow medium porosity on the velocity profile

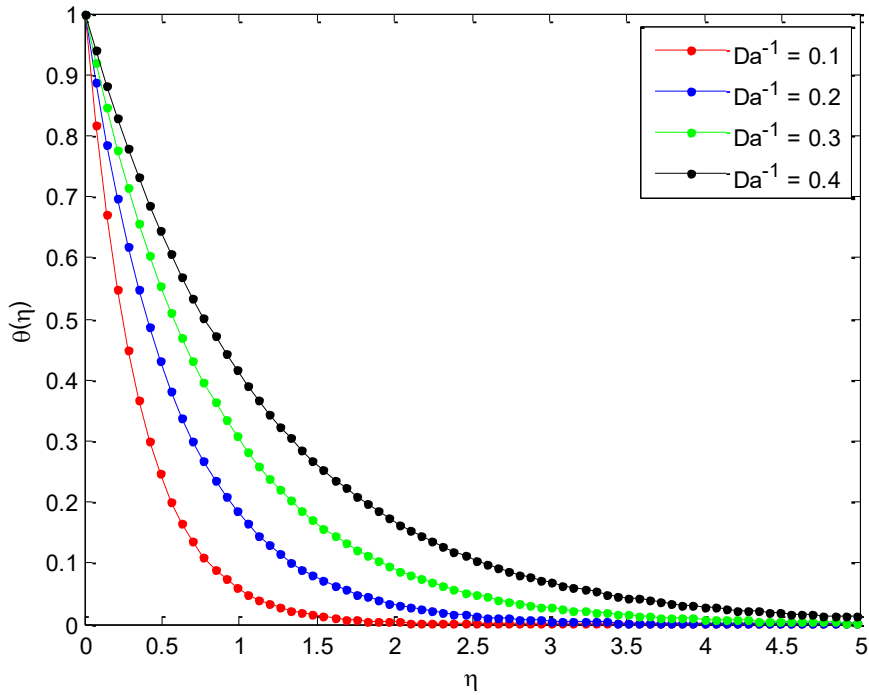


Fig. 6b. Effects of flow medium porosity on temperature profile

Fig. 6 depict the effects of Darcy number on the flow velocity and temperature distributions which by extension shows the influence of flow medium porosity on the flow velocity and temperature distributions. It is inferred from the figures that the flow velocity of the fluid decrease as the porosity parameter increases. Also, it is clear that the velocity profiles attain maximum value near the plate at low value of the porosity. It is shown that the temperature distribution in the flow increases as the Darcy number increases.

7. 4. Effect of Casson parameter on Casson nanofluid velocity and temperature distributions

Figs. 7a and 7b depicts the effects of Casson parameter on velocity and temperature profiles Casson nanofluid, respectively. It is obvious from the figure that Casson the parameter has influence on axial velocity. From Fig. 7a, the magnitude of velocity near the plate for Casson nanofluid parameter decreases for increasing value of the Casson parameter, while temperature increases for increase in Casson fluid parameter as shown in Fig. 7b. Physically, increasing values of Casson parameter develop the viscous forces. These forces have a tendency to decline the thermal boundary layer.

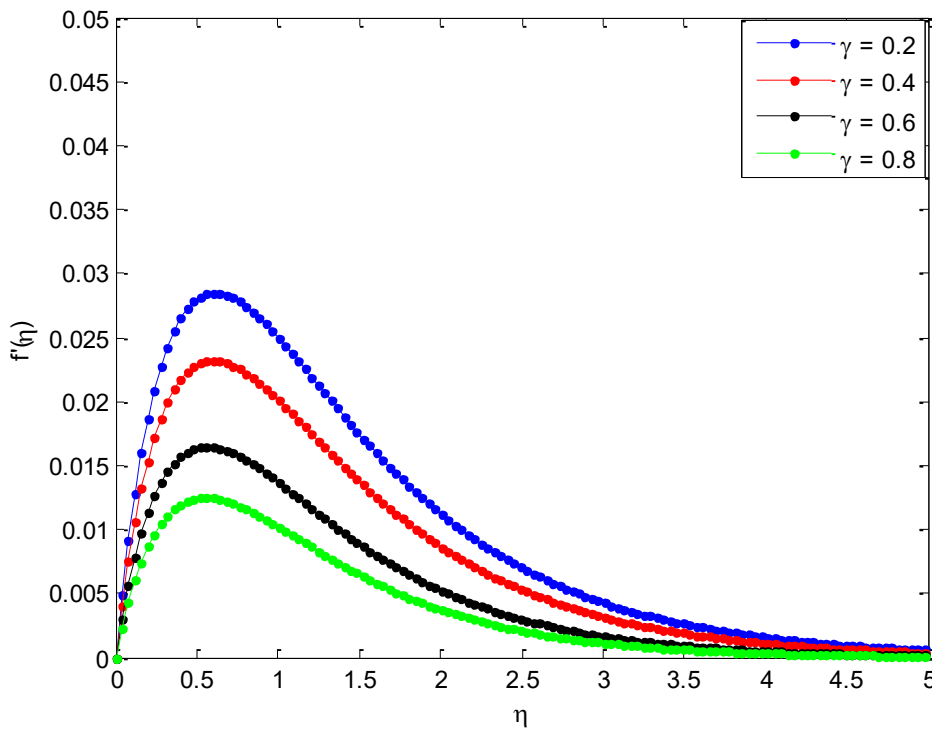


Fig. 7a. Effects of Casson parameter on the velocity profile of the Casson nanofluid

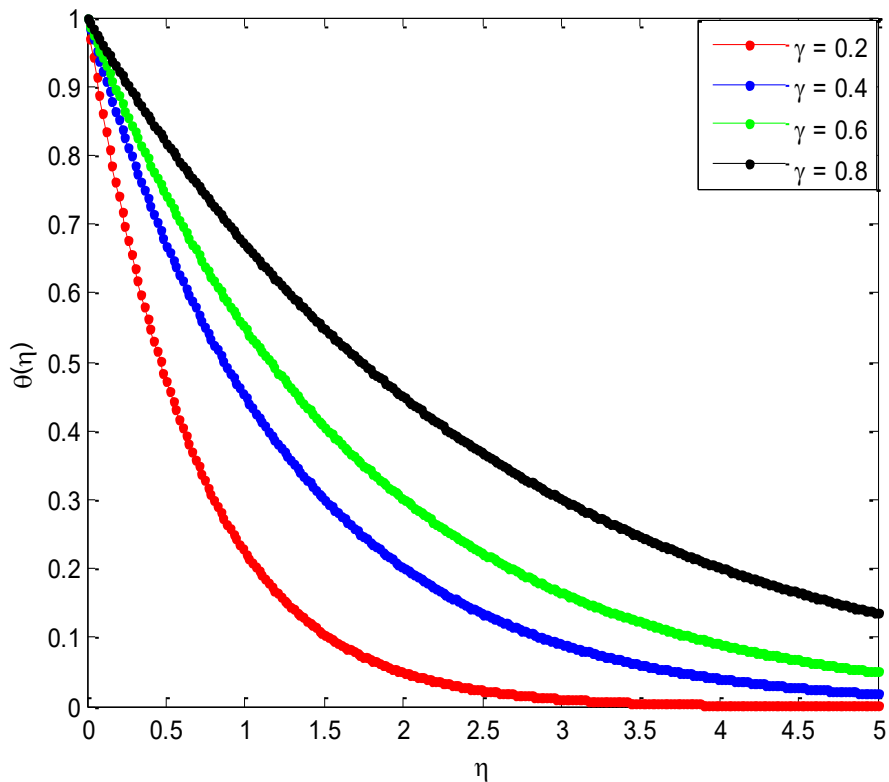


Fig. 7b. Effects of Casson parameter on temperature profile of the Casson nanofluid

7. 5. Effect of thermal radiation parameter on Casson nanofluid velocity and temperature distributions

It is depicted that both viscous and thermal boundary layers increase with the increase of radiation parameter, R . Fig. 8a depicts the effect of thermal radiation parameter on the velocity profiles. From the figure, it is shown that increase in radiation parameter causes the velocity of the fluid to increase. This is because as the radiation parameter is augmented, the absorption of radiated heat from the heated plate releases more heat energy released to the fluid and the resulting temperature increases the buoyancy forces in the boundary layer which also increases the fluid motion and the momentum boundary layer thickness accelerates. This is expected, because the considered radiation effect within the boundary layer increases the motion of the fluid which increases the surface frictions. The maximum velocity for all values of R is at the approximated value of $\eta = 0.5$. Therefore, it can be concluded that the inner viscous layer does not increase for variation of radiation parameter. Only the outer layer thickness has a great influence of thermal radiation, R . Although, the velocity gradient at the surface increase with the increase in radiation parameter, a reverse case has been established in literature when water is used as the fluid under the study of the flow of viscous fluid over a flat surface.

Using a constant value of the Prandtl number, the influence of radiation parameter on the temperature field is displayed in Fig. 8b. Increase in the radiation parameter contributes in general to increase in the temperature.

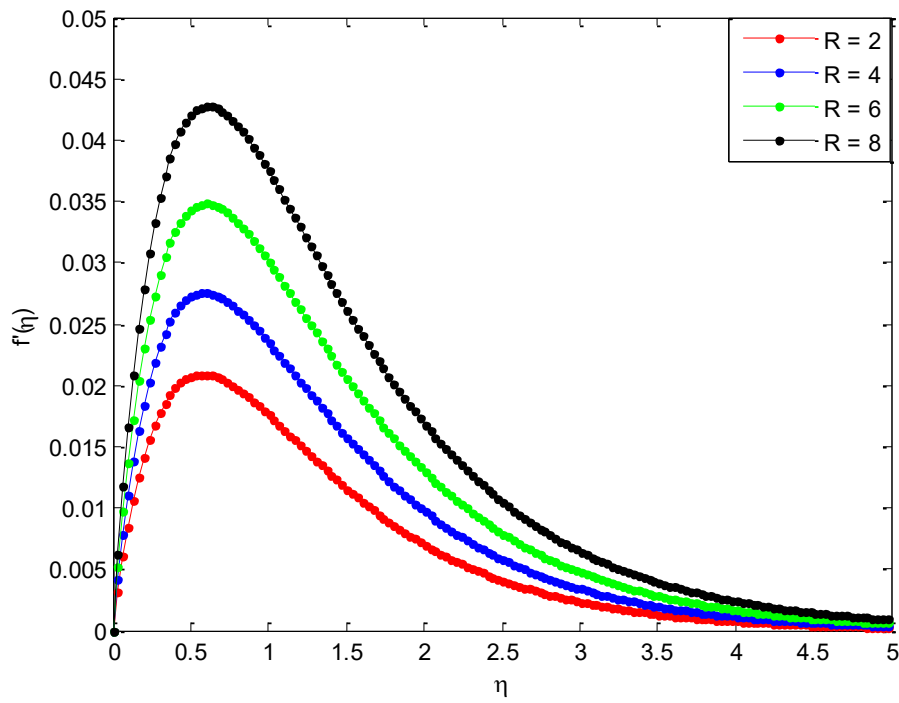


Fig. 8a. Effects of radiation parameter on the velocity profile of the Casson nanofluid

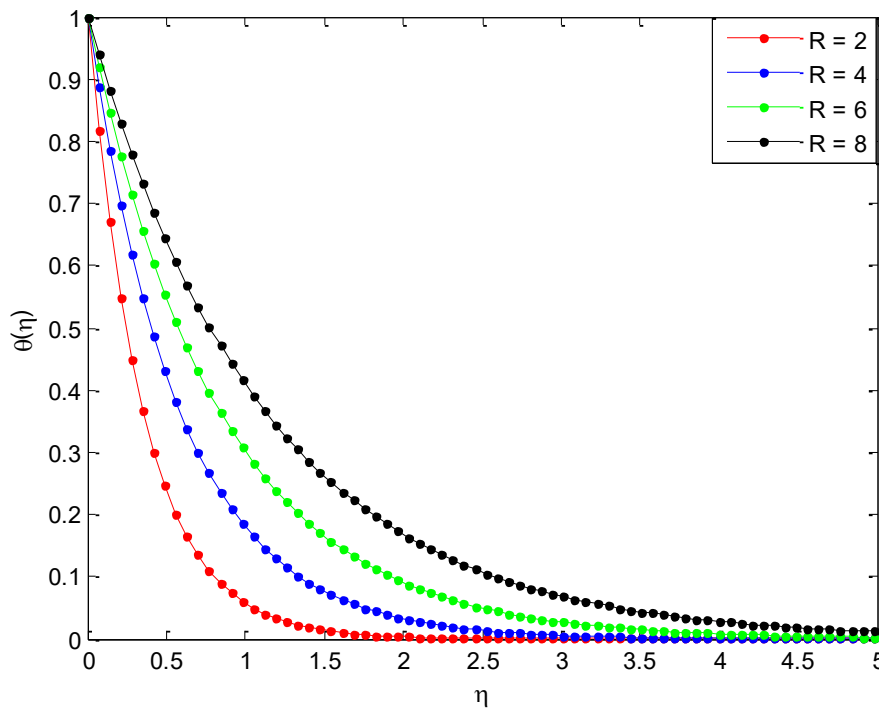


Fig. 8b. Effects of radiation parameter on temperature profile of the Casson nanofluid

This is because, as the thermal radiation increases, the absorption of radiated heat from the heated plate releases heat energy released to the fluid the thermal boundary layer of fluid increases as the temperature near the boundary is enhanced.

This shows that influence of radiation is more effective when high temperature is required for the desired thickness of end product. It is observed that the effect of the radiation parameter is not significant as we move away from the boundary. Also, it is observed that as the temperature of the fluid increases for increasing thermal radiation, the temperature difference between the plate and the ambient fluid reduces which turns to decrease the heat transfer rate in flow region.

7. 6. Effect of nanoparticle volume fraction on Casson nanofluid velocity and temperature distributions for different values of Prandtl number

Figs. 9-12 show the effects nanoparticle concentration/volume fraction and Prandtl number on velocity and temperature profiles Copper(II) Oxide-water Casson nanofluid. It is indicated in the Figures that as the volume-fraction or concentration of the nanoparticle in the nanofluid increases, the velocity decreases. However, an opposite trend or behaviour in the temperature profile is observed i.e. the nanofluid temperature increases as the volume-fraction of the nanoparticles in the base fluid increases. This is because, the solid volume fraction has significant impacts on the thermal conductivity. The increased volume fraction of nanoparticles in the base fluid results in higher thermal conductivity of the base fluid which increases the heat enhancement capacity of the base fluid.

Also, one of the possible reasons for the enhancement on heat transfer of nanofluids can be explained by the high concentration of nanoparticles in the thermal boundary layer at the wall side through the migration of nanoparticles. It should also be stated that the thickness of thermal boundary layer rises with increasing the values of nanoparticle volume fraction. This consequently reduces the velocity of the nanofluid as the shear stress and skin friction are increased.

The figures also show the effects of Prandtl number (Pr) on the velocity and temperature profiles. It is indicated that the velocity of the nanofluid decreases as the Pr increases but the temperature of the nanofluid increases as the Pr increases. This is because the nanofluid with higher Prandtl number has a relatively low thermal conductivity, which reduces conduction, and thereby reduces the thermal boundary-layer thickness, and as a consequence, increases the heat transfer rate at the surface.

For the case of the fluid velocity that decreases with the increase of Pr, the reason is that fluid of the higher Prandtl number means more viscous fluid, which increases the boundary-layer thickness and thus, reduces the shear stress and consequently, retards the flow of the nanofluid. Also, it can be seen that the velocity distribution for small value of Prandtl number consist of two distinct regions. A thin region near the wall of the plate where there are large velocity gradients due to viscous effects and a region where the velocity gradients are small compared with those near the wall. In the later region, the viscous effects are negligible and the flow of fluid in the region can be considered to be inviscid. Also, such region tends to create uniform accelerated flow at the surface of the plate.

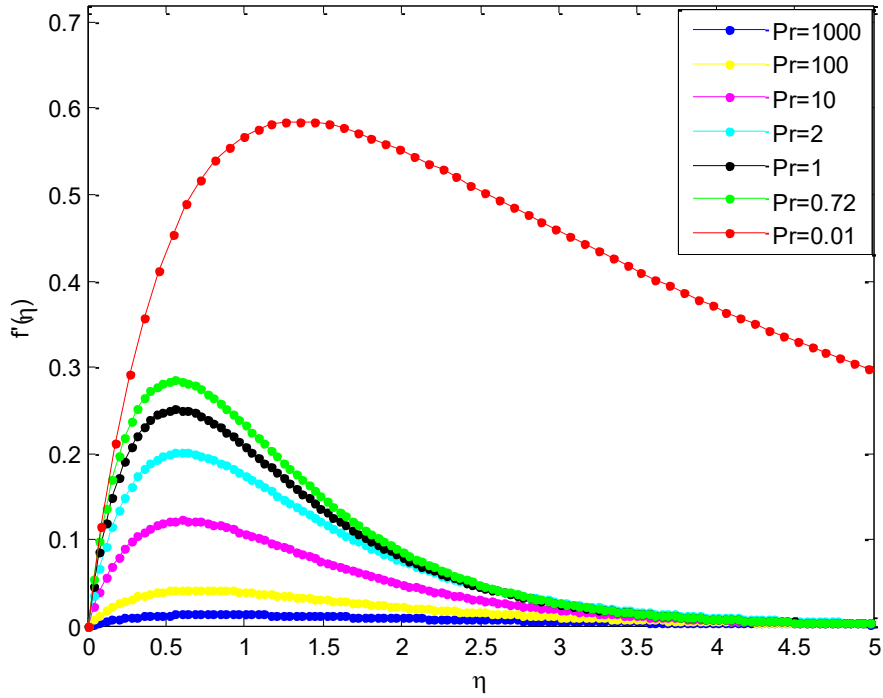


Fig. 9a. Effects of Prandtl number on the velocity profile when $\phi = 0.020$

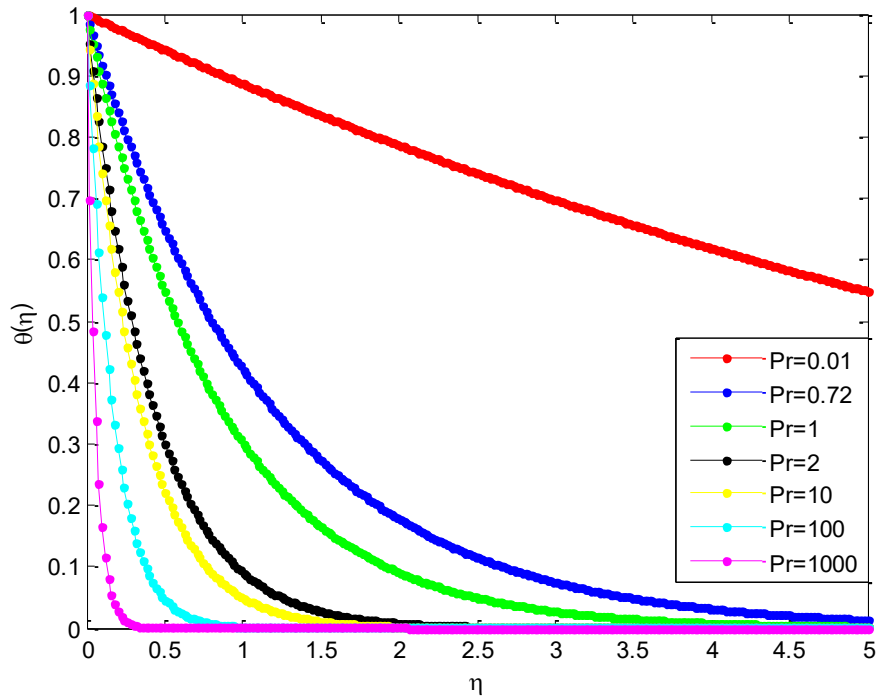


Fig. 9b. Effects of Prandtl number on temperature profile when $\phi = 0.020$

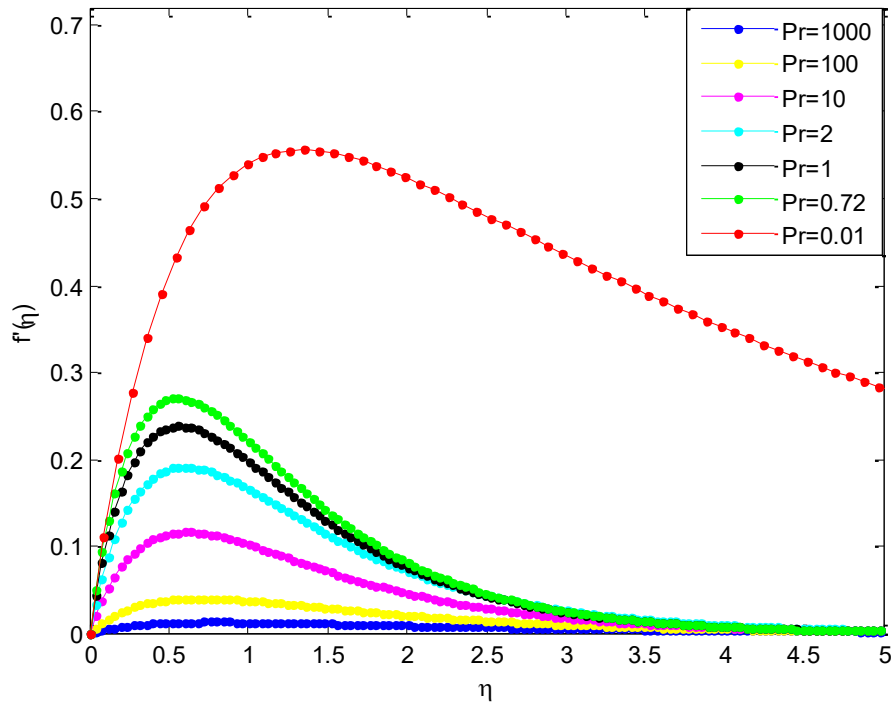


Fig. 10a. Effects of Prandtl number on the velocity profile when $\phi = 0.040$

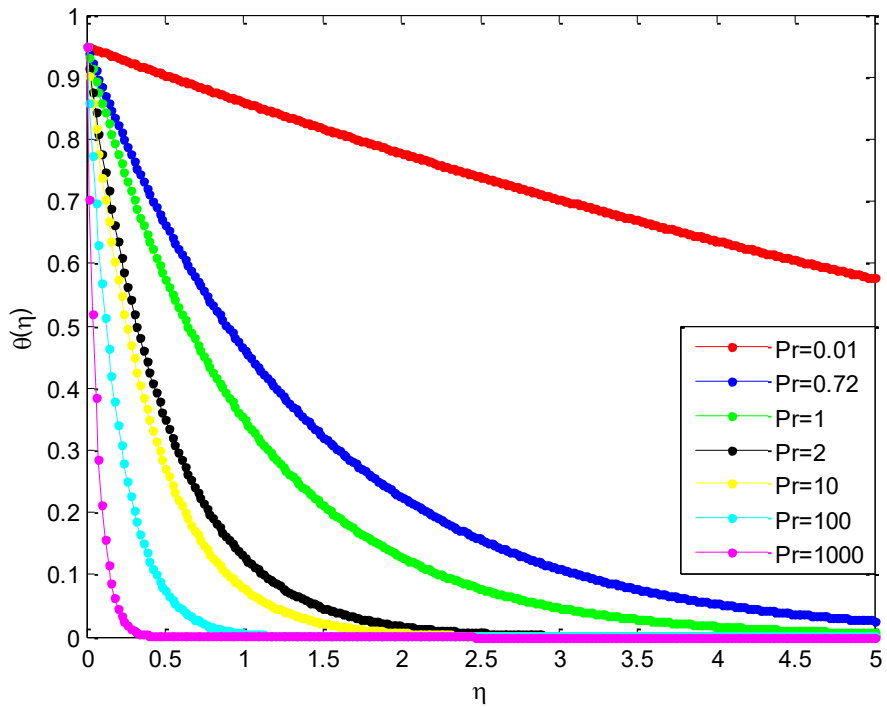


Fig. 10b. Effects of Prandtl number on temperature profile when $\phi = 0.040$

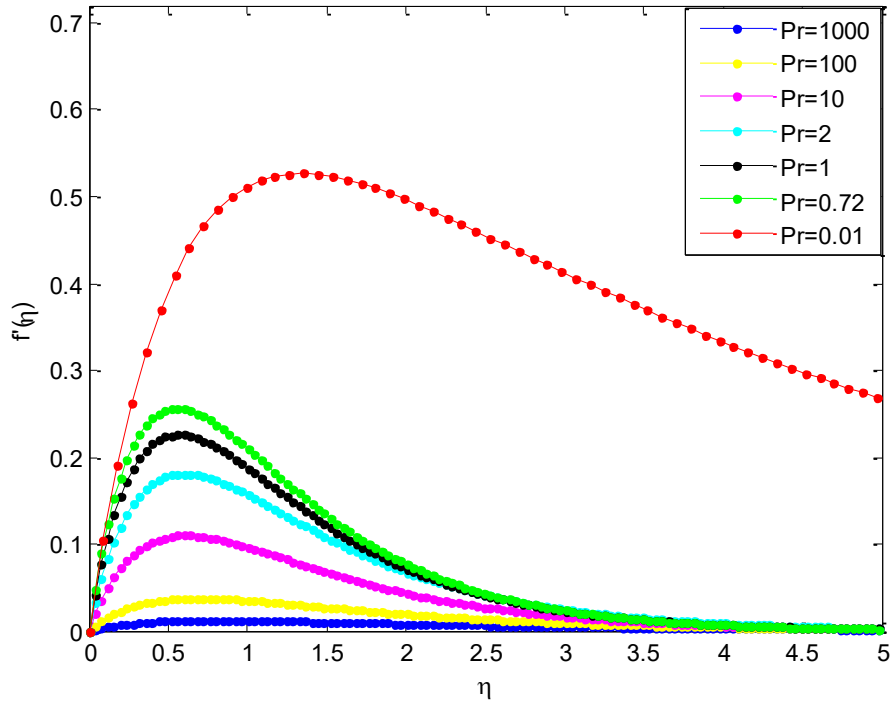


Fig. 11a. Effects of Prandtl number on the velocity profile when $\phi = 0.060$

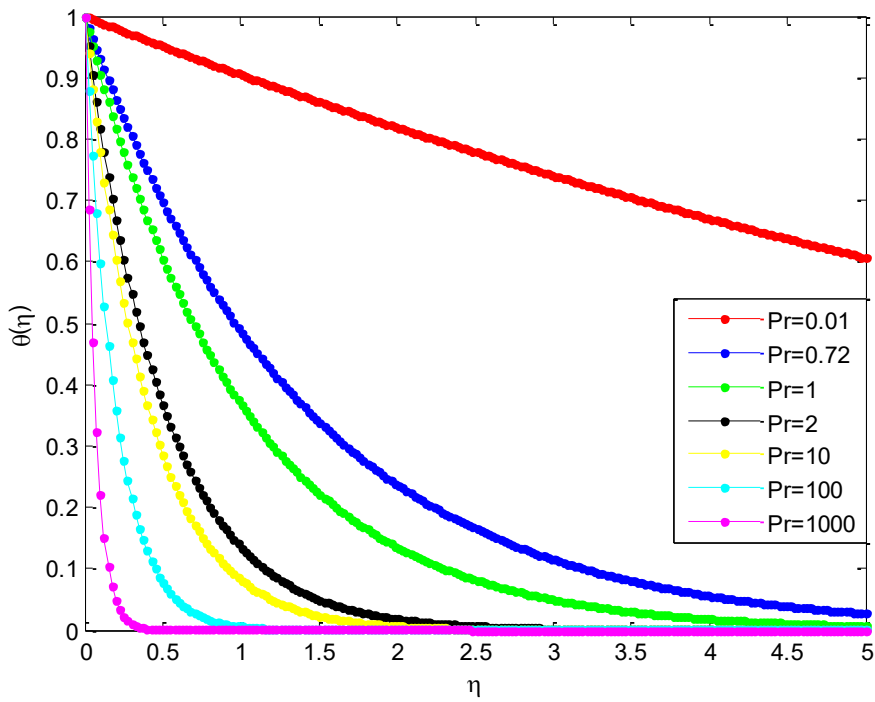


Fig. 11b. Effects of Prandtl number on temperature profile when $\phi = 0.060$

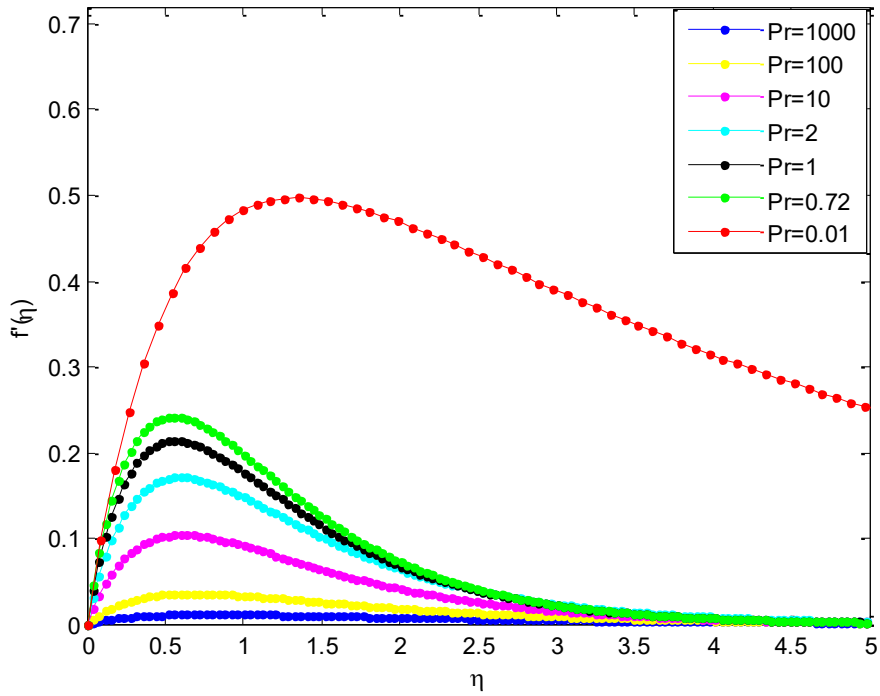


Fig. 12a. Effects of Prandtl number on the velocity profile when $\phi = 0.080$

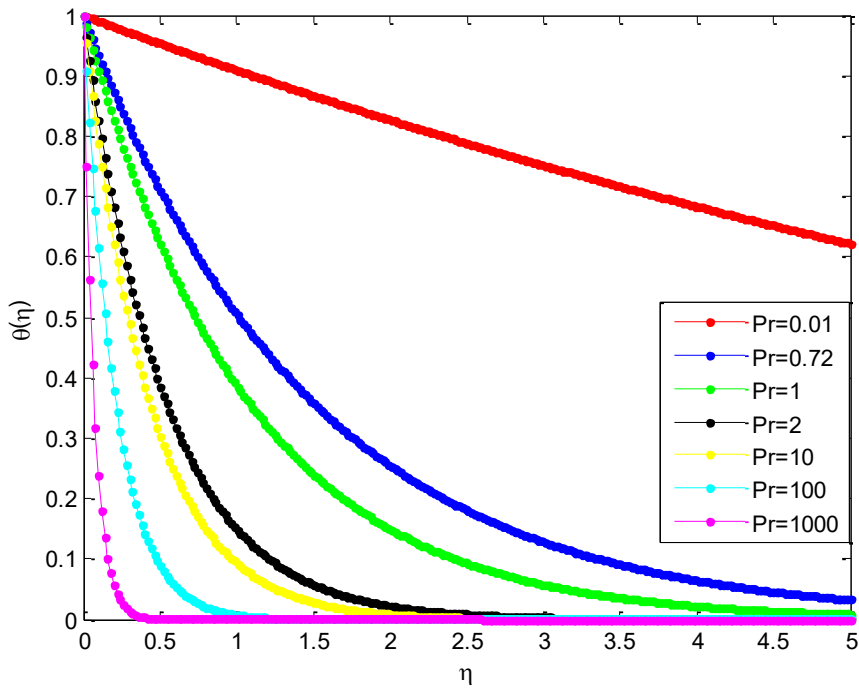


Fig. 12b. Effects of Prandtl number on temperature profile when $\phi = 0.080$

The use of nanoparticles in the fluids exhibited better properties relating to the heat transfer of fluid than heat transfer enhancement through the use of suspended millimeter- or micrometer-sized particles which potentially cause some severe problems, such as abrasion, clogging, high pressure drop, and sedimentation of particles. The very low concentrations applications and nanometer sizes properties of nanoparticles in the base fluid prevent the sedimentation in the flow that may clog the channel. It should be added that the theoretical prediction of enhanced thermal conductivity of the base fluid and prevention of clogging, abrasion, high pressure drop and sedimentation through the addition of nanoparticles in the base fluid have been supported with experimental evidences in literature.

7. 7. Effect of nanoparticle shape on Casson nanofluid velocity and temperature distributions for different values of Prandtl number

It has observed experimentally that the nanoparticle shape has significant impacts on the thermal conductivity. Therefore, the effects of nanoparticle shape at different values of Prandtl number on velocity and temperature profiles of Copper(II) Oxide-water nanofluid are shown in Fig. 13-18. It is indicated that the maximum decrease in velocity and maximum increase in temperature are caused by lamina, platelets, cylinder, bricks and sphere, respectively. It is observed that lamina shaped nanoparticle carries maximum velocity whereas spherical shaped nanoparticle has better enhancement on heat transfer than other nanoparticle shapes.

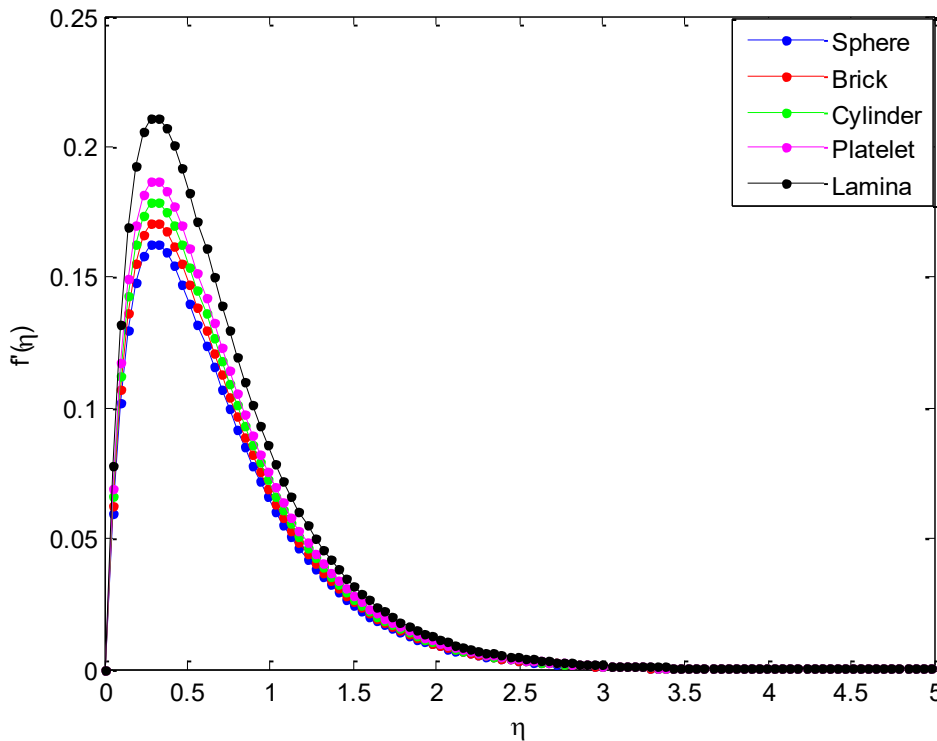


Fig. 13a. Effect of nanoparticle shape on velocity distribution of the nanofluid

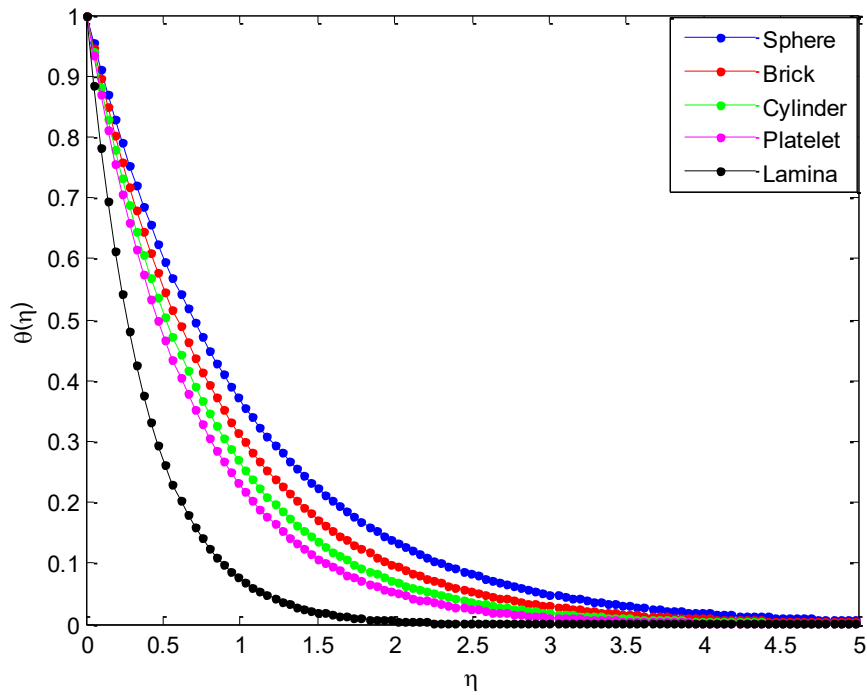


Fig. 13b. Effects of nanoparticle shape on temperature distribution of the nanofluid

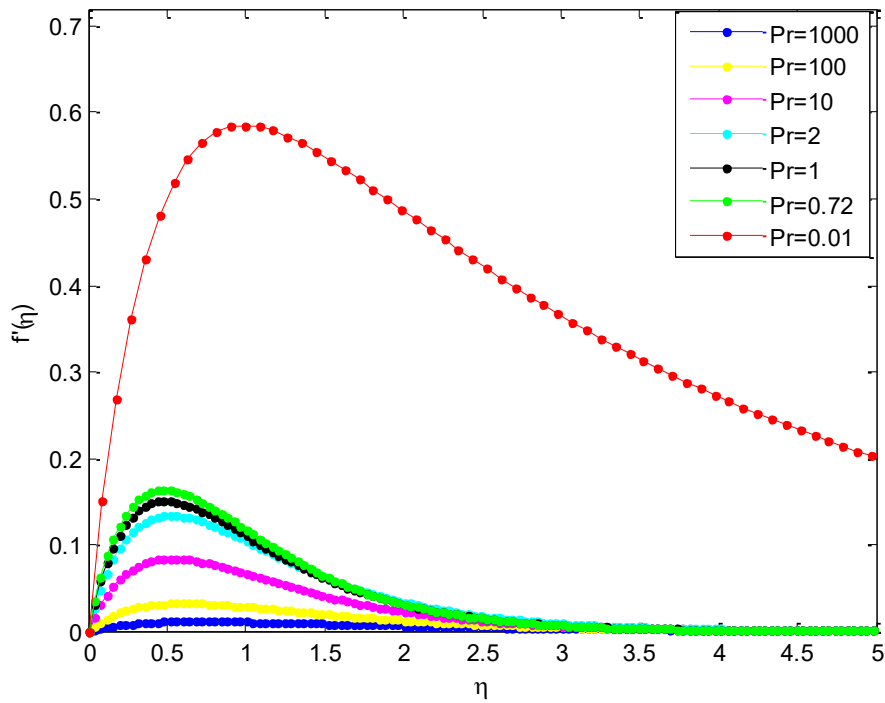


Fig. 14a. Effects of Prandtl number on velocity profile for spherical shape nanoparticle

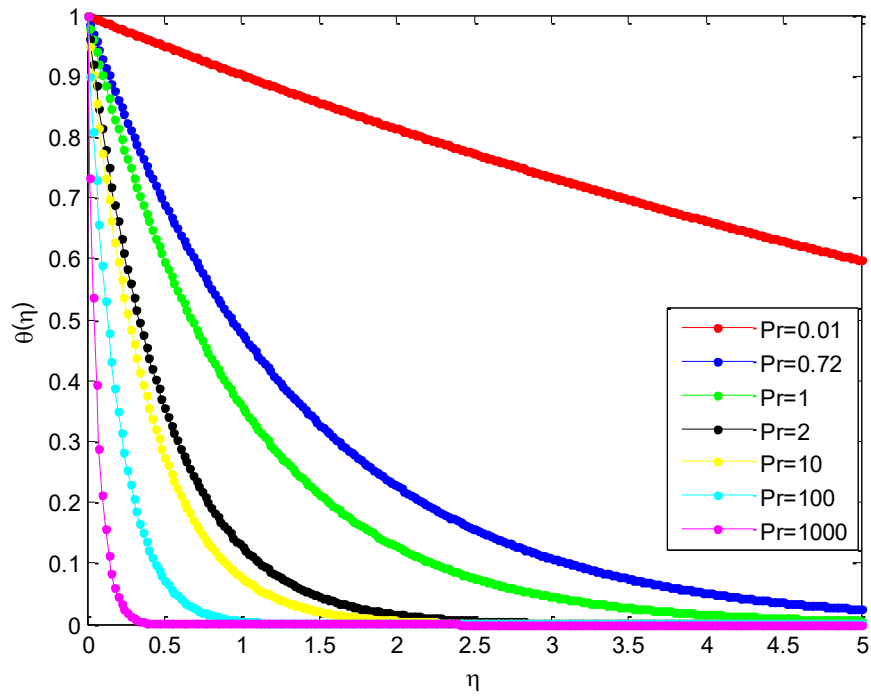


Fig. 14b. Effects of Prandtl number on temperature profile for spherical shape nanoparticle

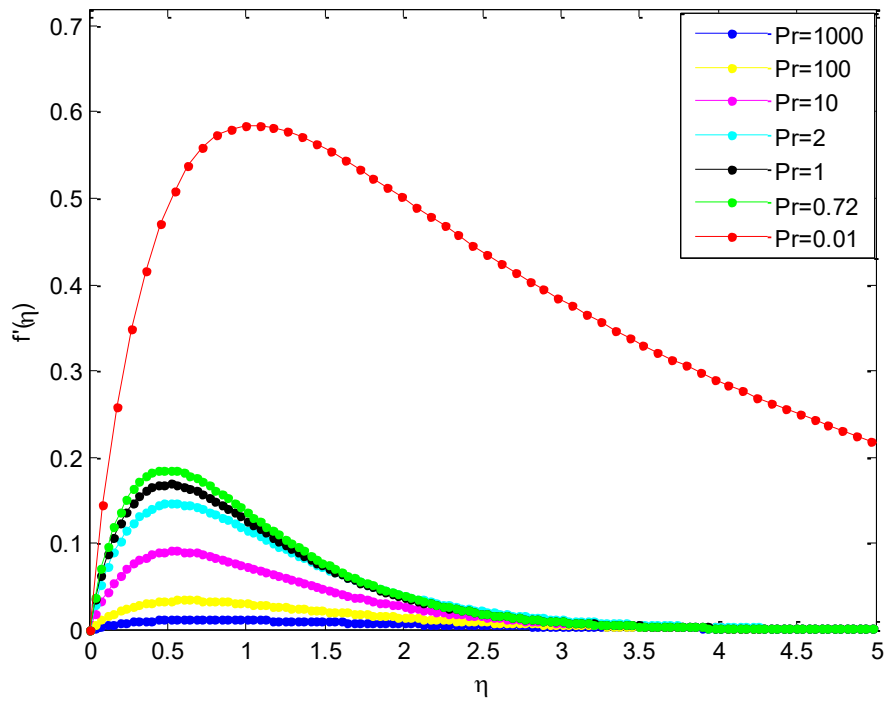


Fig. 15a. Effects of Prandtl number on velocity profile for brick shape nanoparticle

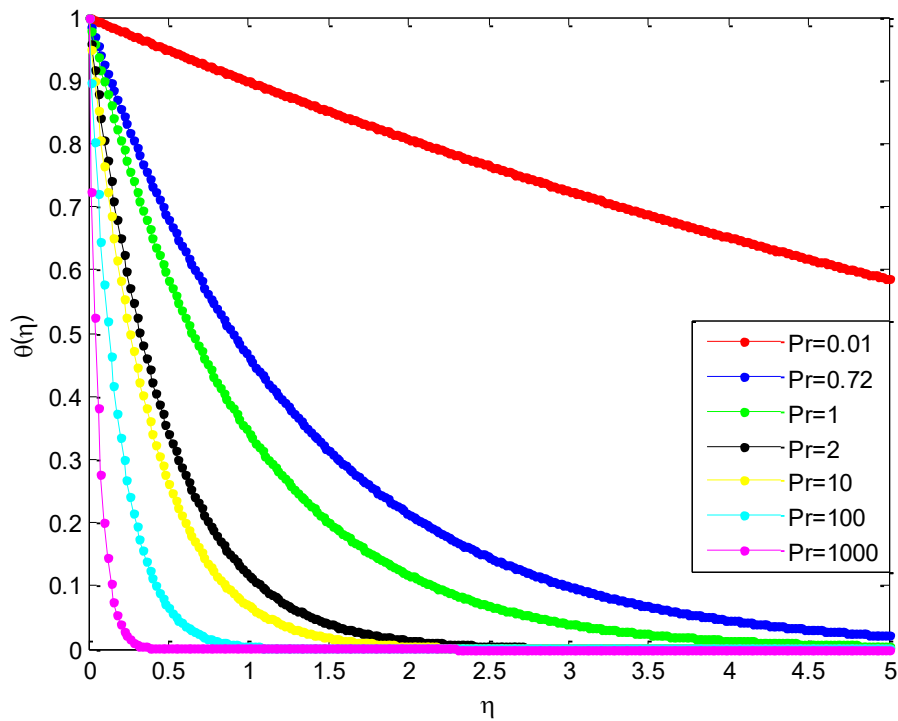


Fig. 15b. Effects of Prandtl number on temperature profile for brick shape nanoparticle

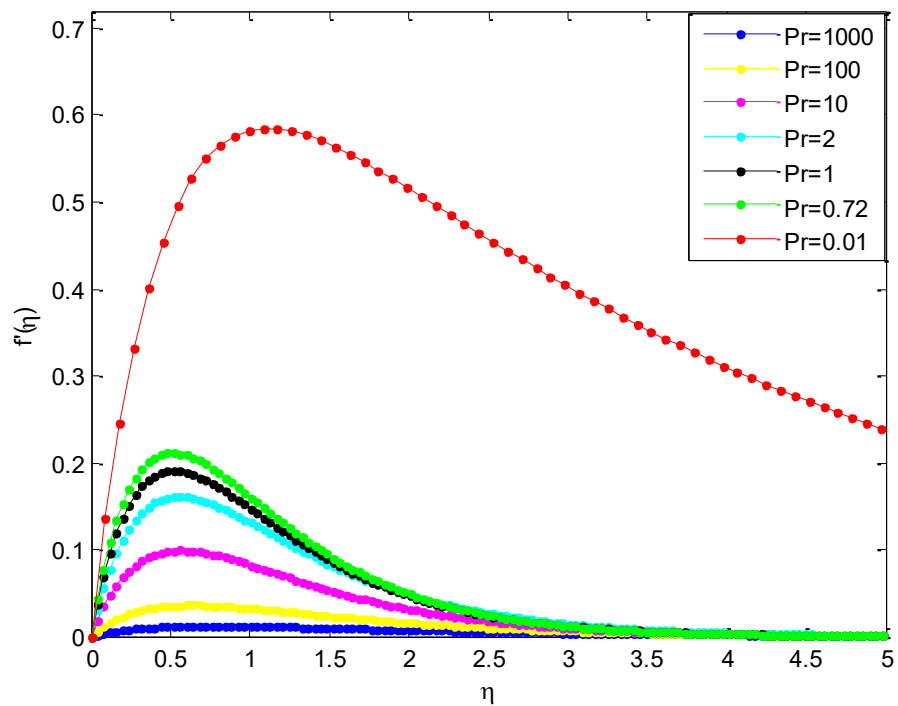


Fig. 16a. Effects of Prandtl number on velocity profile for cylindrical shape nanoparticle

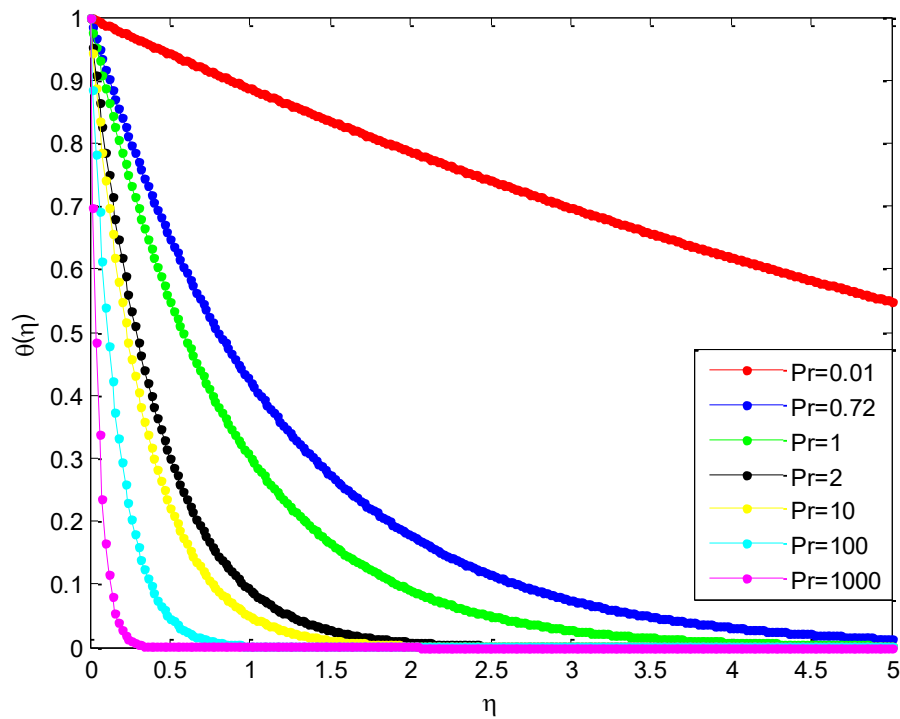


Fig. 16b. Effects of Prandtl number on temperature profile for cylindrical shape nanoparticle

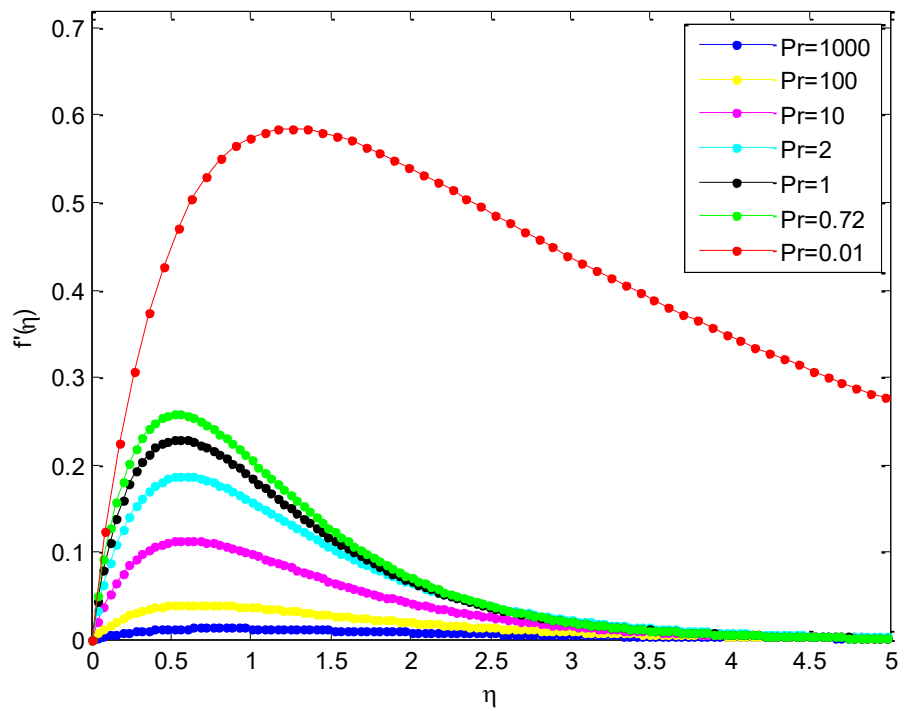


Fig. 17a. Effects of Prandtl number on velocity profile for platelet shape nanoparticle

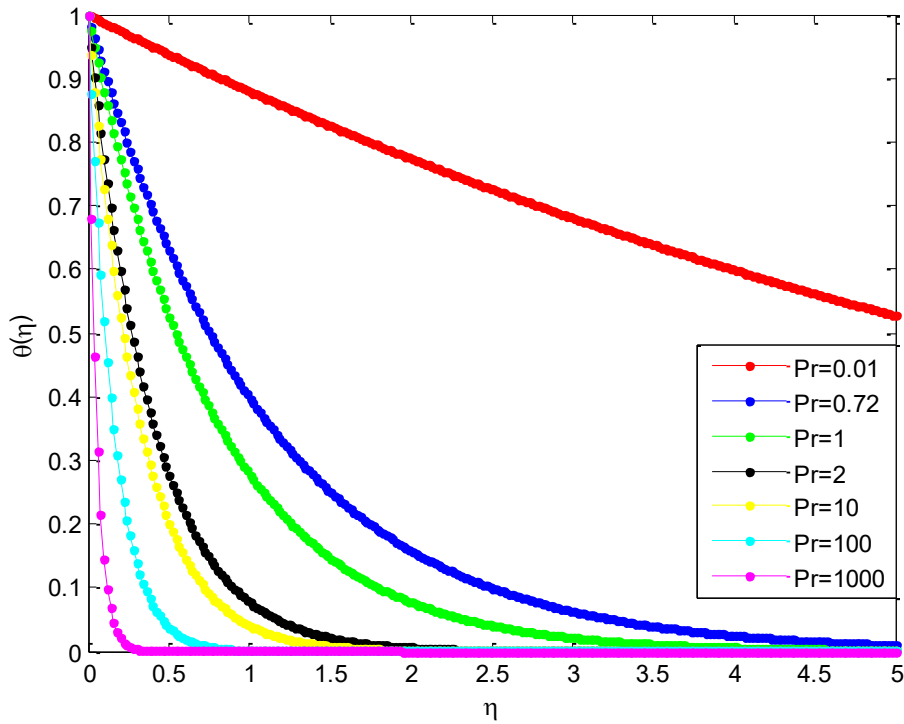


Fig. 17b. Effects of Prandtl number on temperature profile for platelet shape nanoparticle

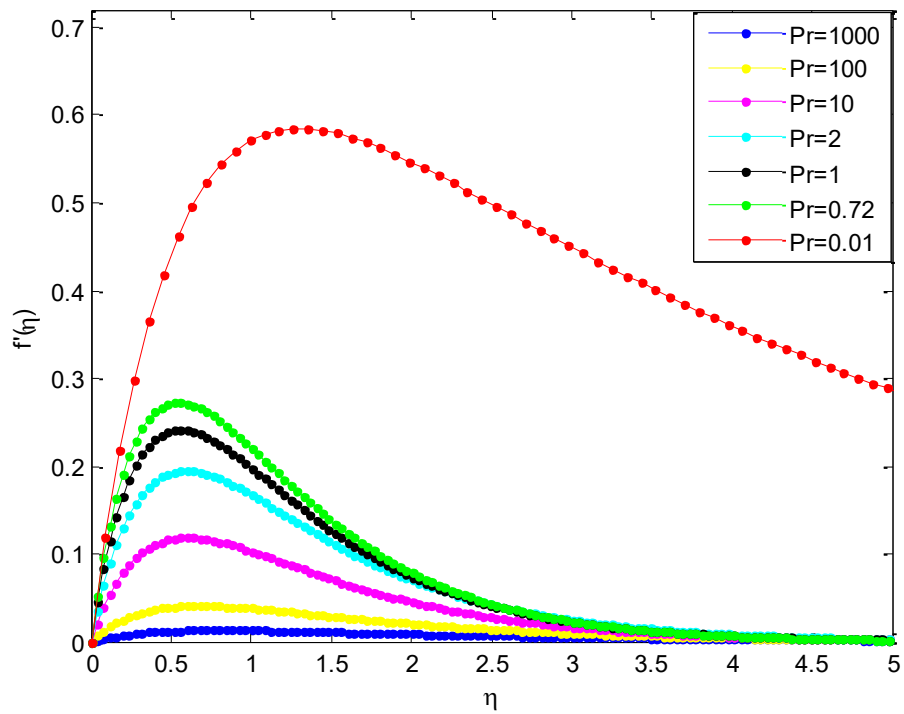


Fig. 18a. Effects of Prandtl number on velocity profile for lamina shape nanoparticle

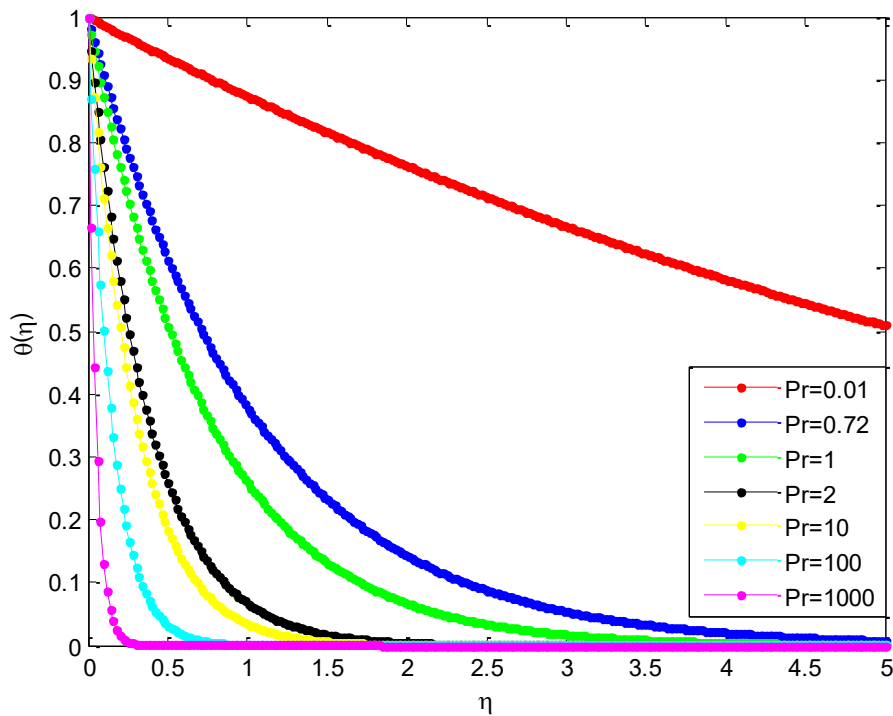


Fig. 18b. Effects of Prandtl number on temperature profile for lamina shape nanoparticle

In fact, it is in accordance with the physical expectation since it is well known that the lamina nanoparticle has greater shape factor than other nanoparticles of different shapes, therefore, the lamina nanoparticle comparatively gains maximum temperature than others. The decrease in velocity is highest in spherical nanoparticles as compared with other shapes. The enhancement observed at lower volume fractions for non-spherical particles is attributed to the percolation chain formation, which perturbs the boundary layer and thereby increases the local Nusselt number values.

It is evident from this study that proper choice of nanoparticles will be helpful in controlling velocity and heat transfer. It is also observed that irreversibility process can be reduced by using nanoparticles, especially the spherical particles. This can potentially result in higher enhancement in the thermal conductivity of a nanofluid containing elongated particles compared to the one containing spherical nanoparticle, as exhibited by the experimental data in the literature. Also, the figure shows that the thickness of this boundary-layer decreases with increase in the Prandtl number implying a slow rate of thermal diffusion as a result of the inhibiting influence of the viscous forces. It should be noted that higher values of Prandtl number leads to faster cooling of the plane sheet. These results will enhance the understanding of free-convective boundary-layer problem especially in glass-fiber production process.

7. 8. Effect of type of nanoparticle on Casson nanofluid velocity and temperature distribution for different values of Prandtl number

The variations of the velocity and temperature profiles against η for various types of nanoparticles (TiO_2 , CuO , Al_2O_3 and SWCNTs) are shown in Fig. 19-22.

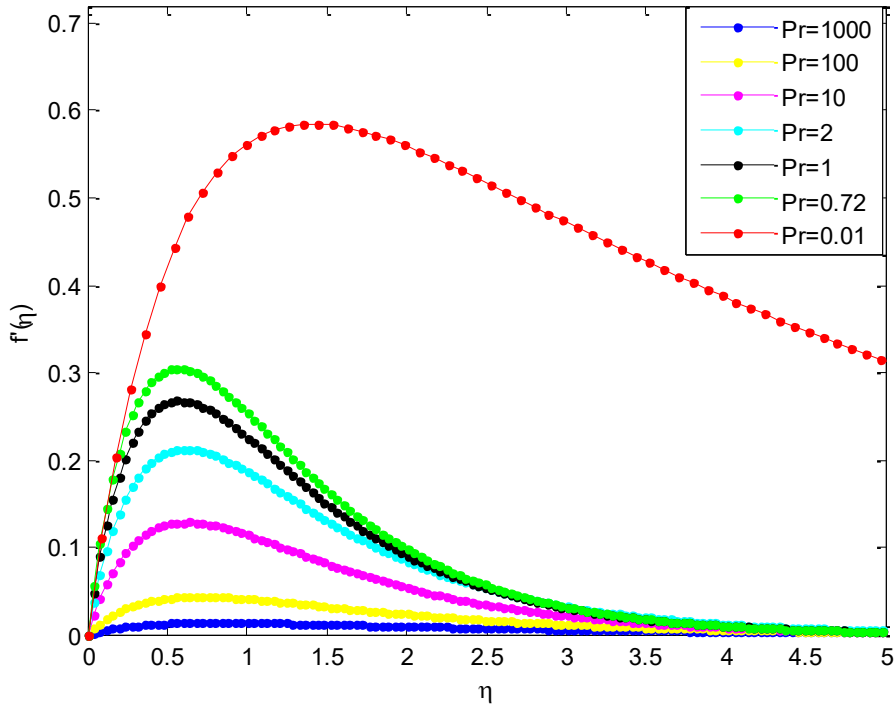


Fig. 19a. Effects of Prandtl number on velocity profile for TiO₂ nanoparticle

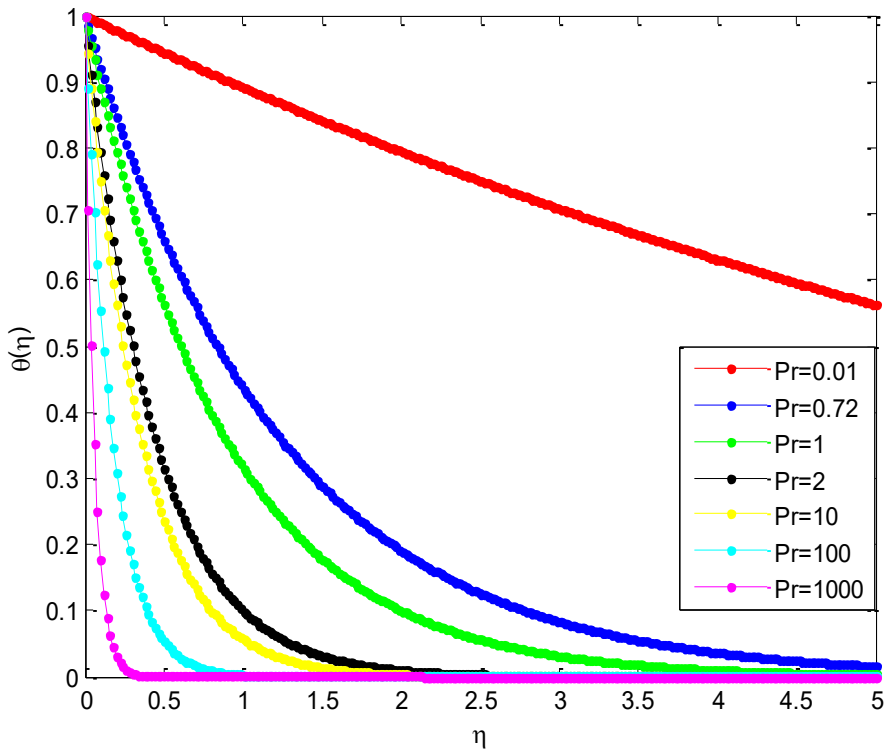


Fig. 19b. Effects of Prandtl number on temperature profile for TiO₂ nanoparticle

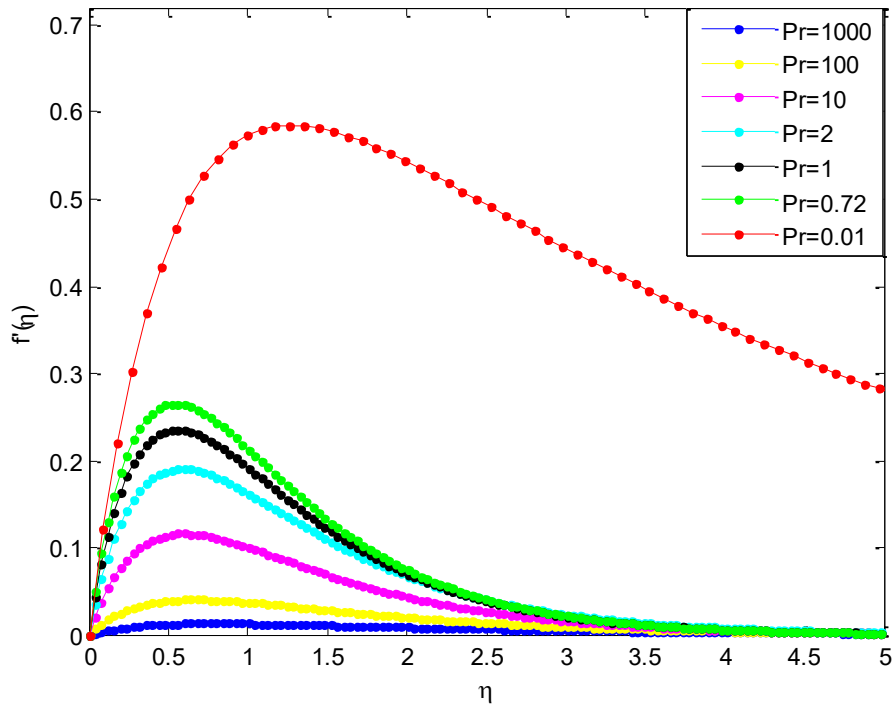


Fig. 20a. Effects of Prandtl number on velocity profile for CuO nanoparticle.

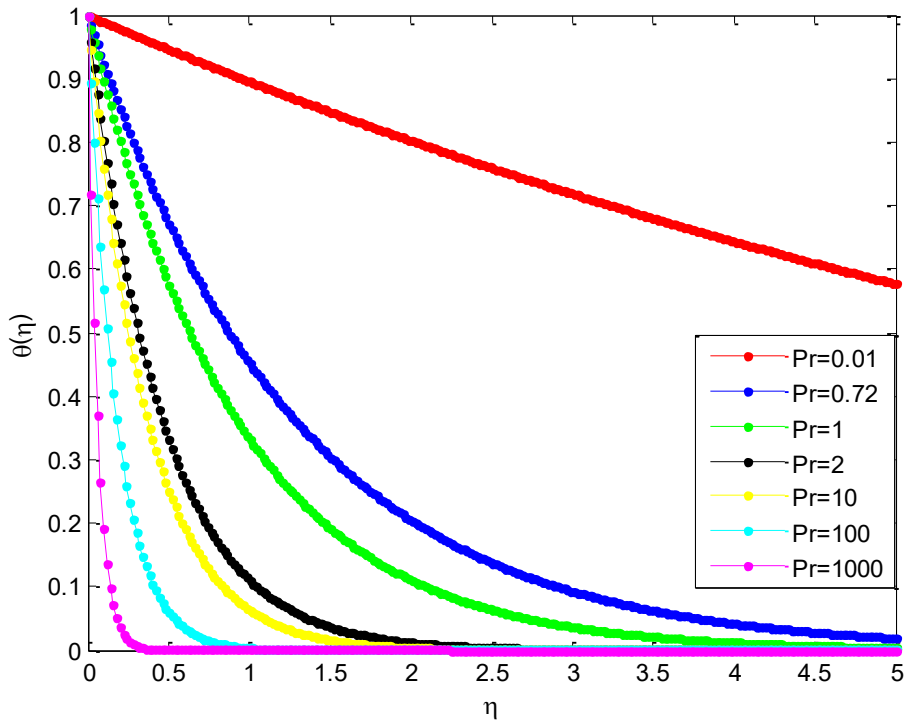


Fig. 20b. Effects of Prandtl number on temperature profile for CuO nanoparticle.

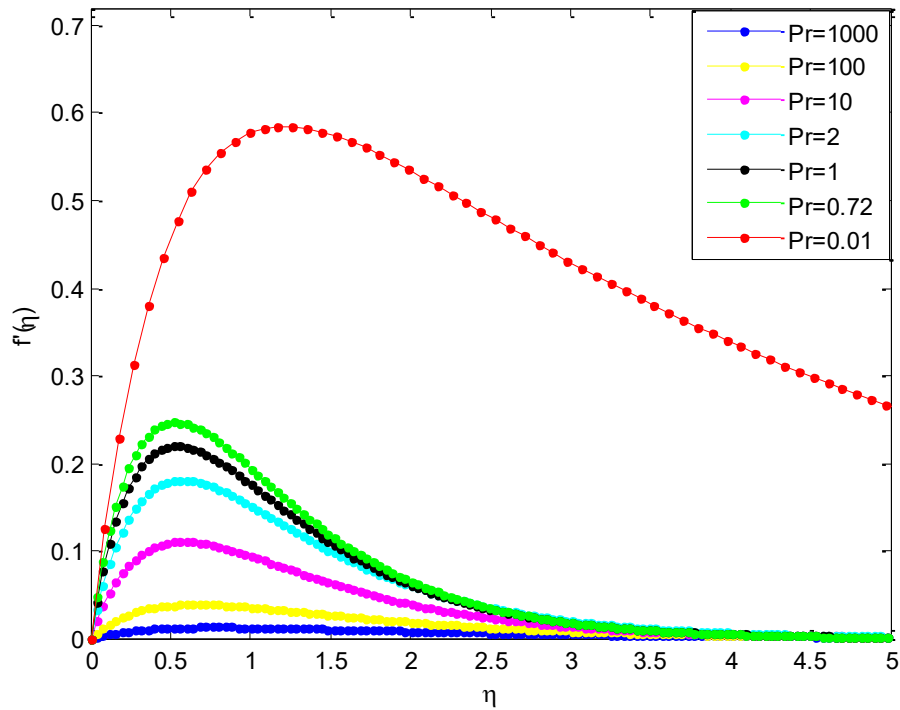


Fig. 21a. Effects of Prandtl number on velocity profile for Al_2O_3 nanoparticle

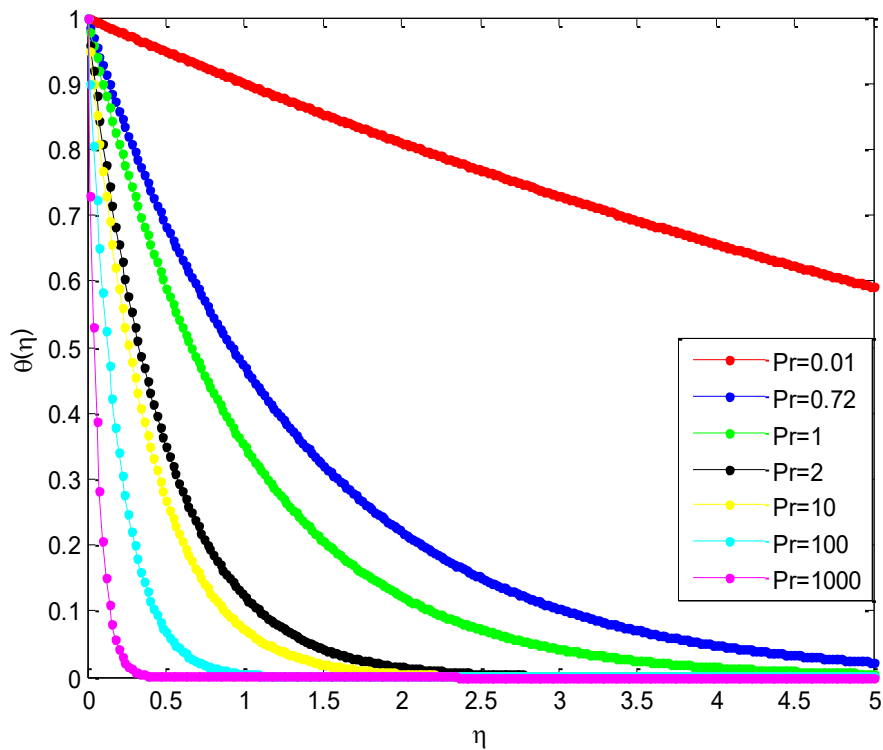


Fig. 21b. Effects of Prandtl number on temperature profile for Al_2O_3 nanoparticle

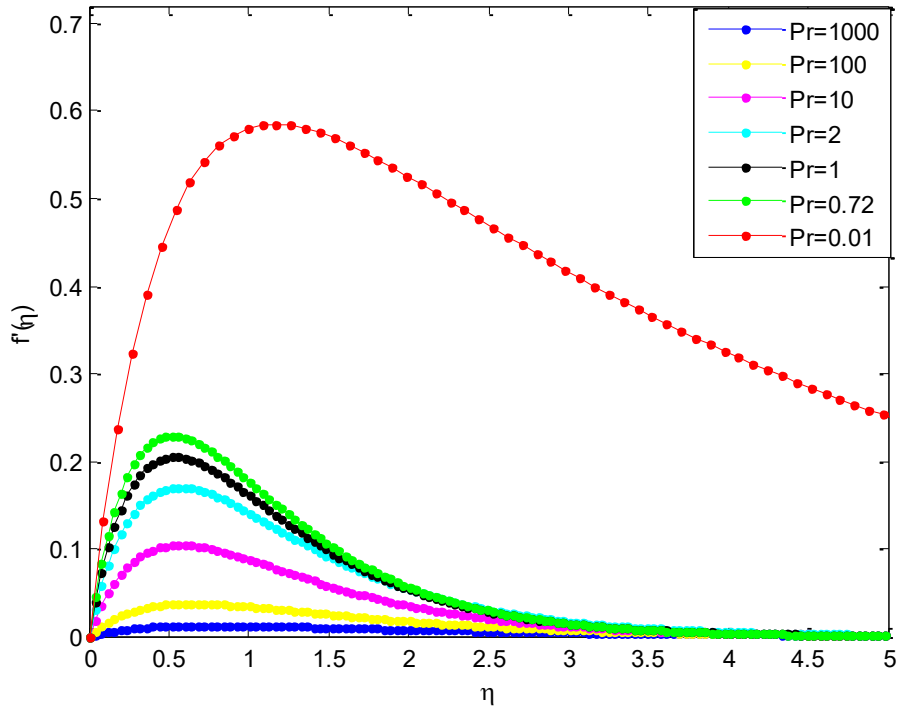


Fig. 22a. Effects of Prandtl number on velocity profile for SWCNTs nanoparticle

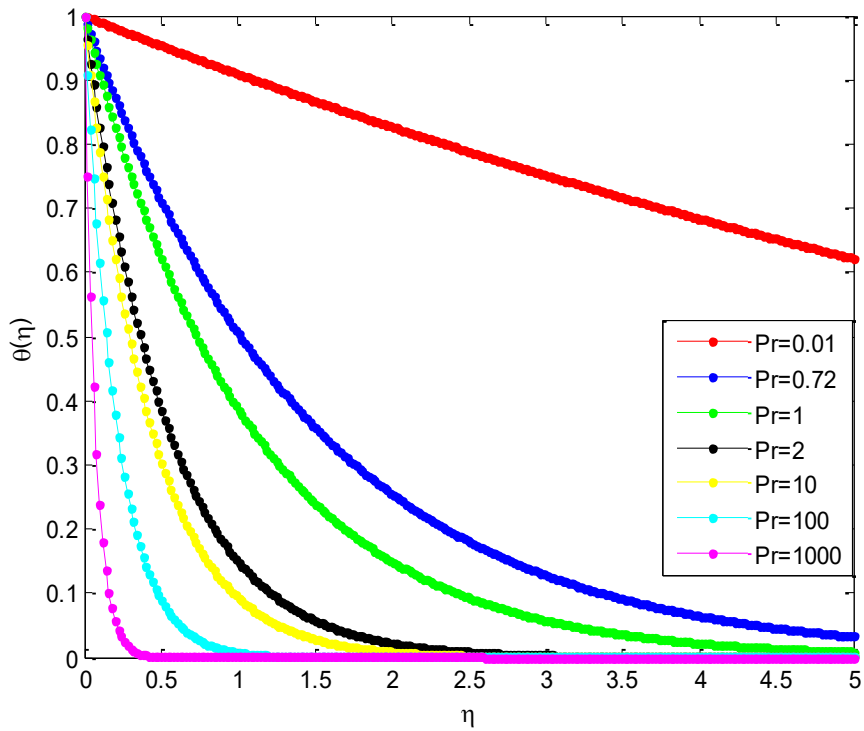


Fig. 22b. Effects of Prandtl number on temperature profile for SWCNTs nanoparticle

Using a common base fluid for all the nanoparticle types, it is observed that the maximum decrease in velocity and maximum increase in temperature are caused by TiO_2 , CuO , Al_2O_3 and SWCNTs, respectively. It is observed that SWCNTs nanoparticle carries maximum decreases velocity but has better enhancement on heat transfer than other nanoparticle shapes. In accordance with the physical expectation well, the SWCNTs nanoparticle has higher thermal conductivity than other types of nanoparticles, therefore, the SWCNTs nanoparticle comparatively gains maximum temperature than others. The increased thermal conductivity of the base fluid due to the use of nanoparticle of higher thermal conductivity increases the heat enhancement capacity of the base fluid.

Also, it is observed that the velocity decreases are maximum in SWCNTs nanoparticles when compared with other type of nanoparticles. This is because, the solid thermal conductivity has significant impacts on the momentum boundary layer of the nanofluid. The thickness of the momentum boundary layer increases with the increase in thermal conductivity. It is observed that the thickness of the thermal boundary layer enhances in presence of higher thermal conductivity nanoparticle. Therefore, the sensitivity of the boundary layer thickness to the type of nanoparticle is correlated to the value of the thermal conductivity of the nanoparticle used which consequently leads to enhancement of thermal conductivity of the nanofluid.

7. 9. Effect of thermal radiation parameter on Casson nanofluid velocity and temperature distributions

It is depicted that both viscous and thermal boundary layers increase with the increase of radiation parameter, R . Fig. 23a depicts the effect of thermal radiation parameter on the velocity profiles. From the figure, it is shown that increase in radiation parameter causes the velocity of the fluid to increase. This is because as the radiation parameter is augmented, the absorption of radiated heat from the heated plate releases more heat energy released to the fluid and the resulting temperature increases the buoyancy forces in the boundary layer which also increases the fluid motion and the momentum boundary layer thickness accelerates. This is expected, because the considered radiation effect within the boundary layer increases the motion of the fluid which increases the surface frictions. The maximum velocity for all values of R is at the approximated value of $\eta = 0.5$.

Therefore, it can be concluded that the inner viscous layer does not increase for variation of radiation parameter. Only the outer layer thickness has a great influence of thermal radiation, R . Although, the velocity gradient at the surface increase with the increase in radiation parameter, a reverse case has been established in literature when water is used as the fluid under the study of the flow of viscous fluid over a flat surface. Using a constant value of the Prandtl number, the influence of radiation parameter on the temperature field is displayed in Fig. 23b. Increase in the radiation parameter contributes in general to increase in the temperature. This is because, as the thermal radiation increases, the absorption of radiated heat from the heated plate releases heat energy released to the fluid the thermal boundary layer of fluid increases as the temperature near the boundary is enhanced. This shows that influence of radiation is more effective when high temperature is required for the desired thickness of end product. It is observed that the effect of the radiation parameter is not significant as we move away from the boundary. Also, it is observed that as the temperature of the fluid increases for increasing thermal radiation, the temperature difference between the plate and the ambient fluid reduces which turns to decrease the heat transfer rate in flow region.

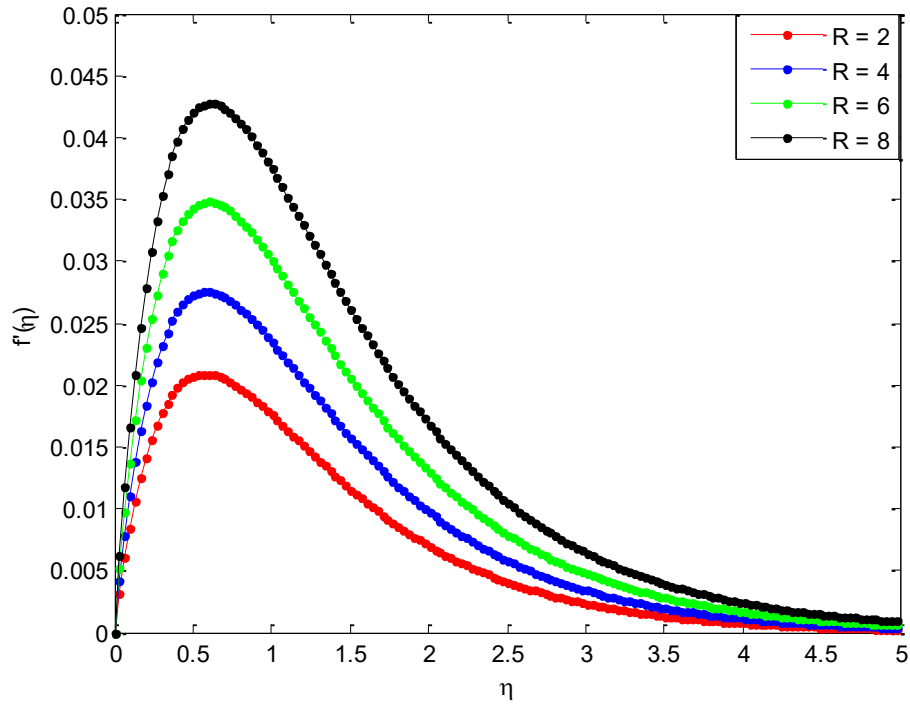


Fig. 23a. Effects of radiation parameter on the velocity profile of the Casson nanofluid

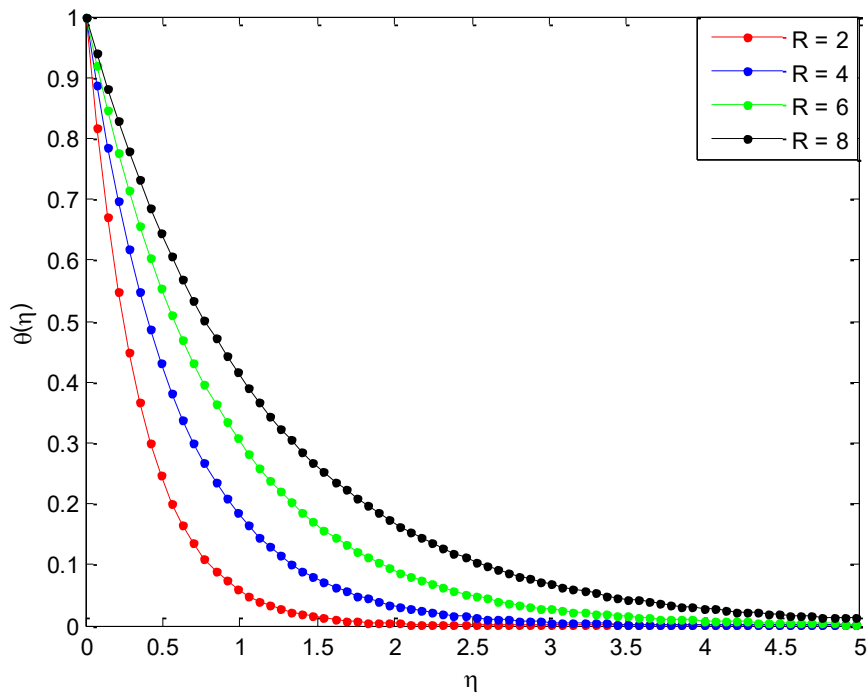


Fig. 23b. Effects of radiation parameter on temperature profile of the Casson nanofluid

This is because the radiation effect within the boundary layer increases the motion of the fluid which increases the surface frictions. As the temperature of the fluid increases for increasing R , consequently, the temperature difference between the plate and the ambient fluid reduces which turns to decrease the heat transfer rate in flow region.

8. CONCLUSIONS

In this work, the influences of inclined magnetic field, flow medium porosity and thermal radiation on free convection flow and heat transfer of Casson nanofluids over a vertical plate have been analyzed using He variational homotopy perturbation method with Padé approximant technique. The accuracies of the developed analytical solutions were verified with the results generated by some other methods as presented in the past works. The developed analytical solutions were used to investigate the effects of Casson parameter, thermal radiation parameter, Prandtl number, nanoparticles size and shapes on the flow and heat transfer behaviour of various Casson nanofluids. From the parametric studies, the following observations were established.

- i. Increase in magnetic field inclination parameter tends to decrease the fluid velocity and increase fluid temperature within the boundary layer, consequently, the skin friction factor in terms of shear stress and heat transfer rate in terms of Nusselt number are decreased.
- ii. The velocity of the fluid and the temperature gradient of the flow decrease as the magnetic field increases. Also, the temperature profiles increase with the increasing values of magnetic field parameter. The flow velocity of the fluid decrease as the porosity parameter increases.
- iii. The magnitude of velocity near the plate for the Casson nanofluid parameter decreases for increasing value of the Casson parameter, while temperature increases for increase in Casson fluid parameter.
- iv. Both the velocity and temperature of the nanofluid as well viscous and thermal boundary layers increase with increase in the radiation parameter.
- v. The velocity of the nanofluid decreases as the Prandtl number increases but the temperature of the nanofluid increases as the Prandtl number increases.
- vi. The velocity of the nanofluid decreases as the volume-fraction or concentration of the nanoparticle in the base fluid increases. However, an opposite trend or behaviour in the temperature profile was observed which showed that as the nanofluid temperature increases as the volume-fraction of the nanoparticles in the base fluid increases.
- vii. The lamina shaped nanoparticle carries maximum velocity whereas spherical shaped nanoparticle has better enhancement on heat transfer than other nanoparticle shapes. The maximum decrease in velocity and maximum increase in temperature are caused by lamina shaped nanoparticle and followed by platelets, cylinder, bricks and sphere shaped nanoparticles, respectively.
- viii. Using a common base fluid to all the nanoparticle types considered in this work, it was observed that SWCNTs nanoparticle carries maximum decrease in velocity but has better enhancement on heat transfer than other nanoparticle shapes. Also, it was observed that that the maximum decrease in velocity and maximum increase in

temperature are caused by TiO₂ and followed by CuO, Al₂O₃ and SWCNTs nanoparticles, in that order.

The present study reveals and exposes the predominant factors affecting the boundary layer of free convection flow and heat transfer of Casson nanofluids. Moreover, the high level of accuracy and versatility of differential transformation method-Padé approximate technique have been demonstrated. It is hoped that the present study will enhance the understanding as it provides physical insights into the free convection boundary-layer problems of Casson nanofluid under various parameters.

Nomenclature

B_o	Electric field intensity
c_p	specific heat capacity
k	thermal conductivity
K	the absorption coefficient, permeability
m	shape factor
p	pressure
p_y	yield stress of the fluid.
Pr	Prandtl number
u	velocity component in x-direction
v	velocity component in z-direction
y	axis perpendicular to plates
x	axis along the horizontal direction
y	axis along the vertical direction

Symbols

β	volumetric extension coefficients
ρ	density of the fluid
μ	dynamic viscosity
η	similarity variable
γ	Casson parameter
λ	sphericity, angle of inclination
ϕ	volume fraction or concentration of the nanofluid
θ	Dimensionless temperature
τ	shear stress,
τ_o	Casson yield stress,
μ	dynamic viscosity,
$\dot{\gamma}$	shear rate, Electric field intensity
e_{ij}	the $(i,j)th$ component of the deformation rate,
π	product of the component of deformation rate with itself
π_c	critical value of this product based on the non-Newtonian model,
μ_B	plastic dynamic viscosity of the non-Newtonian fluid

Subscript

f fluid
s solid
nf nanofluid

Acknowledgement

The author expresses sincere appreciation to University of Lagos, Nigeria for providing material supports and good environment for this work

References

- [1] E. Schmidt and W. Beckmann. Das temperatur-und geschwindigkeitsfeld vor einer wärme abgebenden senkrechter platte bei natürlichelicher convention. *Tech. Mech. U. Thermodynamik, Bd. 1(10)* (1930), 341-349; cont. Bd. 1(11) (1930), 391- 406.
- [2] S. Ostrach, An analysis of laminar free-convection flow and heat transfer about a flat plate parallel to the direction of the generating body force, *NACA Report*, 1111, 1953.
- [3] E.M. Sparrow and J.L. Gregg, Laminar free convection from a vertical plate with uniform surface heat flux, *Trans. A.S.M.E.* 78 (1956) 435-440.
- [4] E.J. Lefevre, Laminar free convection from a vertical plane surface, 9th Intern. Congress on Applied Mechanics, Brussels, paper I, 168 (1956).
- [5] E.M. Sparrow and J.L. Gregg, Similar solutions for free convection from a nonisothermal vertical plate, *Trans. A.S.M.E.* 80 (1958) 379-386.
- [6] K. Stewartson and L.T. Jones, The heated vertical plate at high Prandtl number, *J. Aeronautical Sciences* 24 (1957) 379-380.
- [7] H.K. Kuiken, An asymptotic solution for large Prandtl number free convection, *J. Engng. Math.* 2 (1968) 355-371.
- [8] H.K. Kuiken, Free convection at low Prandtl numbers, *J. Fluid Mech.* 37 (1969) 785-798.
- [9] S. Eshghy, Free-convection layers at large Prandtl number, *J. Applied Math. and Physics* 22 (1971) 275 -292.
- [10] S. Roy, High Prandtl number free convection for uniform surface heat flux, *Trans A.S.M.E.J. Heat Transfer* 95 (1973) 124-126.
- [11] H.K. Kuiken and Z. Rotem, Asymptotic solution for the plume at very large and small Prandtl numbers, *J. Fluid Mech.* 45 (1971) 585-600.
- [12] T.Y. Na, I.S. Habib, Solution of the natural convection problem by parameter differentiation, *Int. J. Heat Mass Transfer* 17 (1974) 457-459.
- [13] J.H. Merkin, A note on the similarity solutions for free convection on a vertical plate, *J. Engng. Math.* 19 (1985) 189-201.

- [14] J.H. Merkin, I. Pop, Conjugate free convection on a vertical surface, *Int. J. Heat Mass Transfer* 39 (1996) 1527–1534.
- [15] F. M. Ali, R. Nazar, and N. M. Arifin, Numerical investigation of free convective boundary layer in a viscous fluid, *The American Journal of Scientific Research*, no. 5, pp. 13–19, 2009.
- [16] S. S. Motsa, S. Shateyi, and Z. Makukula, Homotopy analysis of free convection boundary layer flow with heat and mass transfer, *Chemical Engineering Communications* vol. 198, no.6, pp. 783–795, 2011.
- [17] S. S. Motsa, Z. G. Makukula and S. Shateyi. Spectral Local Linearisation Approach for Natural Convection Boundary Layer Flow. *Mathematical Problems in Engineering*, Volume 2013 (2013), Article ID 765013, 7 pages.
- [18] A.R. Ghotbi, H. Bararnia, G. Domairry, and A. Barari, Investigation of a powerful analytical method into natural convection boundary layer flow, *Communications in Nonlinear Science and Numerical Simulation*, vol. 14, no. 5, pp. 2222–2228, 2009.
- [19] S. Mosayebidorcheh, T. Mosayebidorcheh. Series solution of convective radiative conduction equation of the nonlinear fin with temperature dependent thermal conductivity. *International Journal of Heat and Mass Transfer* 55 (2012), 6589-6594.
- [20] M. Sheikholeslami. CVFEM for magnetic nanofluid convective heat transfer in a porous curved enclosure. *The European Physical Journal Plus*, 2016, 131:413
- [21] M. Sheikholeslami and Davood Domairry Ganji. Hydrothermal Analysis in Engineering Using Control Volume Finite Element Method. First edition, Elsevier.
- [22] M. Sheikholeslami. Application of Control Volume Based Finite Element Method (CVFEM) for Nanofluid Flow and Heat Transfer, First edition, Elsevier.
- [23] M. Sheikholeslami. Numerical study of MHD Natural convection liquid metal flow and heat transfer in a wavy enclosure using CVFEM. *Heat Transfer Research*, 48 (2017), 121-138
- [24] S. Mosayebidorcheh, M. Rahimi-Gorji, D. D. Ganji, T. Moayebidorcheh, O. Pourmehran, M. Biglarian. Transient thermal behavior of radial fins of rectangular, triangular and hyperbolic profiles with temperature-dependent properties using DTM-FDM, *Journal of Central South University* 24 (3), 675-682.
- [25] S. Mosayebidorcheh, Masoud Farzinpoor, D.D. Ganji. Transient thermal analysis of longitudinal fins with internal heat generation considering temperature-dependent properties and different fin profiles, *Energy Conversion and Management* 86 (2014) 365–370.
- [26] S. Mosayebidorcheh, M. M. Rashidi, T. Moayebidorcheh. Analytical solution of the steady state condensation film on the inclined rotating disk by a new hybrid method, *Scientific Research and Essays* 9 (12), 557-565.
- [27] S. Mosayebidorcheh, M. M. Vatani, D. D. Ganji, T. Moayebidorcheh Investigation of the viscoelastic flow and species diffusion in a porous channel with high permeability, *Alexandria Engineering Journal* 53 (4), 779-785.

- [28] S. Mosayebidorcheh and T. Moayebidorcheh Series solution of convective radiative conduction equation of the nonlinear fin with temperature dependent thermal conductivity, *International Journal of Heat and Mass Transfer* 55 (2012) 6589-6594.
- [29] S. Mosayebidorcheh. Analytical Investigation of the Micropolar Flow through a Porous Channel with Changing Walls, *Journal of Molecular Liquids* 196 (2014) 113–119.
- [30] M. Hatami a, S. Mosayebidorcheh, D. Jing, Thermal performance evaluation of alumina-water nanofluid in an inclined direct absorption solar collector (IDASC) using numerical method, *Journal of Molecular Liquids* 231 (2017) 632–639.
- [31] S. Mosayebidorcheh, Solution of the Boundary Layer Equation of the Power-Law Pseudoplastic Fluid Using Differential Transform Method, *Mathematical Problems in Engineering*, Volume 2013, Article ID 685454, 8 pages, 2013.
- [32] S Mosayebidorcheh, M Hatami, DD Ganji, T Mosayebidorcheh, SM Mirmohammadsadeghi, Investigation of Transient MHD Couette flow and Heat Transfer of Dusty Fluid with Temperature-Dependent properties, *Journal of Applied Fluid Mechanics*, 8(4) (2015) 921-929.
- [33] M. Sheikholeslami, S.A. Shehzad. CVFEM for influence of external magnetic source on Fe₃O₄-H₂O nanofluid behavior in a permeable cavity considering shape effect. *International Journal of Heat and Mass Transfer*, Volume 115, Part A, (2017), 180-191
- [34] M. Sheikholeslami, S.A. Shehzad Magnetohydrodynamic nanofluid convective flow in a porous enclosure by means of LBM. *International Journal of Heat and Mass Transfer*, 113 (2017) 796-805
- [35] M. Sheikholeslami, M. Seyednezhad. Nanofluid heat transfer in a permeable enclosure in presence of variable magnetic field by means of CVFEM. *International Journal of Heat and Mass Transfer*, 114 (2017) 1169-1180
- [36] M. Sheikholeslami, H. B. Rokni. Simulation of nanofluid heat transfer in presence of magnetic field: A review. *International Journal of Heat and Mass Transfer*, 115, Part B, (2017) 1203-1233
- [37] M. Sheikholeslami, T. Hayat, A. Alsaedi. On simulation of nanofluid radiation and natural convection in an enclosure with elliptical cylinders. *International Journal of Heat and Mass Transfer*, 115, Part A, (2017) 981-991
- [38] M. Sheikholeslami, Houman B. Rokni. Melting heat transfer influence on nanofluid flow inside a cavity in existence of magnetic field. *International Journal of Heat and Mass Transfer*, 114 (2017) 517-526
- [39] M. Sheikholeslami, M.K. Sadoughi. Simulation of CuO-water nanofluid heat transfer enhancement in presence of melting surface. *International Journal of Heat and Mass Transfer*, 116 (2018) 909-919
- [40] M. Sheikholeslami, Mohammadkazem Sadoughi. Mesoscopic method for MHD nanofluid flow inside a porous cavity considering various shapes of nanoparticles. *International Journal of Heat and Mass Transfer*, 113 (2017) 106-114

- [41] M. Sheikholeslami, M.M. Bhatti. Forced convection of nanofluid in presence of constant magnetic field considering shape effects of nanoparticles. *International Journal of Heat and Mass Transfer*, 111 (2017) 1039-1049
- [42] M. Sheikholeslami, M.M. Bhatti. Active method for nanofluid heat transfer enhancement by means of EHD. *International Journal of Heat and Mass Transfer*, 109 (2017) 115-122
- [43] M. Sheikholeslami, Houman B. Rokni. Nanofluid two phase model analysis in existence of induced magnetic field. *International Journal of Heat and Mass Transfer*, 107 (2017) 288-299
- [44] M. Sheikholeslami, S.A. Shehzad. Magnetohydrodynamic nanofluid convection in a porous enclosure considering heat flux boundary condition. *International Journal of Heat and Mass Transfer*, 106 (2017) 1261-1269
- [45] M. Sheikholeslami, T. Hayat, A. Alsaedi. Numerical simulation of nanofluid forced convection heat transfer improvement in existence of magnetic field using lattice Boltzmann method. *International Journal of Heat and Mass Transfer*, 108, Part B (2017) 1870-1883
- [46] M. Sheikholeslami, T. Hayat, A. Alsaedi. Numerical study for external magnetic source influence on water based nanofluid convective heat transfer. *International Journal of Heat and Mass Transfer*, 106 (2017) 745-755
- [47] M. Sheikholeslami, T. Hayat, A. Alsaedi, S. Abelman. Numerical analysis of EHD nanofluid force convective heat transfer considering electric field dependent viscosity. *International Journal of Heat and Mass Transfer*, 108, Part B (2017) 2558-2565
- [48] J.K. Zhou. *Differential Transformation and Its Applications for Electrical Circuits*. Huazhong University Press, Wuhan, China (1986) (in Chinese).
- [49] L.T. Yu, C.K. Chen, The solution of the Blasius equation by the differential transformation method, *Math. Comput. Modell.* 28 (1998) 101–111.
- [50] B.L. Kuo, Thermal boundary-layer problems in a semi-infinite flat plate by the differential transformation method, *Appl. Math. Comput.* 153 (2004) 143–160.
- [51] B. L. Kuo. Application of the differential transformation method to the solutions of the free convection problem. *Applied Mathematics and Computation* 165 (2005) 63–79.
- [52] M. M. Rashidi, N. Laraqi, S. M. Sadri. A Novel Analytical Solution of Mixed Convection about an Inclined Flat Plate Embedded in a Porous Medium Using the DTM-Pade, *International Journal of Thermal Sciences*, 49 (2010), 12, 2405-2412.
- [53] N. Casson, *Rheology of Dispersed System*, vol.84, Pergamon Press, Oxford, UK, 1959.
- [54] R. K. Dash, K. N. Mehta, and G. Jayaraman, Casson fluid flow in a pipe filled with a homogeneous porous medium. *International Journal of Engineering Science*, vol.34, no.10, pp. 1145–1156, 1996.
- [55] H.I. Andersson and B.S. Dandapat, Flow of a power-law fluid over a stretching sheet. *Applied Analysis of Continuous Media*, vol. 1, no. 339, 1992.

- [56] M. Sajid, I. Ahmad, T. Hayat and M. Ayub, Unsteady flow and heat transfer of a second grade fluid over a stretching sheet. *Communications in Nonlinear Science and Numerical Simulation*, vol.14, no.1, pp. 96–108, 2009.
- [57] N. T. M. Eldabe and M. G. E. Salwa, Heat transfer of mhd non-Newtonian Casson fluid flow between two rotating cylinder. *Journal of the Physical Society of Japan*, vol. 64, p. 4164, 1995.
- [58] S. Nadeem, R. L. Haq, N. S. Akbar, and Z. H. Khan, MHD three-dimensional Casson fluid flow past a porous linearly stretching sheet. *Alexandria. Engineering Journal*, Vol. 52, pp. 577582, (2013).
- [59] A. Raptis, C. Perdikis. Viscoelastic flow by the presence of radiation. *Zeitschrift für Angewandte Mathematik und Mechanik* 1998; 78: 277–9
- [60] M. A. Seddeek. Effects of radiation and variable viscosity on a MHD free convection flow past a semi-infinite flat plate with an aligned magnetic field in the case of unsteady flow. *Int. J. Heat Mass Transfer* 2002; 45: 931–5
- [61] F. Mabood, M. Imtiaz, A. Alsaedi, T. Hayat. Unsteady convective boundary layer flow of Maxwell fluid with nonlinear thermal radiation: A Numerical study. *Int. J. Nonlinear Sci. Num. Simul.* 2016; 17: 221–9
- [62] T. Hayat, T. Muhammad, A. Alsaedi, M. S. Alhuthali. Magnetohydrodynamic threedimensional flow of viscoelastic nanofluid in the presence of nonlinear thermal radiation. *J. Magn. Magn. Mater.* 2015; 385: 222–9
- [63] M. Farooq, M.I., Khan, M. Waqas, T. Hayat, A. Alsaedi, M.I. Khan. MHD stagnation point flow of viscoelastic nanofluid with non-linear radiation effects. *J. Mol. Liq.* 2016; 221, 1097–103
- [64] S. A. Shehzad, Z. Abdullah, A. Alsaedi, Abbasi FM, Hayat T. Thermally radiative three-dimensional flow of Jeffrey nanofluid with internal heat generation and magnetic field. *J. Magn. Magn. Mater.* 2016; 397: 108–14
- [65] N. Casson: A flow equation for the pigment oil suspension of the printing ink type. In: *Rheology of Disperse Systems*, 84-102. Pergamon, New York (1959).
- [66] N. S. Akbar and A. W. Butt. Ferro-magnetic effects for peristaltic flow of Cu-water nanofluid for different shapes of nano-size particles. *Appl. Nanosci.* 6 (2016) 379-385.
- [67] M. Sheikholesmi and M. M. Bhatti. Free convection of nanofluid in the presence of constant magnetic field considering shape effects of nanoparticles. *International Journal of Heat and Mass Transfer*, 111 (2017) 1039-1049.
- [68] R. Ul Haq, S. Nadeem, Z.H. Khan, N.F.M. Noor, Convective heat transfer in MHD slip flow over a stretching surface in the presence of carbon nanotubes, *Physica B*, 457 (2015) 40–47.
- [69] L. D. Talley, G. L. Pickard, W. J. Emery, J. H. Swift, Descriptive Physical Oceanography, Physical Properties of Sea Water, sixth ed., Elsevier Ltd, 2011, pp. 29–65.

- [70] M. Pastoriza-Gallego, L. Lugo, J. Legido, M. Piñeiro, Thermal conductivity and viscosity measurements of ethylene glycol-based Al₂O₃ nanofluids, *Nanoscale Res Lett.* 6 (221) 1–11.
- [71] S. Aberoumand and A. Jafarimoghaddam, Experimental study on synthesis, stability, thermal conductivity and viscosity of Cu–engine oil nanofluid, *Journal of the Taiwan Institute of Chemical Engineers*, 71 (2017) 315–322.
- [72] G.A. Baker, P. Graves-Morris, Pade Approximants, Cambridge U.P., 1996.
- [73] H. K. Kuiken. On boundary layers in fluid mechanics that decay algebraically along stretches of wall that are not vanishingly small. *IMA Journal of Applied Mathematics*, 27(4) (1981) 387–405.
- [74] W. Daungthongsuk and Somchai Wongwises, A critical review of convective heat transfer of nanofluids, *Renewable and Sustainable Energy reviews*, 11 (2007) 797-817.
- [75] S. Kakac and Anchasa Pramuanjaroenkij, Review of convective heat transfer enhancement with nanofluids, *International Journal of Heat and Mass Transfer* 52 (2009) 3187-3196.
- [76] Y. Ding, Haisheng Chen, Yurong He, Alexei Lapkin, Mahboubeh Yeganeh, Lidija Siller and Yuriy V. Butenko, Forced convective heat transfer of nanofluids, *Advanced Powder Technology*, 18 (2007) 813-824.
- [77] L. Godson Asirvatham, B. Raja, D. Mohan Lal and Somchai Wongwises, *Convective heat transfer of nanofluids with correlations*, 9 (2011) 626-631.
- [78] C. Zhang, L. Zheng, X. Zhang and G. Chen. MHD flow and radiation heat transfer of nanofluids in porous media with variable surface heat flux and chemical reaction, *Applied Mathematical Modelling*, 39 (2015) 165-181.
- [79] G.S. Seth, S.M. Hussain and S. Sarkar, Hydromagnetic natural convection flow with heat and mass transfer of a chemically reacting and heat absorbing fluid past an accelerated moving vertical plate with ramped temperature and ramped surface concentration through a porous medium, *Journal of the Egyptian Mathematical Society*, 23 (2015) 197-207.
- [80] D. Srinivasacharya and G. Swamy Reddy, Chemical reaction and radiation effects on mixed convection heat and mass transfer over a vertical plate in power-law fluid saturated porous medium, *Journal of the Egyptian Mathematical Society*, 24 (2016) 108-115.
- [81] F.S. Ibrahim, A.M. Elaiw and A.A. Bakr, Effect of the chemical reaction and radiation absorption on the unsteady MHD free convection flow past a semi-infinite vertical permeable moving plate with heat source and suction, *Nonlinear Science and Numerical Simulation*, 13 (2008) 1056-1066.
- [82] K. Das, Pinaki Ranjan Duari and Prabir Kumar Kundu, Nanofluid over an unsteady stretching surface in presence of thermal radiation, *Alexandria Engineering Journal*, 53 (2014) 737-745.

- [83] R.S. Tripathy, G.C. Dash, S.R. Mishra and S. Baag, Chemical reaction effects on MHD free convective surface over a moving vertical plate through porous medium. *Alexandria Engineering Journal*, 54 (2015) 673-679.
- [84] P.M. Patil and P.S. Kulkarni, Effects of chemical reaction on free convective flow of a polar fluid through a porous medium in the presence of internal heat generation, *International Journal of Thermal Science*, 47 (2008) 1043-1054.
- [85] M. Mehdi Rashidi, B. Rotami, N. Freidoonimehr and S. Abbasbandy, Free convective heat and mass transfer for MHD Fluid flow over a permeable vertical stretching sheet in the presence of the radiation and Buoyancy effects, *Ain Shams Engineering Journal*, 5 (2014) 901-912.
- [86] S. Nadeem, R.U. Haq and Z.H. Khan, Heat transfer analysis of water-based nanofluid over an exponentially stretching sheet. *Alexandria Engineering Journal* Volume 53, Issue 1, March 2014, Pages 219-224
- [87] N. Sandeep, A. Malvandi, Enhanced heat transfer in liquid thin film flow of non-Newtonian nanofluids embedded with graphene nanoparticles, *Advanced Powder Technology*, 27 (2017) 2448–2456.
- [88] S. Mosayebidorcheh, O.D. Makinde, D.D. Ganji, M. A. Chermahini. DTM-FDM hybrid approach to unsteady MHD Couette flow and heat transfer of dusty fluid with variable properties, *Thermal Science and Engineering Progress* 2 (2017) 57-63.
- [89] M. E. Ali, N. Sandeep, Cattaneo-Christov model for radiative heat transfer of magnetohydrodynamic Casson-ferrofluid: A numerical study, *Results in Physics*, 7 (2017) 21-30.
- [90] R.N. Barik, Chemical reaction and radiation effects of MHD free convective flow an impulsively moving vertical plate with ramped wall temperature and concentration, *European Journal of Advanced in Engineering and Technology*, 1 (2014) 56-68.
- [91] C. Sulochana, M.K. Kishore Kumar and N. Sandeep, Radiation and chemical reaction effects on MHD thermosolutal nanofluid flow over a vertical plate in porous medium, *Chemical and Process Eng. Research*, 34 (2015) 28-37.
- [92] A. Rao, S. Shivaiah and Sk. Nuslin, Radiation effects on an unsteady MHD free convective flow a vertical porous plate in the presence of sores, *Advanced in Applied Science Research*, 3 (2012) 1663-1676.
- [93] N. Sandeep, M.Gnaneswar Reddy, Heat transfer of nonlinear radiative magnetohydrodynamic Cu-water nanofluid flow over two different geometries, *Journal of Molecular Liquids*, 225 (2017) 87-94.
- [94] N. Sandeep, Ram Prakash Sharma, M. Ferdows, Enhanced heat transfer in unsteady magnetohydrodynamic nanofluid flow embedded with aluminum alloy nanoparticles, *Journal of Molecular Liquids* 234 (2017) 437–443.
- [95] P. Mohan Krishna, N. Sandeep, Ram Prakash Sharma, Computational analysis of plane and parabolic flow of MHD Carreau fluid with buoyancy and exponential heat source effects, *European Physical Journal Plus*, 132 (2017) 202.

- [96] A. Ishak, R. Nazar, I. Pop. Heat transfer over an unsteady stretching permeable surface with prescribed wall temperature. *Nonlinear Analysis: Real World Applications*, 10 (2009) 2909-2913
- [97] N. Sandeep, Effect of Aligned Magnetic field on liquid thin film flow of magnetic-nanofluid embedded with graphene nanoparticles, *Advanced Powder Technology*, 28 (2017) 865–875.
- [98] M .Jayachandra Babu, N. Sandeep, UCM flow across a melting surface in the presence of double stratification and cross-diffusion effects, *Journal of Molecular Liquids*, 232 (2017) 27-35.
- [99] G. Kumaran, N. Sandeep, Thermophoresis and Brownian moment effects on parabolic flow of MHD Casson and Williamson fluids with cross diffusion, *Journal of Molecular Liquids* 233 (2017) 262–269.
- [100] O. D. Makinde, F. Mabood, W.A. Khan, M.S. Tshehla, MHD flow of a variable viscosity nanofluid over a radially stretching convective surface with radiative heat. *Journal of Molecular Liquids*, 219 (2016) 624-630.
- [101] W.A. Khan, O.D. Makinde, Z.H. Khan, Non-aligned MHD stagnation point flow of variable viscosity nanofluids past a stretching sheet with radiative heat, *Int. J. Heat Mass Transfer*, 96 (2016) 525-534.
- [102] O.D. Makinde, W.A. Khan, J.R. Culham, MHD variable viscosity reacting flow over a convectively heated plate in a porous medium with thermophoresis and radiative heat transfer, *Int. J. Heat Mass Transfer*, 93 (2016) 595-604.
- [103] O.D. Makinde, I.L. Animasaun, Thermophoresis and Brownian motion effects on MHD bioconvection of nanofluid with nonlinear thermal radiation and quartic chemical reaction past an upper horizontal surface of a paraboloid of revolution. *Journal of Molecular Liquids*. 221 (2016) 733-743.
- [104] W. N. Mutuku and O. D. Makinde. Hydromagnetic bioconvection of nanofluid over a permeable vertical plate due to gyrotactic microorganisms. *Computers & Fluids*, 95 (2014) 88–97.
- [105] O.D. Makinde, I. L. Animasaun: Bioconvection in MHD nanofluid flow with nonlinear thermal radiation and quartic autocatalysis chemical reaction past an upper surface of a paraboloid of revolution. *International Journal of Thermal Sciences*, 109 (2016) 159-171.
- [106] W.A. Khan, O.D. Makinde, Z.H. Khan: MHD boundary layer flow of a nanofluid containing gyrotactic microorganisms past a vertical plate with Navier slip. *International Journal of Heat and Mass Transfer* 74 (2014), 285–291.
- [107] W.A. Khan, O.D. Makinde: MHD nanofluid bioconvection due to gyrotactic microorganisms over a convectively heat stretching sheet. *International Journal of Thermal Sciences* 81 (2014) 118-124.
- [108] S. T. Mohyud-Din, M. A. Noor, and K. I. Noor, On the coupling of polynomials with correction functional. *International Journal of Modern Physics B*. In press.

- [109] S. T. Mohyud-Din, Solving heat and wave-like equations using He's polynomials. *Mathematical Problems in Engineering*, vol. 2009, Article ID 427516, 12 pages, 2009.
- [110] M. A. Noor and S. T. Mohyud-Din, Variational iteration method for solving higher-order nonlinear boundary value problems using He's polynomials. *International Journal of Nonlinear Sciences and Numerical Simulation*, 9(2) (2008) 141–157.
- [111] N. Herisanu and V. Marinca, A modified variational iteration method for strongly nonlinear problems, *Nonlinear Science Letters A*, 1 (2010) 183–192
- [112] J.-H. He, Variational iteration method—some recent results and new interpretations, *Journal of Computational and Applied Mathematics*, 207(1) (2007) 3–17.
- [113] J. H. He, Variational iteration method, a kind of non-linear analytical technique, some examples, *International Journal of Non-Linear Mechanics*, 34(4) (1999) 699–708.
- [114] J.-H. He, Variational iteration method for autonomous ordinary differential systems, *Applied Mathematics and Computation*, 114(2-3) (2000) 115–123.
- [115] J.-H. He, The variational iteration method for eighth-order initial-boundary value problems, *Physica Scripta*, 76(6) (2007) 680–682.
- [116] J.-H. He and X.-H. Wu, Variational iteration method: new development and applications, *Computers & Mathematics with Applications*, 54(7-8) (2007) 881–894.
- [117] J.-H. He and X.-H. Wu, Construction of solitary solution and compaction-like solution by variational iteration method, *Chaos, Solitons & Fractals*, 29(1) (2006) 108–113.
- [118] J. H. He, An elementary introduction of recently developed asymptotic methods and nanomechanics in textile engineering, *International Journal of Modern Physics B*, 22(21) (2008), 3487–4578
- [119] J.-H. He, Some asymptotic methods for strongly nonlinear equations, *International Journal of Modern Physics B*, 20(10) (2006) 1141–1199.
- [120] S. A. Kechil and I. Hashim, Non-perturbative solution of free-convective boundary-layer equation by Adomian decomposition method, *Physics Letters A*, 363 (2007) 110–114.
- [121] J.-H. He, Recent development of the homotopy perturbation method, *Topological Methods in Nonlinear Analysis*, 31(2) (2008) 205–209.
- [122] J.-H. He, Comparison of homotopy perturbation method and homotopy analysis method, *Applied Mathematics and Computation*, 156(2) (2004) 527–539
- [123] J. H. He, Homotopy perturbation method for bifurcation of nonlinear problems, *International Journal of Nonlinear Science and Numerical Simulation*, 6(2) (2005), 207–208.
- [124] J.-H. He, The homotopy perturbation method nonlinear oscillators with discontinuities, *Applied Mathematics and Computation*, 151(1) (2004) 287–292.
- [125] J.-H. He, A coupling method of a homotopy technique and a perturbation technique for non-linear problems, *International Journal of Non-Linear Mechanics*, 35(1) (2000) 37–43.